Crack Tip Plasticity in Mixed Mode Loading Under Contained Yielding Conditions

by

Md. Moshiur Rahman

Thesis submitted to the Department of Mechanical Engineering, Faculty of Engineering, University of Glasgow for the degree of Master of Science

November, 2002

Abstract

Mode I, mode II and mixed mode I/II asymptotic crack tip fields have been studied under contained yielding conditions using plane strain and plane stress boundary layer formulations. The effect of the non-singular term in the asymptotic elastic expansion (Williams, 1957) on the plastic zone at the crack tip has been determined. Plane stress mode I, mode II and mixed mode I/II crack tip fields have also been investigated analytically. Analytical solutions were developed by assembling constant stress, fan and elastic sectors. Slip line theory (Hill, 1950) was used to solve constant stress and fan sectors while the stress fields in elastic sectors were solved using the semi-infinite wedge solution of Timoshenko and Goodier (1970). Analytical solutions were validated by numerical results, and represented as slip line fields.

Acknowledgement

I would like to express my profound gratitude to my supervisor Prof. John W. Hancock for his sincere guidance, encouragement and specially for his kindness and financial support during this work.

I acknowledge access to the computer codes given in Appendices I & II from Prof. Hancock, and the use of ABAQUS under academic license from HKS Inc.

I would acknowledge the financial support of Bangladesh Atomic Energy Commission under the project "Research Development & Training Project of BAEC" for this research.

I wish to thank my friends and colleagues in Glasgow who have encouraged and helped me during my research.

I am thankful to my father, mother and relatives for their encouragement and support during this work.

Finally, I would like to express my profound thanks to my wife, Nazma and daughter, Nishat for their continuous support during this work.

Contents

List of Figures

List of Tables

Chapter 1 Introduction

Engineering structures and components may contain cracks or defects which may compromise their structural integrity. Fracture mechanics is intended to ensure the safety of structures such as nuclear installation, aircraft and chemical plant, and thus avoid loss of life, as well as providing financial savings.

Fracture mechanics can be used both in the design and maintenance of structures and components. Conventional methods based on strength, use two variables: the applied load and the yield strength or ultimate tensile strength of the material. In design based on fracture mechanics, three variables are considered: the applied load, the fracture toughness and the absolute defect size. Fracture toughness is a material property, which quantifies the material resistance to fracture. Fracture mechanics attempts to establish the critical combinations of load, fracture toughness and defect size to ensure that an existing defect does not extend.

The field of fracture mechanics developed following the failure of the Liberty ships developed in the United States during the second world war. The Liberty ships were fabricated by welding instead of using traditional riveted joints. Out of about 2700 Liberty ships, fractures occurred in around 400 vessels. Subsequent fracture analysis identified three different causes of failure: defects or cracks in welded joints, stress concentration at square hatch corners on the deck and poor fracture toughness of the structural steel. As a result improved quality control measures were implemented.

Research in the field of fracture mechanics can be categorised into materials research and structural research. Materials research is intended to give a better understanding of material behaviour. This includes material properties, process control, defects control and control of microstructure to obtain improved material performance and reliability. Structural research is intended to improve the life and design of structures. Thus fracture mechanics research potentially saves significant costs arising from both material and structural failures.

A component containing crack-like defects, may be loaded in three distinct modes: mode I (opening), mode II (in-plane shear) and mode III (out of plane shear) or any combination of these modes. In many practical cases, structures or components are subject to mixed mode (I/II, I/III, II/III) loadings rather than a single mode. The current work investigates the mixed mode I/II crack tip fields in elastic perfectly-plastic material in plane strain and plane stress, and is intended to provide insight into the structure of the crack tip field within the plastic zone, which develops at the crack tip.

Following this Introduction, Chapter 2 reviews the basic concepts of stress, strain and elastic stress-strain relations, plane stress and plane strain and concludes with a discussion on yielding and plasticity. Chapter 3 introduces the fundamental concepts of linear elastic fracture mechanics, which are central to this work. Chapter 4 establishes the concepts of plane strain and plane stress slip line fields and reviews existing solutions of plane strain and plane stress mixed mode (I/II) slip line fields.

Chapter 5 reviews the literature on cleavage and ductile fracture under mixed mode (I/II) loading. This leads to the numerical methods employed in the analysis including boundary layer formulations, which are discussed in Chapter 6. Chapter 7 presents the results of the numerical study, which focus on the structure of elastic perfectly-plastic crack tip fields in mixed mode I/II loading. Here a technique for expressing numerical results as slip line fields is developed in both plane strain and plane stress. Chapter 8 develops analytical solutions of the plane stress problems in mode I and mixed mode I/II loading. Finally, Chapter 9 discusses the results and the main conclusions of the work are summarised in Chapter 10.

Chapter 2 Stress, strain and stress-strain relations

2.1 Stress and strain

2.1.1 Stress

Stress is a fundamental concept in the mechanics of materials, and indicates how a force is transmitted through a solid body. To illustrate this, consider a small cubic element in Figure 2.1 subjected to arbitrary forces in an orthogonal Cartesian co-ordinate system x_i (i = 1, 2, 3). As the element is small, the forces are assumed to be uniformly distributed over the faces of the element. Force is a vector F_j, and A_i is the area of a face normal to the i direction. The stress on the element can be defined as:

$$\sigma_{ij} = \lim_{A_i \to 0} \frac{F_j}{A_i} \tag{2.1}$$

where i, j = 1, 2, 3. Stress σ_{ij}, is a second order tensor, in which the first suffix, i refers to the direction of the normal to the plane on which the stress acts, and the second suffix, j refers to the direction of force component. Normal stresses occur when i = j and shear stresses when i ≠ j. Thus a normal stress σ_{11} evolves from the force component on a plane in the x_1 direction and where the direction of the normal to the plane is also x_1. As illustrated in Figure 2.1, the stress components σ_{11}, σ_{22}, σ_{33} are the normal stress components on the element in x_1, x_2 and x_3 direction. σ_{12} and σ_{13} are shear stress components on the x_2x_3 face. Similarly σ_{21} and σ_{23} are shear stress components on the x_1x_3 face, and σ_{31} and σ_{32} are the components on the x_1x_2 face. Equilibrium of moments requires that $\sigma_{ij} = \sigma_{ji}$ allowing the stress tensor at a point be described by six independent components σ_{11}, σ_{22}, σ_{33}, σ_{12}, σ_{23} and σ_{31}.

If a body is under static equilibrium, the stress components must satisfy a set of differential equations known as the linear equilibrium equations:

$$\frac{\partial\sigma_{11}}{\partial x_1} + \frac{\partial\sigma_{12}}{\partial x_2} + \frac{\partial\sigma_{31}}{\partial x_3} + X_1 = 0$$

$$\frac{\partial\sigma_{22}}{\partial x_2} + \frac{\partial\sigma_{12}}{\partial x_1} + \frac{\partial\sigma_{23}}{\partial x_3} + X_2 = 0$$

$$\frac{\partial\sigma_{33}}{\partial x_3} + \frac{\partial\sigma_{23}}{\partial x_2} + \frac{\partial\sigma_{31}}{\partial x_1} + X_3 = 0 \tag{2.2}$$

where, X_1, X_2 and X_3 are the components of the body force per unit volume in the x_1, x_2 and x_3 directions.

Stresses can be transformed from one co-ordinate system to another system using the stress transformation equations. Figures 2.2 & 2.3 show the stresses on an element near the crack tip in Cartesian and polar co-ordinate systems. If the Cartesian stress components are σ_{11}, σ_{22} and σ_{12}, the stress components in a polar co-ordinate system (r,θ) are:

$$\sigma_{rr} = \sigma_{11}\cos^2\theta + \sigma_{22}\sin^2\theta + 2\sigma_{12}\sin\theta\cos\theta$$

$$\sigma_{\theta\theta} = \sigma_{11}\sin^2\theta + \sigma_{22}\cos^2\theta - 2\sigma_{12}\sin\theta\cos\theta$$

$$\sigma_{r\theta} = (\sigma_{22} - \sigma_{11})\sin\theta\cos\theta + \sigma_{12}(\cos^2\theta - \sin^2\theta) \qquad (2.3)$$

where, σ_{rr} is the normal stress component in the radial direction, $\sigma_{\theta\theta}$ is the normal stress component in the circumferential direction, $\sigma_{r\theta}$ is the shear stress component and θ is the angle (taken as positive anti-clockwise) which the element makes with the x_1 axis.

Similarly, stresses in the Cartesian co-ordinate system can be obtained from the polar co-ordinate system by the reverse transformation:

$$\sigma_{11} = \sigma_{rr}\cos^2\theta + \sigma_{\theta\theta}\sin^2\theta - 2\sigma_{r\theta}\sin\theta\cos\theta$$

$$\sigma_{22} = \sigma_{rr}\sin^2\theta + \sigma_{\theta\theta}\cos^2\theta + 2\sigma_{r\theta}\sin\theta\cos\theta$$

$$\sigma_{12} = (\sigma_{rr} - \sigma_{\theta\theta})\sin\theta\cos\theta + \sigma_{r\theta}(\cos^2\theta - \sin^2\theta) \qquad (2.4)$$

The maximum and the minimum normal stresses in an element are the principal stresses. The planes on which principal stresses act are called principal planes, which are not subject to shear stresses. Using Mohr's circle in Figures 2.4a & b, the maximum and minimum normal stresses i.e., the principal stresses on the element are:

$$\sigma_{1,2} = \frac{\sigma_{11} + \sigma_{22}}{2} \pm \sqrt{\left(\frac{\sigma_{11} - \sigma_{22}}{2}\right)^2 + \sigma_{12}^2} \qquad (2.5)$$

The principal planes and the principal stresses are shown in Figure 2.4c, and are perpendicular to each other.

Consideration of the element shown in Figure 2.4, indicates the maximum and minimum shear stresses in the element obtained from Mohr's circle construction are:

$$\tau_{\substack{max\\min}} = \pm\sqrt{\left(\frac{\sigma_{11} - \sigma_{22}}{2}\right)^2 + \sigma_{12}^2} \qquad (2.6)$$

The minimum shear stress is negative with an absolute value equal to the maximum shear stress. Figure 2.4d shows the maximum and the minimum shear stresses and the planes on which they occur. The two planes are orthogonal. The normal stresses, σ_n, on the planes of maximum and minimum shear stresses are identical and can be given as:

$$\sigma_n = \frac{\sigma_{11} + \sigma_{22}}{2} \tag{2.7}$$

The plane of maximum shear stress makes an angle of 45^0 with principal planes.

2.1.2 Strain

Strain is a measure of the distortion of a body, possibly as the result of an applied stress. A body subject to an external force, may undergo deformation as well as a rigid body motion. In multi-axial loading, the strain at a point in the body is specified by the components of strain in x_1, x_2 and x_3 directions. Like stress, the strain components are denoted as normal and shear strains and give the strain values of an infinitesimal element which is initially parallel to the co-ordinate axes. Normal strains are denoted by ε_{ij} $(i = j)$ and shear strains by γ_{ij} $(i \neq j)$. If the displacement components of a particle in a deformed body in x_1, x_2 and x_3 directions are u, v, and w, the normal and shear strain components are:

$$\varepsilon_{11} = \frac{\partial u}{\partial x_1}, \varepsilon_{22} = \frac{\partial v}{\partial x_2} \text{ and } \varepsilon_{33} = \frac{\partial w}{\partial x_3}$$

$$\gamma_{12} = \frac{\partial u}{\partial x_2} + \frac{\partial v}{\partial x_1}$$

$$\gamma_{23} = \frac{\partial v}{\partial x_3} + \frac{\partial w}{\partial x_2}$$

$$\gamma_{31} = \frac{\partial w}{\partial x_1} + \frac{\partial u}{\partial x_3} \tag{2.8}$$

As the six strain components are functions of the three displacement components, they can not vary independently and are related by a set of differential equations. The differential equations are called compatibility equations and can be written as:

$$\frac{\partial^2 \varepsilon_{11}}{\partial x_2^2} + \frac{\partial^2 \varepsilon_{22}}{\partial x_1^2} = \frac{\partial^2 \gamma_{12}}{\partial x_1 \partial x_2}$$

$$\frac{\partial^2 \varepsilon_{22}}{\partial x_3^2} + \frac{\partial^2 \varepsilon_{33}}{\partial x_2^2} = \frac{\partial^2 \gamma_{23}}{\partial x_2 \partial x_3}$$

$$\frac{\partial^2 \varepsilon_{33}}{\partial x_1^2} + \frac{\partial^2 \varepsilon_{11}}{\partial x_3^2} = \frac{\partial^2 \gamma_{13}}{\partial x_1 \partial x_3}$$

$$2\frac{\partial^2 \varepsilon_{11}}{\partial x_2 \partial x_3} = \frac{\partial}{\partial x_1}\left(-\frac{\partial \gamma_{23}}{\partial x_1} + \frac{\partial \gamma_{13}}{\partial x_2} + \frac{\partial \gamma_{12}}{\partial x_3}\right)$$

$$2\frac{\partial^2 \varepsilon_{22}}{\partial x_1 \partial x_3} = \frac{\partial}{\partial x_2}\left(\frac{\partial \gamma_{23}}{\partial x_1} - \frac{\partial \gamma_{13}}{\partial x_2} + \frac{\partial \gamma_{12}}{\partial x_3}\right)$$

$$2\frac{\partial^2 \varepsilon_{33}}{\partial x_1 \partial x_2} = \frac{\partial}{\partial x_3}\left(\frac{\partial \gamma_{23}}{\partial x_1} + \frac{\partial \gamma_{13}}{\partial x_2} - \frac{\partial \gamma_{12}}{\partial x_3}\right) \tag{2.9}$$

The strain components must satisfy the compatibility equations.

2.1.3 Elastic stress strain relations

Consider a bar of isotropic linear-elastic material subjected to uniaxial tensile stress σ_{22} as illustrated in Figure 2.5. The corresponding strains are:

$$\varepsilon_{22} = \frac{\sigma_{22}}{E}, \varepsilon_{11} = \varepsilon_{33} = -\nu\frac{\sigma_{22}}{E} \tag{2.10}$$

where, $\varepsilon_{11}, \varepsilon_{22}$ and ε_{33} are strain components in x_1, x_2 and x_3 direction respectively, E is Young's modulus and ν is Poisson's ratio. Similarly for uniaxial tensile stresses σ_{11} and σ_{33} the stress strain relations are:

$$\varepsilon_{11} = \frac{\sigma_{11}}{E}, \varepsilon_{22} = \varepsilon_{33} = -\nu\frac{\sigma_{11}}{E} \text{ and}$$

$$\varepsilon_{33} = \frac{\sigma_{33}}{E}, \varepsilon_{11} = \varepsilon_{22} = -\nu\frac{\sigma_{33}}{E} \tag{2.11}$$

By superimposing these equations for the strain components, the stress strain relations for multi-axial loading are:

$$\varepsilon_{11} = \frac{1}{E}[\sigma_{11} - \nu(\sigma_{22} + \sigma_{33})]$$

$$\varepsilon_{22} = \frac{1}{E}[\sigma_{22} - \nu(\sigma_{11} + \sigma_{33})]$$

$$\varepsilon_{33} = \frac{1}{E}[\sigma_{33} - \nu(\sigma_{11} + \sigma_{22})] \tag{2.12}$$

The shear strain components are obtained from the shear stresses as:

$$\gamma_{12} = \frac{\sigma_{12}}{G}, \gamma_{23} = \frac{\sigma_{23}}{G}, \gamma_{31} = \frac{\sigma_{31}}{G} \tag{2.13}$$

where, G is the shear modulus, which can be written in terms of Young's modulus and Poisson's ratio:

$$G = \frac{E}{2(1+\nu)} \tag{2.14}$$

2.2 Plane stress and plane strain

2.2.1 Plane stress

Plane stress and plane strain are concepts which are intended to simplify full three dimensional problems allowing them to become more amenable to analysis. Consider a thin plate, loaded as in Figure 2.6. The forces are uniformly distributed over the boundary of the plate, and act parallel to its plane, such that there is no stress component in the direction perpendicular to the plane of the plate (i.e., in the x_3 direction), and other stress components (x_1 and x_2) do not vary in that direction. This state is defined as plane stress and can be specified by the stress components σ_{11}, σ_{22} and σ_{12}.

Plane stress is defined such that in direction x_3,

$$\sigma_{33} = \sigma_{13} = \sigma_{23} = 0 \text{ and } \frac{\partial \sigma_{ij}}{\partial x_3} = 0 \tag{2.15}$$

2.2.2 Plane strain

Consider a long cylindrical body loaded as in Figure 2.7. The forces are uniformly distributed over the surface of the body, and act parallel to the faces of the cylinder. The stress components (x_1, x_2 and x_3) do not vary along the longitudinal axis (represents the x_3 direction) of the cylinder. Moreover, the cylinder is fixed between two rigid plates, such that it does not displace in the axial direction. Therefore, strain components of the body in the x_3 direction are zero. This state is defined as plane strain.

Plane strain is defined such that in direction x_3,

$$\varepsilon_{33} = \gamma_{13} = \gamma_{23} = 0 \tag{2.16}$$

From Hooke's law, the strain in the x_3 direction:

$$\varepsilon_{33} = \frac{1}{E}\left[\sigma_{33} - \nu\left(\sigma_{11} + \sigma_{22}\right)\right] \tag{2.17}$$

where ν represents Poisson's ratio and E is modulus of elasticity. Substituting $\varepsilon_{33} = 0$ in Equation 2.17, the normal stress in direction x_3 is:

$$\sigma_{33} = \nu\left(\sigma_{11} + \sigma_{22}\right) \tag{2.18}$$

The out of plane stress, σ_{33}, maintains the plane strain condition. Again, from stress-strain relations:

$$\gamma_{13} = \frac{1}{G}\sigma_{13},\ \gamma_{23} = \frac{1}{G}\sigma_{23} \text{ and } \gamma_{12} = \frac{1}{G}\sigma_{12} \tag{2.19}$$

Substituting from Equation 2.16, Equations 2.19 give the condition of plane strain as:

$$\varepsilon_{33} = \gamma_{13} = \gamma_{23} = \sigma_{13} = \sigma_{23} = 0 \text{ and } \gamma_{12} = \frac{1}{G}\sigma_{12} \tag{2.20}$$

2.3 Yielding and plasticity

2.3.1 The Tresca yield criterion

The Tresca yield criterion (Tresca, 1864) suggests that multiaxially loaded material yields and exhibits irreversible plastic deformation when the maximum shear stress exceeds a critical value equal to the yield strength in shear. The maximum shear stress is given by:

$$\tau_{max} = \tau_y = \sigma_0/2 = \text{Maximum of } \left|\frac{\sigma_1 - \sigma_2}{2}\right|, \left|\frac{\sigma_1 - \sigma_3}{2}\right|, \left|\frac{\sigma_2 - \sigma_3}{2}\right| \tag{2.21}$$

where, σ_1, σ_2 and σ_3 are the three principal stresses. The Tresca criterion indicates that the yield stress in shear is one-half the tensile yield strength.

2.3.2 The von Mises yield criterion

The von Mises yield criterion (von Mises, 1913) indicates that yielding occurs when the elastic distortional energy per unit volume in a tensile test equals the distortional energy per unit volume in the component under multi-axial loading. The distortional energy within a component under multi-axial loading can be characterised by an equivalent stress:

$$\sigma_e = \frac{1}{\sqrt{2}}\left[(\sigma_1 - \sigma_2)^2 + (\sigma_2 - \sigma_3)^2 + (\sigma_3 - \sigma_1)^2\right]^{\frac{1}{2}} \tag{2.22}$$

where, σ_1, σ_2 and σ_3 are the three principal stresses. Yielding occurs in a multi-axially loaded component if the equivalent stress, σ_e equals the uni-axial yield strength, σ_0.

The von Mises yield criterion can be expressed in terms of non-principal stresses. As discussed in Section 2.1.1, the principal stresses can be written as:

$$\sigma_1 = \frac{\sigma_{11} + \sigma_{22}}{2} + \left[\left(\frac{\sigma_{11} - \sigma_{22}}{2}\right)^2 + \sigma_{12}^2\right]^{\frac{1}{2}}$$

$$\sigma_2 = \frac{\sigma_{11} + \sigma_{22}}{2} - \left[\left(\frac{\sigma_{11} - \sigma_{22}}{2}\right)^2 + \sigma_{12}^2\right]^{\frac{1}{2}} \tag{2.23}$$

The principal stress in x_3 direction can be given as:

$$\sigma_3 = 0 \tag{2.24}$$

in plane stress, and

$$\sigma_3 = \nu(\sigma_1 + \sigma_2) \tag{2.25}$$

in plane strain, where ν is Poison's ratio.

Substituting Equations 2.23 in Equation 2.25 gives:

$$\sigma_3 = \nu(\sigma_{11} + \sigma_{22}) \tag{2.26}$$

Substituting Equations 2.23 & 2.24 in Equation 2.22 gives von Mises equation in terms of non-principal stresses for plane stress:

$$\sigma_e = \frac{1}{\sqrt{2}}\left[6\left(\frac{\sigma_{11}-\sigma_{22}}{2}\right)^2 + 2\left(\frac{\sigma_{11}+\sigma_{22}}{2}\right)^2 + 6\sigma_{12}^2\right]^{\frac{1}{2}} \tag{2.27}$$

Again substituting Equations 2.23 & 2.26 in Equation 2.22 gives the corresponding equation for plane strain:

$$\sigma_e = \frac{1}{\sqrt{2}}\left[6\left(\frac{\sigma_{11}-\sigma_{22}}{2}\right)^2 + 2\left(\frac{\sigma_{11}+\sigma_{22}}{2}\right)^2(1-2\nu)^2 + 6\sigma_{12}^2\right]^{\frac{1}{2}} \tag{2.28}$$

2.3.3 Equivalent stress and equivalent strain

If yielding is assumed to occur under the von Mises yield criterion, the tendency for further plastic flow can be quantified by the equivalent stress, $\bar{\sigma}$ which can be expressed in terms of principal stresses, $\sigma_1, \sigma_2, \sigma_3$ as:

$$\bar{\sigma} = \sqrt{1/2[(\sigma_1-\sigma_2)^2 + (\sigma_2-\sigma_3)^2 + (\sigma_3-\sigma_1)^2]} \tag{2.29}$$

The equivalent stress can also be written in terms of the Cartesian stresses as:

$$\begin{aligned}\bar{\sigma} = &\sqrt{1/2[(\sigma_{11}-\sigma_{22})^2 + (\sigma_{22}-\sigma_{33})^2 + (\sigma_{33}-\sigma_{11})^2]} \\ &+ \sqrt{3}\sigma_{12} + \sqrt{3}\sigma_{23} + \sqrt{3}\sigma_{31}\end{aligned} \tag{2.30}$$

In uni-axial tension the equivalent stress, $\bar{\sigma}$ is equal to the yield or flow strength of the material. For an elastic-perfectly plastic material during plastic deformation the equivalent stress remains constant. However, if the material strain hardens, the equivalent stress increases with plastic deformation, due to changes in the dislocation structure of the material.

Since the equivalent stress depends on plastic strain, it is necessary to quantify strain with a parameter which corresponds to the equivalent stress, $\bar{\sigma}$. The appropriate parameter is the equivalent plastic strain, $\bar{e}^p$, which can be defined as:

$$\bar{e}^p = \sqrt{2/9[(e_1^p-e_2^p)^2 + (e_2^p-e_3^p)^2 + (e_3^p-e_1^p)^2]} \tag{2.31}$$

where, e_1^p, e_2^p and e_3^p are principal plastic strains. The equivalent plastic strain in terms of Cartesian strains can be given as:

$$\bar{e}^p = \sqrt{2/9[(e_{11}^p - e_{22}^p)^2 + (e_{22}^p - e_{33}^p)^2 + (e_{33}^p - e_{11}^p)^2] + \frac{1}{3}(\gamma_{12})^2 + \frac{1}{3}(\gamma_{23})^2 + \frac{1}{3}(\gamma_{31})^2} \tag{2.32}$$

In uni-axial tension the equivalent strain, $\bar{e}^p$ is equal to the axial strain, e_1^p for incompressible deformation. The equivalent plastic strain, $\bar{e}^p$ quantifies the total dislocation activity associated with a shape change. Under uni-axial tension ($\sigma_2 = \sigma_3 = 0$) an axial tensile plastic strain, $e_1^p = 0.02$, gives rise to transverse plastic strains, $e_2^p = e_3^p = -0.01$, with no volume change. Although the volumetric shape change ($e_1^p + e_2^p + e_3^p$) is zero, the equivalent plastic strain ($\bar{e}^p = e_1^p$) is 0.02.

The equivalent plastic strain can be written in an incremental form as:

$$d\bar{e}^p = \sqrt{2/9[(de_1^p - de_2^p)^2 + (de_2^p - de_3^p)^2 + (de_3^p - de_1^p)^2]} \tag{2.33}$$

where, de_1^p, de_2^p and de_3^p are the principal plastic strain increments. Using Cartesian strains the equivalent plastic strain increment is:

$$d\bar{e}^p = \sqrt{2/9[(de_{11}^p - de_{22}^p)^2 + (de_{22}^p - de_{33}^p)^2 + (de_{33}^p - de_{11}^p)^2] + \frac{1}{3}(d\gamma_{12})^2 + \frac{1}{3}(d\gamma_{23})^2 + \frac{1}{3}(d\gamma_{31})^2} \tag{2.34}$$

The total equivalent plastic strain is then given by summing the equivalent strain increments over the strain history:

$$\bar{e}^p = \int d\bar{e}^p \tag{2.35}$$

Thus a tensile strain of 0.02 ($e_1^p = 0.02$, $e_2^p = e_3^p = -0.01$) followed by a compressive strain of 0.02 ($e_1^p = -0.02$, $e_2^p = e_3^p = +0.01$) recovers the original shape of the body but gives a total equivalent plastic strain of 0.04.

The relation between equivalent stress and equivalent plastic strain is independent of loading history as well as state of stress. Therefore, the equivalent stress-strain relation in tension is identical to that in bending or torsion.

The plastic stress-strain equations can be written in similar form to the elastic equations, thus:

$$\varepsilon_{11} = \frac{1}{E}[\sigma_{11} - \nu(\sigma_{22} + \sigma_{33})]$$

$$\varepsilon_{22} = \frac{1}{E}[\sigma_{22} - \nu(\sigma_{11} + \sigma_{33})]$$

$$\varepsilon_{33} = \frac{1}{E}[\sigma_{33} - \nu(\sigma_{11} + \sigma_{22})] \tag{2.36}$$

$$\gamma_{12} = \frac{\sigma_{12}}{G}\ ,\ \gamma_{23} = \frac{\sigma_{23}}{G}\ ,\ \gamma_{31} = \frac{\sigma_{31}}{G} \tag{2.37}$$

where, G is shear modulus and $G = E / 2(1+\nu)$.

Plastic deformation occurs with no volume change, so that the volumetric strain is:

$$\frac{\Delta V}{V} = \varepsilon_{11} + \varepsilon_{22} + \varepsilon_{33} = 0 \tag{2.38}$$

Substituting from Equations 2.36, Equation 2.38 gives:

$$\frac{\Delta V}{V} = \frac{1-2\nu}{E}(\sigma_{11} + \sigma_{22} + \sigma_{33}) = 0 \tag{2.39}$$

Equation 2.39 shows that for an incompressible material Poisson's ratio is ½, giving the shear modulus, $G = E/3$. Substituting into Equations 2.37 gives:

$$\gamma_{12} = \frac{3\sigma_{12}}{E}\ ,\ \gamma_{23} = \frac{3\sigma_{23}}{E}\ ,\ \gamma_{31} = \frac{3\sigma_{31}}{E} \tag{2.40}$$

To describe non-linear deformation, the modulus of elasticity, E, can be replaced with the ratio of equivalent stress to equivalent strain, $\overline{\sigma}/\overline{e}$, in Equations 2.36 & 2.40 to give a set of equations:

$$\varepsilon_{11} = \frac{\overline{e}}{\overline{\sigma}}[\sigma_{11} - \frac{1}{2}(\sigma_{22} + \sigma_{33})] \qquad \gamma_{12} = 3\frac{\overline{e}}{\overline{\sigma}}\sigma_{12}$$

$$\varepsilon_{22} = \frac{\overline{e}}{\overline{\sigma}}[\sigma_{22} - \frac{1}{2}(\sigma_{11} + \sigma_{33})] \qquad \gamma_{23} = 3\frac{\overline{e}}{\overline{\sigma}}\sigma_{23}$$

$$\varepsilon_{33} = \frac{\overline{e}}{\overline{\sigma}}[\sigma_{33} - \frac{1}{2}(\sigma_{11} + \sigma_{22})] \qquad \gamma_{31} = 3\frac{\overline{e}}{\overline{\sigma}}\sigma_{31} \tag{2.41}$$

These equations describe deformation plasticity, which is applicable to both linear and non-linear elasticity. A non-linear elastic material can not be distinguished from a plastic material unless unloading is allowed, and given this type of loading history (proportional loading) Equations 2.41 are also applicable to a material under deformation plasticity.

Non-linear elastic and plastically deforming materials can be distinguished if the deformation history involves unloading as the elastic strains are recovered on unloading and plastic strains are permanent. The total plastic strain is the sum of the increments of the strain in the deformation history. Replacing strains by plastic strain increments, Equations 2.41 gives the flow rule as:

$$d\varepsilon_{11}^{p} = [\sigma_{11} - \frac{1}{2}(\sigma_{22} + \sigma_{33})]\frac{d\bar{e}^{p}}{\bar{\sigma}} \qquad d\gamma_{12}^{p} = 3\frac{d\bar{e}^{p}}{\bar{\sigma}}\sigma_{12}$$

$$d\varepsilon_{22}^{p} = [\sigma_{22} - \frac{1}{2}(\sigma_{11} + \sigma_{33})]\frac{d\bar{e}^{p}}{\bar{\sigma}} \qquad d\gamma_{23}^{p} = 3\frac{d\bar{e}^{p}}{\bar{\sigma}}\sigma_{23}$$

$$d\varepsilon_{33}^{p} = [\sigma_{33} - \frac{1}{2}(\sigma_{11} + \sigma_{22})]\frac{d\bar{e}^{p}}{\bar{\sigma}} \qquad d\gamma_{31}^{p} = 3\frac{d\bar{e}^{p}}{\bar{\sigma}}\sigma_{31} \tag{2.42}$$

The Equations 2.42 describe incremental plasticity, where the total strain is obtained from the elastic strain calculated from instantaneous stresses and the total plastic strain obtained by summing the plastic strain increments:

$$d\varepsilon_{11} = d\varepsilon_{11}^{el} + d\varepsilon_{11}^{p} \qquad d\gamma_{12} = d\gamma_{12}^{el} + d\gamma_{12}^{p}$$

$$d\varepsilon_{22} = d\varepsilon_{22}^{el} + d\varepsilon_{22}^{p} \qquad d\gamma_{23} = d\gamma_{23}^{el} + d\gamma_{23}^{p}$$

$$d\varepsilon_{33} = d\varepsilon_{33}^{el} + d\varepsilon_{33}^{p} \qquad d\gamma_{31} = d\gamma_{31}^{el} + d\gamma_{31}^{p} \tag{2.43}$$

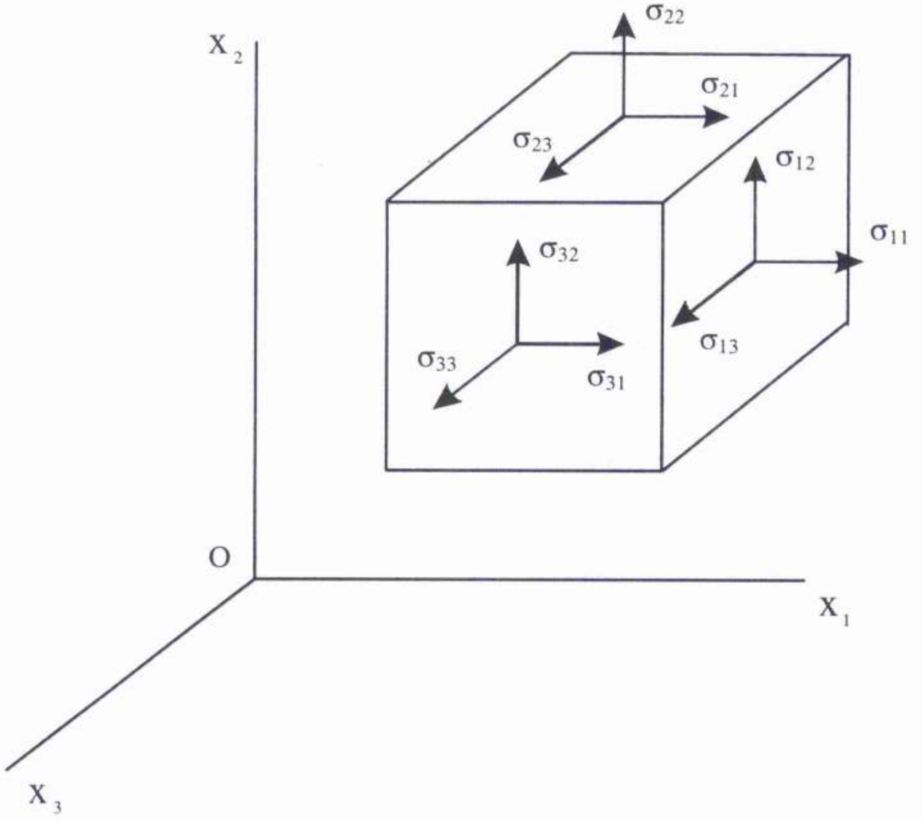

Figure 2.1: Stress components referred to Cartesian co-ordinate axes.

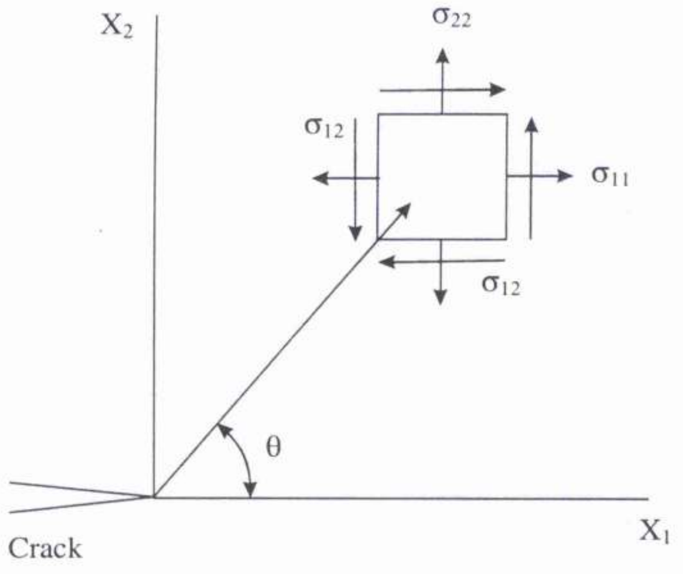

Figure 2.2: Stresses on an element near the crack tip in Cartesian co-ordinate system.

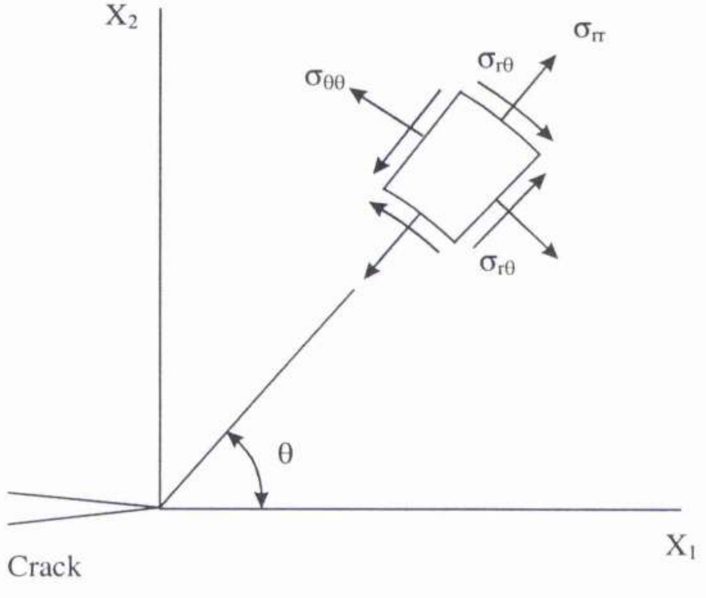

Figure 2.3: Stresses on an element near the crack tip in polar co-ordinate system.

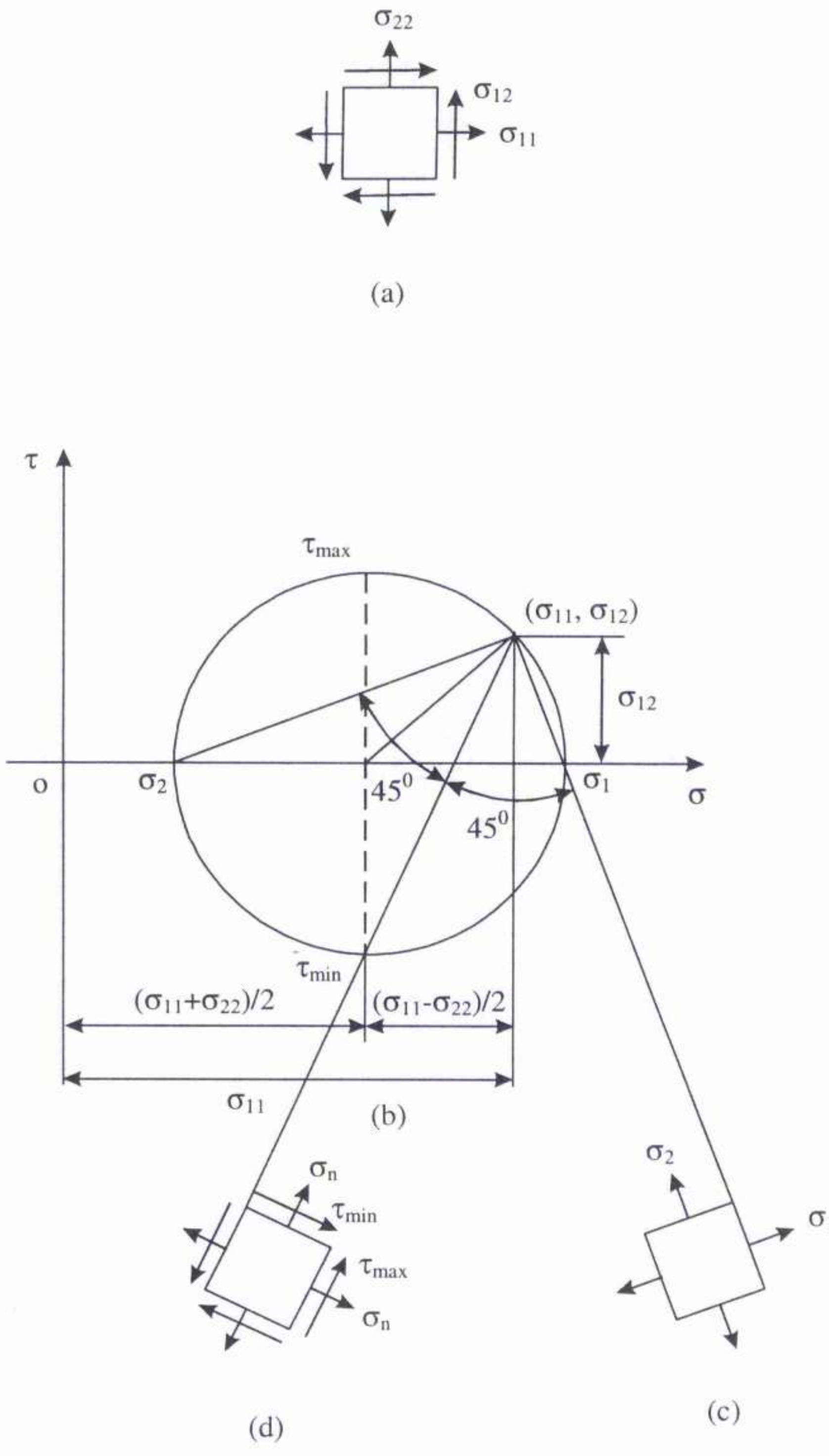

Figure 2.4: Stresses on element (a) and its corresponding Mohr's circle (b) showing the principal stresses (c) and maximum and minimum shear stresses (d).

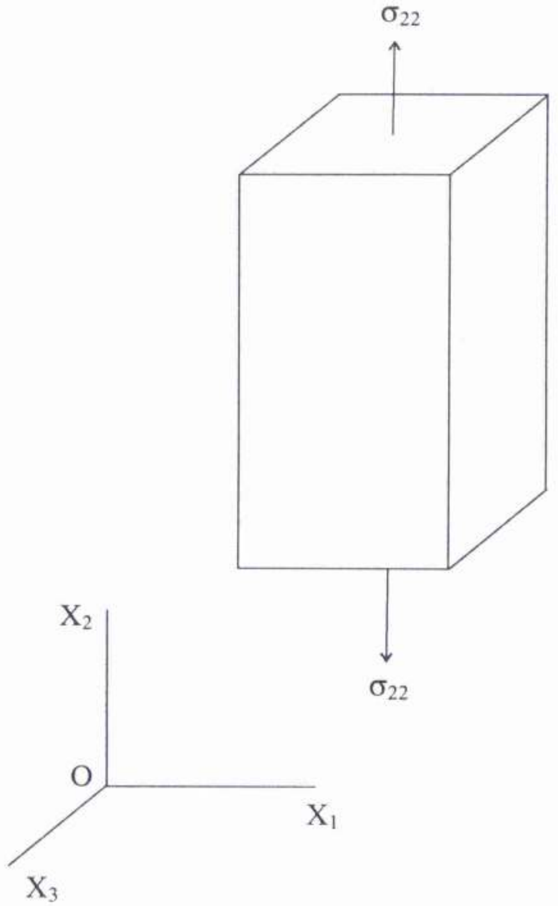

Figure 2.5: Bar subjected to uniaxial tension.

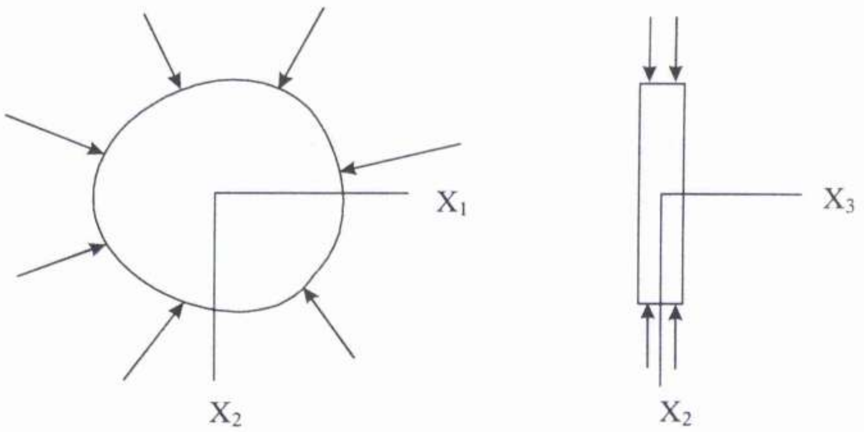

Figure 2.6: Forces at the boundary of a thin plate.

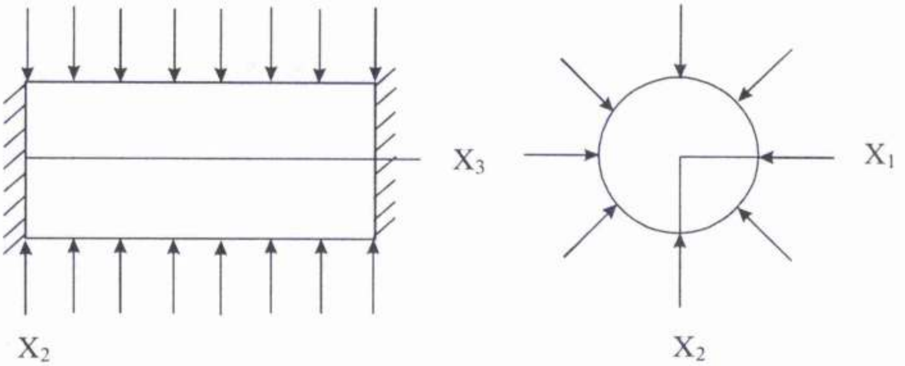

Figure 2.7: Cylindrical body is loaded by forces perpendicular to the longitudinal axis.

Chapter 3 Linear elastic fracture mechanics

3.1 Griffith Criterion

According to the Griffith criterion (1920), crack propagation occurs if the energy available for crack growth is greater than the energy absorbed by the material. Griffith (1920) used a thermodynamic principle which states that a system loses energy when it goes from a non-equilibrium to an equilibrium state, but if it is already in equilibrium the energy will remain unchanged. Hence, an existing crack will advance if the total energy in the system decreases or remains constant.

Consider an infinite plate subject to a remote tensile stress σ as illustrated in Figure 3.1. The plate contains a crack of length 2a. Following Griffith (1920), the surface energy associated with the crack will be $4at\gamma_s$ (the product of the total crack surface area, 4at, and the specific surface energy, γ_s). According to an analysis due to Inglis (1913), the decrease in elastic potential energy of the plate due to introducing a crack of length 2a is $(\pi\sigma^2a^2t)/E'$, where $E' = E$ in plane stress and $E/(1-v^2)$ in plane strain. The change in potential energy of the plate due to the introduction of a crack can be given as:

$$U - U_0 = -\frac{\pi\sigma^2a^2t}{E'} + 4at\gamma_s \tag{3.1}$$

where, U is the potential energy of the plate with a crack, U_0 is the potential energy of the plate without a crack, a is one-half the crack length, t is the thickness of the plate and γ_s is the specific surface energy.

Equation 3.1 can be rewritten in the form:

$$U = 4at\gamma_s - \frac{\pi\sigma^2a^2t}{E'} + U_0 \tag{3.2}$$

The equilibrium condition is given by the minimum potential energy, U with respect to crack length

$$\frac{\partial U}{\partial a} = 4t\gamma_s - \frac{2\pi\sigma^2a\,t}{E'} + 0 = 0 \tag{3.3}$$

Equation 3.3 gives the equilibrium condition as:

$$2\gamma_s = \frac{\pi\sigma^2a}{E'} \tag{3.4}$$

The second derivative of U in Equation 3.3 can be written as:

$$\frac{\partial^2U}{\partial a^2} = -\frac{2\pi\sigma^2t}{E'} \tag{3.5}$$

A negative value of the second derivative indicates unstable equilibrium in which the crack continues to grow. Equation 3.4 can finally be written in the form, which relates the fracture stress to the crack length:

$$\sigma = \sqrt{\frac{2E'\gamma_s}{\pi a}} \tag{3.6}$$

Equation 3.6 is valid for ideally brittle materials in which cracks propagate by breaking the atomic bonds, such that the energy of the broken bonds per unit area is given by surface energy per unit area, γ_s. However, in the case of metals and polymers, which undergo plastic deformation, a major portion of the fracture energy is contributed by plastic work (Irwin, 1948, Orowan, 1948). Therefore, plastic work per unit area of surface must be included in surface energy term.

In order to apply Griffith's relation to a plastically deforming material, Irwin (1948) defined the elastic strain energy release rate, $G = \partial U / \partial a$, which gives the relation:

$$\sigma\sqrt{\pi a} = \sqrt{E'G} \tag{3.7}$$

Fracture occurs when the strain energy release rate reaches a critical value, G_c. This critical strain energy release rate, G_c, is a material property and is independent of geometry. Substituting $G = G_c$ in Equation 3.7 gives relation between failure stress and critical strain energy release rate as:

$$\sigma_f\sqrt{\pi a} = \sqrt{E'G_c} \tag{3.8}$$

For an elastic plastic material strain energy release rate, G = J, a path independent contour integral surrounding the crack tip (Rice, 1968), which characterises the elastic plastic crack tip condition. Following Rice (1968), the J integral can be given as:

$$J = \int_{\Gamma}\left(w\,dy - T_i \frac{\partial u_i}{\partial x} ds \right) \tag{3.9}$$

where, Γ is an arbitrary contour surrounding the crack tip, w is the strain energy density, T_i are components of traction vector (normal to the contour), u_i are the components of displacement vector and ds is the increment of length along the contour. The strain energy density, w, can be given as:

$$w = \int_0^{\varepsilon_{ij}} \sigma_{ij}\, d\varepsilon_{ij} \tag{3.10}$$

where, σ_{ij} and ε_{ij} are the stress and strain tensors. Under linear elasticity J is identical to the strain energy release rate, G.

3.2 Stress Intensity Factor (SIF)

A parallel approach to the energetics of the crack advance considers the stress field at the crack tip. Using a cylindrical co-ordinate system centred at the crack tip the Williams (1957) expansion of the asymptotic elastic field can be given as:

$$\sigma_{ij} = A_{ij}(\theta)r^{-1/2} + B_{ij}(\theta)r^{0} + C_{ij}(\theta)r^{1/2} + \cdots \tag{3.11}$$

Focusing on the first and second terms that are non-zero at the tip, the stress field can be written as:

$$\sigma_{ij} = \frac{K}{\sqrt{2\pi r}} f_{ij}(\theta) + \begin{bmatrix} T & 0 \\ 0 & 0 \end{bmatrix} \qquad (i, j = 1, 2) \tag{3.12}$$

where, σ_{ij} is the stress tensor, $f_{ij}(\theta)$ is a dimensionless function of θ, K is the stress intensity factor and T is a uni-axial stress (tensile or compressive) parallel to the crack flanks. The first term in Equation 3.12 is singular at the crack tip and K describes the amplitude of singularity. T-stress is independent of radial distance but depends on geometry and load. Focussing on the first term, the asymptotic stress field for mode I loading can be given as:

$$\sigma_{ij} = \frac{K_I}{\sqrt{2\pi r}} f_{ij}(\theta) \tag{3.13}$$

where, K_I is mode I stress intensity factor. The Stress Intensity Factor (henceforth SIF) characterises the amplitude of the stress singularity at the tip of a crack in a linear elastic material. If the SIF is known, all the components of stress, strain and displacement at a point near the crack tip can be determined as a function of distance from the crack tip r and angle θ. The stress intensity factor is denoted by K_I, K_{II} and K_{III} depending upon the mode of loading (i.e., opening, in-plane shear and out-of-plane shear respectively). Figure 3.2 illustrates three different modes of loading. In mode I, the load is applied normal to the crack plane, and the crack opens symmetrically about the crack plane. Mode II corresponds to in-plane shear loading and tends to slide one crack face with respect to the other. Mode III corresponds to out of plane shear.

Consider an element located at (r,θ) near the crack tip in Figure 3.3. Westergaard (1939) has given the mode I stresses on the element in Cartesian co-ordinates:

$$\sigma_{11} = \frac{K_I}{\sqrt{2\pi r}} \cos\left(\frac{\theta}{2}\right)\left[1 - \sin\left(\frac{\theta}{2}\right)\sin\left(\frac{3\theta}{2}\right)\right]$$

$$\sigma_{22} = \frac{K_I}{\sqrt{2\pi r}} \cos\left(\frac{\theta}{2}\right)\left[1 + \sin\left(\frac{\theta}{2}\right)\sin\left(\frac{3\theta}{2}\right)\right]$$

$$\sigma_{12} = \frac{K_I}{\sqrt{2\pi r}} \cos\left(\frac{\theta}{2}\right)\sin\left(\frac{\theta}{2}\right)\cos\left(\frac{3\theta}{2}\right) \tag{3.14}$$

On the crack plane, $\theta = 0$, Equations 3.14 can be written as:

$$\sigma_{11} = \sigma_{22} = \frac{K_I}{\sqrt{2\pi r}}$$

$$\sigma_{12} = 0 \tag{3.15}$$

On the crack plane the shear stress is zero, so that for mode I loading the crack plane is a principal plane. The normal and shear stresses in the x_3 direction:

$\sigma_{33} = \nu\ (\sigma_{11} + \sigma_{22})$, in plane strain

$\sigma_{33} = 0$, in plane stress and

$\sigma_{13} = \sigma_{23} = 0$, both in plane stress and strain (3.16)

The Cartesian displacements (u_1, u_2) at (r,θ) for mode I can be given as:

$$u_1 = \frac{K_I}{2G}\left(\frac{r}{2\pi}\right)^{\frac{1}{2}}\left(\cos\frac{\theta}{2}\left(\kappa - 1 + 2\sin^2\frac{\theta}{2}\right)\right)$$

$$u_2 = \frac{K_I}{2G}\left(\frac{r}{2\pi}\right)^{\frac{1}{2}}\left(\sin\frac{\theta}{2}\left(\kappa + 1 - 2\cos^2\frac{\theta}{2}\right)\right) \tag{3.17}$$

where, $\kappa = (3 - 4\nu)$ for plane strain and $\kappa = (3-\nu)/(1+\nu)$ for plane stress, and G is the shear modulus. Stresses on the element in Figure 3.3 due to mode II loading can be given as:

$$\sigma_{11} = -\frac{K_{II}}{\sqrt{2\pi r}}\sin\left(\frac{\theta}{2}\right)\left[2 + \cos\left(\frac{\theta}{2}\right)\cos\left(\frac{3\theta}{2}\right)\right]$$

$$\sigma_{22} = \frac{K_{II}}{\sqrt{2\pi r}}\sin\left(\frac{\theta}{2}\right)\cos\left(\frac{\theta}{2}\right)\cos\left(\frac{3\theta}{2}\right)$$

$$\sigma_{12} = \frac{K_{II}}{\sqrt{2\pi r}}\cos\left(\frac{\theta}{2}\right)\left[1 - \sin\left(\frac{\theta}{2}\right)\sin\left(\frac{3\theta}{2}\right)\right] \tag{3.18}$$

Finally Cartesian displacements at (r,θ) for mode II loading can be written as:

$$u_1 = \frac{K_{II}}{2G}\left(\frac{r}{2\pi}\right)^{\frac{1}{2}}\left(\sin\frac{\theta}{2}\left(\kappa + 1 + 2\cos^2\frac{\theta}{2}\right)\right)$$

$$u_2 = \frac{K_{II}}{2G}\left(\frac{r}{2\pi}\right)^{\frac{1}{2}}\left(-\cos\frac{\theta}{2}\left(\kappa - 1 - 2\sin^2\frac{\theta}{2}\right)\right) \tag{3.19}$$

Linear elastic fields can be superimposed to produce a general mixed mode I/II loading. The stresses are given by summing Equations 3.14 and 3.18 and displacements by adding Equations 3.17 and 3.19. The strain energy release rate, G is given as:

$$G = \frac{K_I^2}{E'} + \frac{K_{II}^2}{E'} \tag{3.20}$$

where $E' = E$ for plane stress, and $E' = E/(1-\nu^2)$ for plane strain.

3.3 Stress intensity factor and specimen geometry

The stress intensity factor for a central through crack in an infinite plate, illustrated in Figure 3.4 is:

$$K_I = \sigma\sqrt{\pi a} \tag{3.21}$$

where, σ is remotely applied stress, and a is one-half the crack length. This makes contact with the Griffith's solution shown in Equation 3.6. This can be expressed as:

$$K_I = \sqrt{2E'\gamma_s} \tag{3.22}$$

The stress intensity factor must always involve the product of the applied stress and a characteristic distance such as the crack length. However the definition may involve a dimensionless constant which depends on geometry.

As an example consider an edge crack in a semi-infinite plate shown in Figure 3.5. The stress intensity factor given by Brown & Srawley (1966) is:

$$K_I = 1.12\,\sigma\sqrt{\pi a} \tag{3.23}$$

For an edge crack the stress intensity factor is 12% higher than that of a Griffith crack.

An important test geometry is that of an edge cracked bar of height 2h, width b and crack length a, subjected to a uniform tensile stress, σ as shown in Figure 3.6. For the condition without bending constraint, Brown & Srawley's (1966) polynomial for stress intensity factor is:

$$\frac{K_I}{K_o} = 1.12 - 0.23\,(a/b) + 10.6\,(a/b)^2 - 21.7\,(a/b)^3 + 30.4\,(a/b)^4 \tag{3.24}$$

where $K_0 = \sigma\sqrt{\pi a}$, the stress intensity factor for Griffith crack. Brown & Srawley (1966) estimate the accuracy of the stress intensity factor calculated from this equation to be within 1% for specimen with $h/b \geq 1.0$, and $a/b \leq 0.6$.

For an edge cracked bar (Figure 3.7) of width b and crack length a, subjected to pure bending, Brown & Srawley's (1966) polynomial for stress intensity factor is:

$$\frac{K_I}{K_o} = 1.12 - 1.39\,(a/b) + 7.32\,(a/b)^2 - 13.1\,(a/b)^3 + 14.0\,(a/b)^4 \qquad (3.25)$$

$$\text{where, } K_0 = \frac{6M\sqrt{\pi a}}{b^2} \qquad (3.26)$$

M is bending moment per unit thickness. The accuracy of result, obtained from the polynomial is estimated to be within 1% for $a/b \leq 0.6$.

As a further example consider an edge cracked bar of width b and crack length a, subjected to three point bending as shown is Figure 3.8. P is the applied load per unit thickness and l is the distance of each support from the line of crack. Brown & Srawley's (1966) stress intensity factor polynomials for l /b = 2 and 4 are given in Equations 3.27 and 3.28 respectively:

$$\frac{K_I}{K_o} = 1.11 - 1.55\,(a/b) + 7.71\,(a/b)^2 - 13.5\,(a/b)^3 + 14.2\,(a/b)^4 \qquad (3.27)$$

$$\frac{K_I}{K_o} = 1.09 - 1.73\,(a/b) + 8.20\,(a/b)^2 - 14.2\,(a/b)^3 + 14.6\,(a/b)^4 \qquad (3.28)$$

where K_0 is calculated from Equation 3.26. The bending moment:

$$M = Pl/2 \qquad (3.29)$$

3.4 Estimate of plastic zone radius

Much of the work of fracture involves crack tip plasticity (Irwin, 1948, Orowan, 1948). It is therefore important to estimate the radius of the plastic zone at the crack tip. The crack tip plastic zone radius can be estimated by applying the Tresca or von Mises yield criterion to the Westergaard (1939) equations:

$$\sigma_{11} = \frac{K_I}{\sqrt{2\pi r}}\cos\left(\frac{\theta}{2}\right)\left[1 - \sin\left(\frac{\theta}{2}\right)\sin\left(\frac{3\theta}{2}\right)\right]$$

$$\sigma_{22} = \frac{K_I}{\sqrt{2\pi r}}\cos\left(\frac{\theta}{2}\right)\left[1 + \sin\left(\frac{\theta}{2}\right)\sin\left(\frac{3\theta}{2}\right)\right]$$

$$\sigma_{12} = \frac{K_I}{\sqrt{2\pi r}}\cos\left(\frac{\theta}{2}\right)\sin\left(\frac{\theta}{2}\right)\cos\left(\frac{3\theta}{2}\right) \qquad (3.30)$$

The Tresca Equation is:

$$\tau_{max} = \frac{\sigma_1 - \sigma_3}{2} \qquad (\sigma_1 \geq \sigma_2 \geq \sigma_3) \qquad (3.31)$$

where, σ_1 is the largest principal stress, and σ_3 is the smallest principal stress.

The von Mises equation is:

$$\sigma_e = \frac{1}{\sqrt{2}}\left[(\sigma_1 - \sigma_2)^2 + (\sigma_2 - \sigma_3)^2 + (\sigma_3 - \sigma_1)^2\right]^{\frac{1}{2}} \quad (3.32)$$

where, σ_1, σ_2 and σ_3 are the three principal stresses. Using Mohr's circle σ_1, σ_2 and σ_3 can be given as:

$$\sigma_1 = \frac{\sigma_{11} + \sigma_{22}}{2} + \left[\left(\frac{\sigma_{11} - \sigma_{22}}{2}\right)^2 + \sigma_{12}^2\right]^{\frac{1}{2}}$$

$$\sigma_2 = \frac{\sigma_{11} + \sigma_{22}}{2} - \left[\left(\frac{\sigma_{11} - \sigma_{22}}{2}\right)^2 + \sigma_{12}^2\right]^{\frac{1}{2}}$$

$\sigma_3 = 0$, for plane stress

$\sigma_3 = \nu\,(\sigma_1 + \sigma_2)$, for plane strain (3.33)

where, ν is Poison's ratio.

Substituting Equations 3.30 into Equations 3.33 gives:

$$\sigma_1 = \frac{K_I}{\sqrt{2\pi r}}\cos\left(\frac{\theta}{2}\right)\left[1 + \sin\left(\frac{\theta}{2}\right)\right]$$

$$\sigma_2 = \frac{K_I}{\sqrt{2\pi r}}\cos\left(\frac{\theta}{2}\right)\left[1 - \sin\left(\frac{\theta}{2}\right)\right]$$

$\sigma_3 = 0$, for plane stress

$$\sigma_3 = \frac{2\nu K_I}{\sqrt{2\pi r}}\cos\left(\frac{\theta}{2}\right), \text{ for plane strain} \quad (3.34)$$

Following the Tresca criterion, yielding occurs when $\tau_{max} = \sigma_0/2$. Substituting Equations 3.34 into Equation 3.31 and setting $r = r_0$, the radius of Tresca plastic zone can be given as:

$$r_0 = \frac{K_I^2}{2\pi\sigma_0^2}\left[\cos\left(\frac{\theta}{2}\right)\left(1 + \sin\left(\frac{\theta}{2}\right)\right)\right]^2 \quad (3.35)$$

for plane stress, and the larger of

$$r_0 = \frac{K_I^2}{2\pi\sigma_0^2}\cos^2\left(\frac{\theta}{2}\right)\left[1 - 2\nu + \sin\left(\frac{\theta}{2}\right)\right]^2$$

and

$$r_0 = \frac{K_I^2}{2\pi\sigma_0^2}\sin^2\theta \qquad (3.36)$$

for plane strain.

Following the von Mises criterion, yielding occurs when the equivalent stress, σ_e, equals the uniaxial yield strength, σ_0. Substituting Equations 3.34 into Equation 3.32 and setting r = r_0, the radius of von Mises plastic zone can be given as:

$$r_0 = \frac{K_I^2}{4\pi\sigma_0^2}\left[1 + \cos\theta + \frac{3}{2}\sin^2\theta\right] \qquad (3.37)$$

for plane stress

$$r_0 = \frac{K_I^2}{4\pi\sigma_0^2}\left[(1 - 2\nu)^2(1 + \cos\theta) + \frac{3}{2}\sin^2\theta\right] \qquad (3.38)$$

for plane strain. Figures 3.9 & 3.10 show the plastic zone shapes estimated from Tresca and von Mises yield criteria.

3.5 The effect of thickness on fracture toughness

Fracture toughness varies with the thickness of the specimen (Irwin & Kies, 1954). If the thickness is small compared the plastic zone size, plane stress conditions occur at the crack tip. In this case, a high fracture toughness results, because of the energy absorbed by the large plastic zone.

If the specimen is thick compared to the plastic zone size, plane strain conditions develop in the centre of the crack plane. In this case, a limiting lower fracture toughness is obtained. This plane strain fracture toughness is denoted, K_{IC}, which is a material property and independent of geometry.

Figure 3.11 shows the effect of thickness on the fracture toughness schematically. A high K_C value occurs at small thicknesses. The K_C value decreases, as thickness increases until the limiting K_{IC}, the toughness is obtained, which does not change further with thickness.

3.6 LEFM fracture toughness (K_{IC}) test procedure

In Linear Elastic Fracture Mechanics the plane strain fracture toughness, K_{IC} is a material property, which must be measured in a laboratory test. Standard K_{IC} test methods include ASTM E 399 (1983) and BS 5447 (1974).

ASTM E 399 allows four possible specimen configurations for the K_{IC} test: the compact tension specimen (CTS), the single edge notched bend (SENB) specimen as well as the arc-shaped and disk-shaped specimens illustrated in Figure 3.12. A specimen for a K_{IC} test has three characteristic dimensions, the crack length, a, the thickness, B and the width, W. Specimens are fatigue pre-cracked under controlled conditions before the test is performed. The dimensions of the specimens are such that the thickness, B, equal to one half the width, W, and the crack length to the width ratio, a/W, is kept between 0.45 and 0.55.

To obtain a valid K_{IC}, the dimensions of the specimens must be large compared to the plastic zone radius. A preliminary validity check is recommended by ASTM E 399 to determine the specimen dimensions. The required dimensions are:

$$B, a \geq 2.5\left(\frac{K_{IC}}{\sigma_0}\right)^2 \qquad \text{and } 0.45 \leq a/W \leq 0.55 \tag{3.39}$$

where, σ_0 is the uniaxial yield strength. To determine the specimen dimensions, an anticipated fracture toughness is estimated using data for similar materials. If data are not available, a strength-thickness table provided by the ASTM standard can be used. However, this table is not strongly recommended as there is no unique relationship between K_{IC} and σ_0, and the data can only be used when better data are not available.

Before fatigue pre-cracking the specimen, the maximum allowable fatigue load is determined from the estimated K_{IC} value. During fatigue pre-cracking an optimum load is selected as pre-cracking would take longer time with low loads, and on the other hand there is a possibility of excessive crack tip plasticity at high loads. ASTM E 399 recommends that the maximum stress intensity factor, K_{max} in a cycle should be kept within 0.8 K_{IC} during initial stages of pre-cracking, and should be reduced to within 0.6 K_{IC} during the final stages.

In the test, the specimen is loaded until it fails and the load and displacement are monitored throughout the loading. From the load-displacement curve, the critical load, P_Q, is determined. Three different load-displacement curves are possible depending upon the material behaviour as shown in Figure 3.13. After performing the test the crack length, a, is measured as the average of three evenly spaced measurements through the thickness. A provisional fracture toughness, K_Q, is then calculated using the equation:

$$K_Q = \frac{P_Q}{B\sqrt{W}} f\,(a/W) \tag{3.40}$$

where, f (a/W) is a dimensionless function obtained from a polynomial or the table provided in the ASTM E 399. Upon the fulfilment of the requirements in the standard and the conditions imposed by the equations given below, K_Q would be the fracture toughness, K_{IC} of the material:

$$B, a \geq 2.5\left(\frac{K_Q}{\sigma_0}\right)^2,\ 0.45 \leq a/W \leq 0.55 \text{ and } P_{max} \leq 1.10 P_Q \tag{3.41}$$

where, P_{max} is the maximum load in the test.

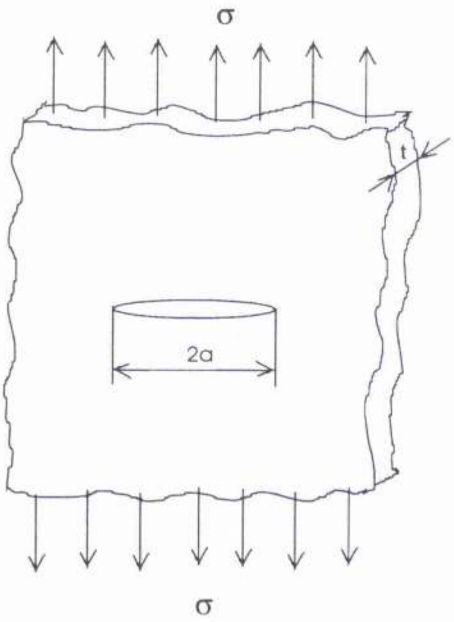

Figure 3.1: Through thickness crack in an infinite plate subjected to a remote tensile stress.

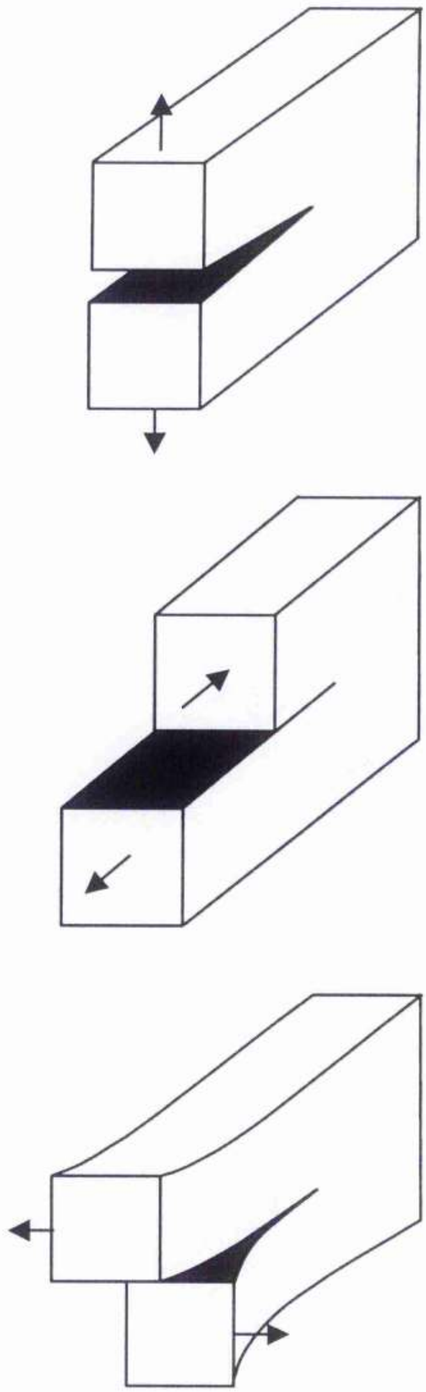

a) Mode I (Opening)

b) Mode II (In-Plane Shear)

c) Mode III (Out-of-Plane Shear)

Figure 3.2: Three modes of loading applicable to a crack.

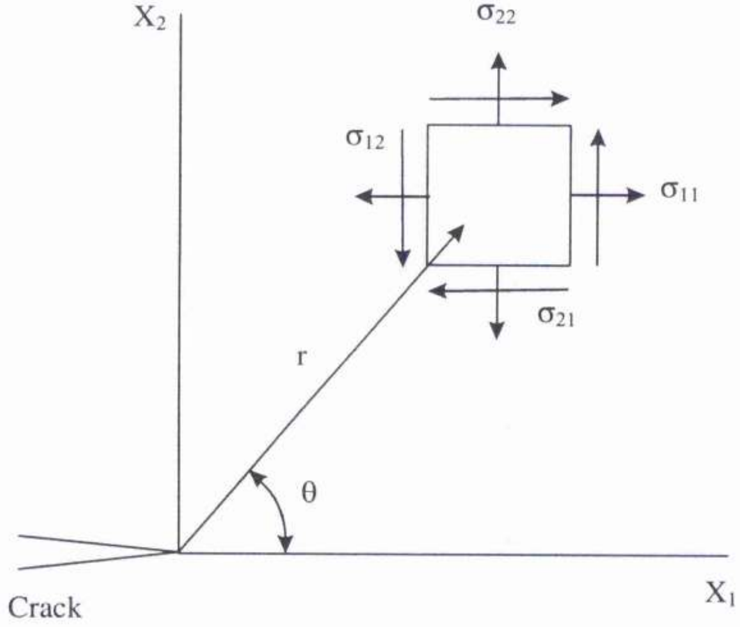

Figure 3.3: Stresses on an element near the crack tip in a linear elastic material.

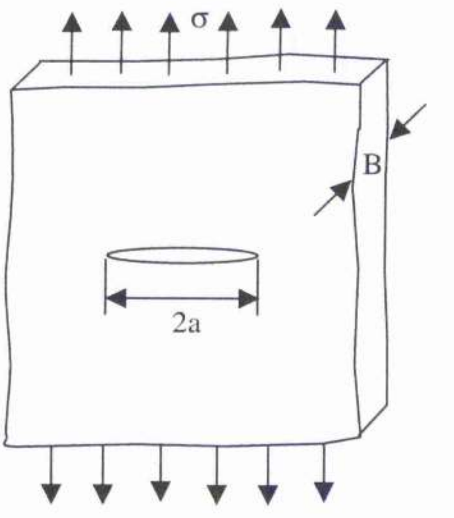

Figure 3.4: Through crack in an infinite plate.

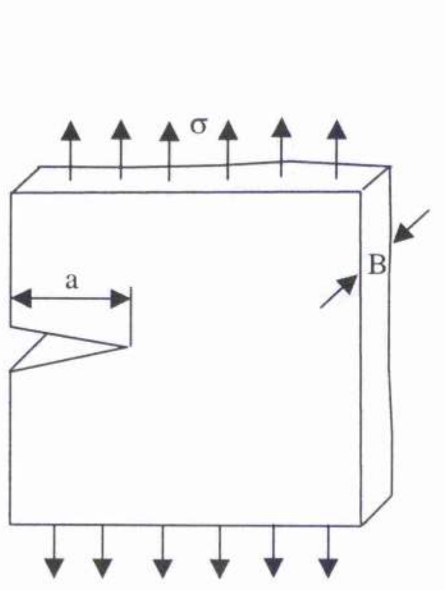

Figure 3.5: Edge crack in a semi-infinite plate.

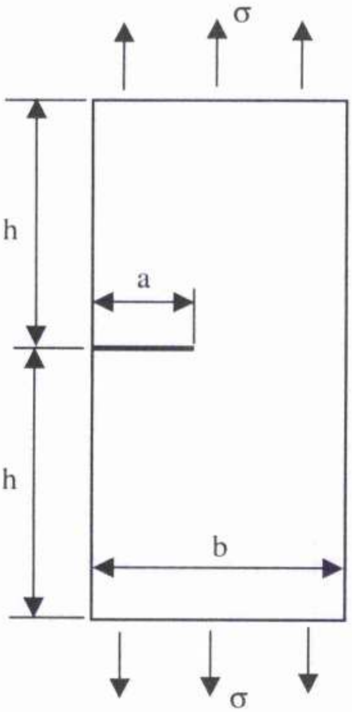

Figure 3.6: Edge cracked bar in tension.

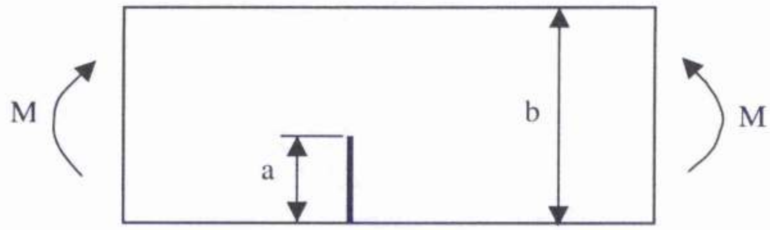

Figure 3.7: Edge cracked bar in pure bending.

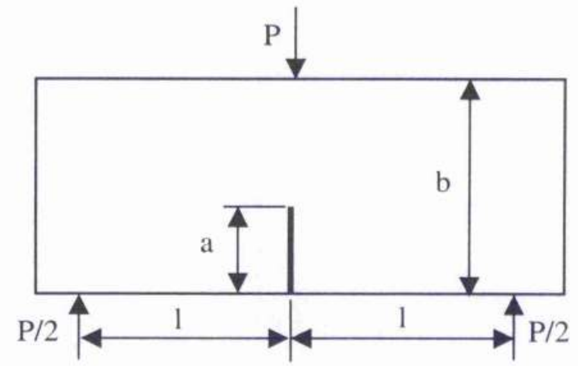

Figure 3.8: Edge cracked bar in three point bending.

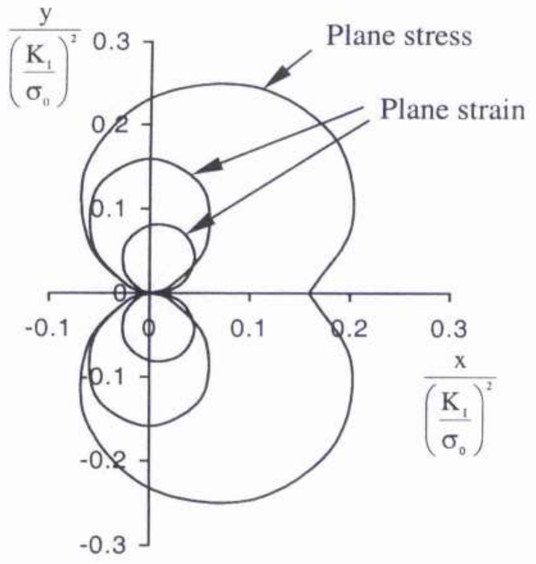

Figure 3.9: Plastic zone shapes estimated from Tresca yield criterion.

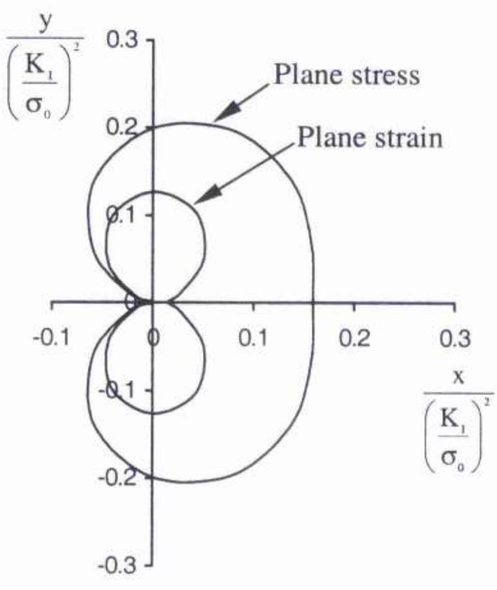

Figure 3.10: Plastic zone shapes estimated from von Mises yield criterion.

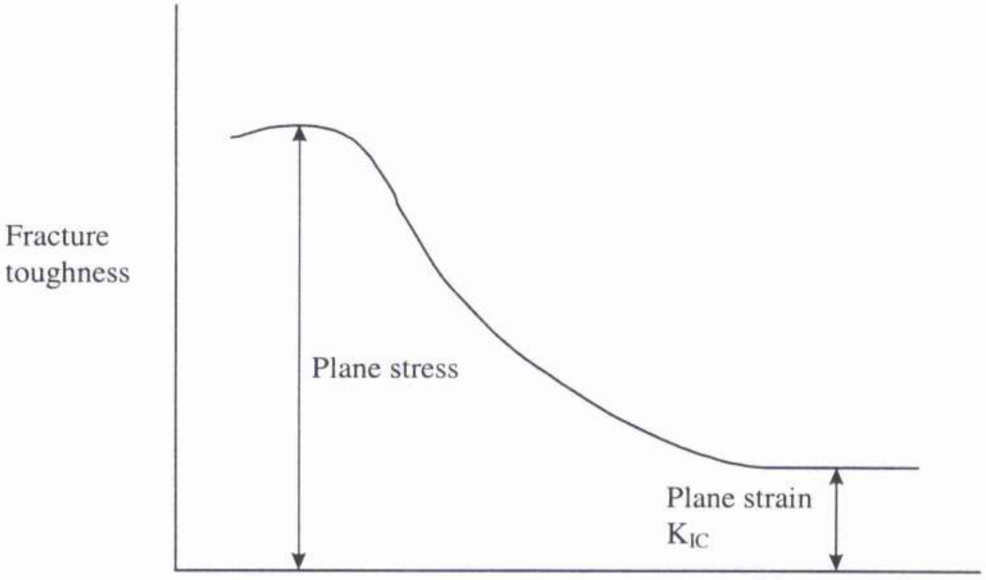

Figure 3.11: Effect of thickness on the fracture toughness.

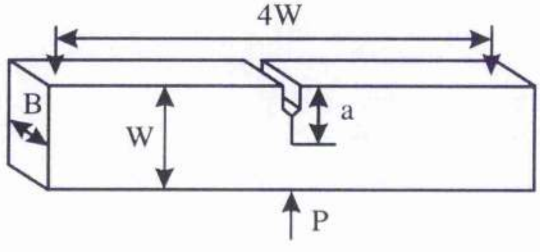

a) SENB specimen

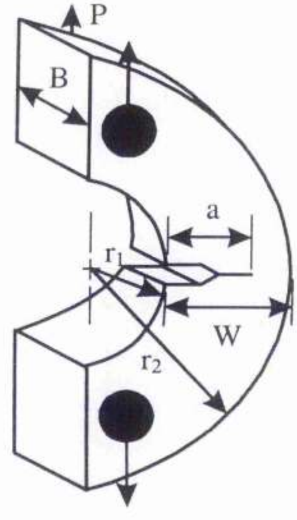

b) Arc shaped specimen

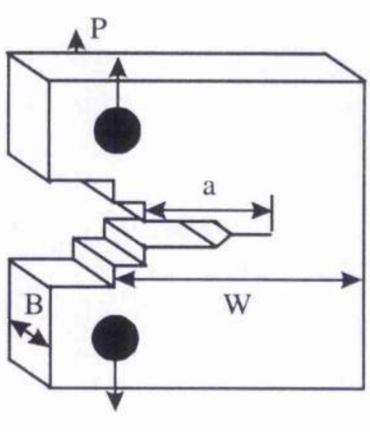

c) Compact specimen

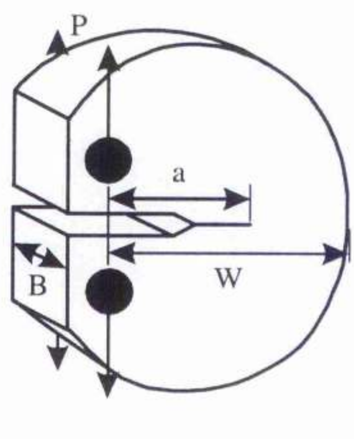

d) Disk shaped specimen

Figure 3.12: Four types of specimens for K_{IC} test.

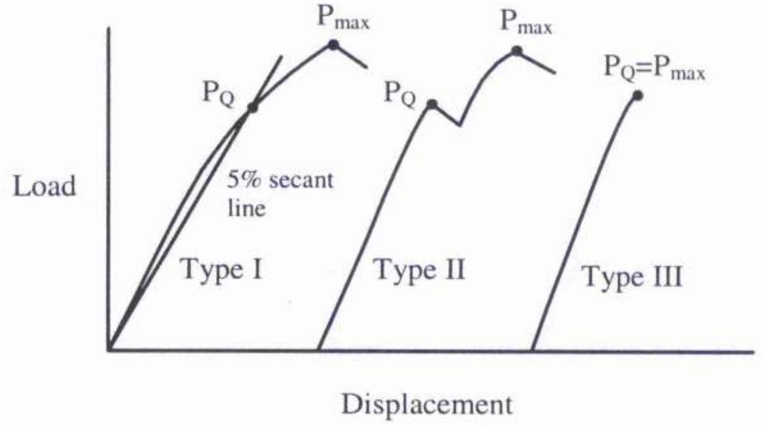

Figure 3.13: Three types of load-displacement curves in K_{IC} test.

Chapter 4 Slip line fields

4.1 Plane strain slip line fields

Two dimensional elastic perfectly-plastic plane strain problems can be expressed in terms of slip line fields (Hill, 1950). This allows material deformation to be regarded as a planar shear process in which blocks of material slide over one another at constant volume.

For plane strain in the out-of-plane direction, x_3, σ_{33} is a principal stress which can be written for incompressible flow as:

$$\sigma_{33} = \sigma_3 = \sigma_m = \frac{1}{2}(\sigma_{11} + \sigma_{22}) \tag{4.1}$$

where, σ_m is mean stress. From the yield criterion the principal stresses can be written as:

$$\sigma_1 = \sigma_m + k$$

$$\sigma_2 = \sigma_m - k$$

$$\sigma_3 = \sigma_m \tag{4.2}$$

where, k is the yield stress in shear. The yield stress in shear, k can be expressed in terms of the yield stress in tension, σ_0. $k = \frac{\sigma_0}{\sqrt{3}}$ using the von Mises yield criterion and $k = \frac{\sigma_0}{2}$ using the Tresca criterion.

The direction of the maximum shear stress bisects the principal directions. The orthogonal lines of maximum shear stresses are slip lines and designated as α and β. The α, β lines represent a new system of curvilinear co-ordinate axes, in which an α line makes an angle of 45^0 clockwise from the maximum principal direction and a β line is oriented 45^0 anticlockwise from the same principal direction. Thus the maximum principal stress lies in first and third quadrants of the α-β co-ordinate system as shown in Figure 4.1. As the stress system changes the α and β axes rotate and consequently the α, β axes can be curved but they are always orientated at $\pm 45^0$ from the principal directions.

The equilibrium equations referred to the α, β lines are known as the Hencky equations (Hencky, 1923):

$$\sigma_m = 2k\theta + C_\alpha \quad \text{on an } \alpha \text{ line} \tag{4.3}$$

$$\sigma_m = -2k\theta + C_\beta \quad \text{on a } \beta \text{ line} \tag{4.4}$$

$$\Delta\sigma_m = 2k\Delta\theta \quad \text{on } \alpha \text{ line} \tag{4.5}$$

$$\Delta\sigma_m = -2k\Delta\theta \quad \text{on } \beta \text{ line} \tag{4.6}$$

where C_α and C_β are constants on given α, β lines. The Hencky equations represent the equilibrium equations for a material deforming plastically, and allow the change in mean stress, σ_m, from a point where the stresses are known to a new point to be determined from the rotation of the slip lines ($\Delta\theta$).

Without loss of generality, the asymptotic crack tip stress field can be divided into elastic and plastic sectors. The angular span over which yield criterion is not satisfied defines the elastic sector. The von Mises yield criterion can be written in cylindrical co-ordinate system (r,θ) as:

$$(\sigma_{\theta\theta} - \sigma_{rr})^2 + 4\sigma_{r\theta}^2 = 4k^2 \qquad (4.7)$$

Rice (1974) has shown that for an incompressible material ($\nu = 1/2$) undergoing plastic deformation, the assumption that the crack tip stresses are finite plus the plane strain condition allows the asymptotic equilibrium equations to be written as:

$$\frac{\partial\sigma_m}{\partial\theta}\cdot\frac{\partial\sigma_{r\theta}}{\partial\theta} = 0 \qquad (4.8)$$

where, σ_m and $\sigma_{r\theta}$ are mean and shear stresses. Equation 4.8 has two simple solutions:

$$\frac{\partial\sigma_m}{\partial\theta} = 0,\ \ \frac{\partial\sigma_{r\theta}}{\partial\theta} \neq 0 \qquad (4.9)$$

and

$$\frac{\partial\sigma_{r\theta}}{\partial\theta} = 0,\ \ \frac{\partial\sigma_m}{\partial\theta} \neq 0 \qquad (4.10)$$

The first solution given by Equation 4.9 is a plastic sector in which mean stress, σ_m, does not vary with angle, and is known as a constant stress sector. A constant stress sector is represented by a slip line field with straight α and β lines as shown in Figure 4.2. The stresses can be written as:

$$\sigma_m = \sigma_{33} = \frac{1}{2}(\sigma_{11} + \sigma_{22}) = \frac{1}{2}(\sigma_{rr} + \sigma_{\theta\theta}) = \text{constant} \qquad (4.11)$$

The second solution given by Equation 4.10 corresponds to a centred fan in which the shear stress, $\sigma_{r\theta}$, equals the yield stress in shear, k, and the mean stress, σ_m, varies linearly with the angle. This type of slip line field is represented by a set of straight radial lines focussed at the crack tip and a set of concentric arcs as illustrated in Figure 4.2. The stresses within the centred fan can be given as:

$$\sigma_{rr} = \sigma_{\theta\theta} = \sigma_{33} = \sigma_m$$

$$\sigma_{r\theta} = \pm\ k \qquad (4.12)$$

4.1.1 Plane strain mode I crack tip fields

As an example of slip line field analysis it is appropriate to consider the Prandtl slip line field (Prandtl, 1920) illustrated in Figure 4.3. The Prandtl field is developed on the assumption that the plasticity fully surrounds the crack tip. The stresses for this field can be solved starting from the traction free crack surface, where the stresses are known. The Cartesian stresses at the crack surface of region I can be given as:

$$\sigma_{11} = 2k$$

$$\sigma_{22} = 0$$

$$\sigma_{12} = 0$$

$$\sigma_{33} = \sigma_m = k \qquad (4.13)$$

where, k is the yield stress in shear. The Hencky equilibrium equations indicate that the Cartesian stresses are constant throughout the region I, as the slip lines in this region are straight and thus region I is called a constant stress sector. In a cylindrical co-ordinate system (r,θ), the stresses in the region I can be given as:

$$\sigma_{rr} = k\,(1 + \cos 2\theta)$$

$$\sigma_{\theta\theta} = k\,(1 - \cos 2\theta)$$

$$\sigma_{zz} = \sigma_m = k$$

$$\sigma_{r\theta} = k \sin 2\theta \qquad (4.14)$$

where, $\pi \geq \theta \geq 3\pi/4$. The constant stress sector I is followed by a centred fan, denoted by II. The stresses in this region can be derived from Hencky equations following a β (negative) line:

$$\sigma_{rr} = \sigma_{\theta\theta} = \sigma_{zz} = \sigma_m = k\,(1 + 3\pi/2 - 2\theta)$$

$$\sigma_{r\theta} = k \qquad (4.15)$$

where, $3\pi/4 \geq \theta \geq \pi/4$. The centred fan is leading to a diamond shaped constant stress sector denoted by III. Following the same slip line (negative β), the stresses in this region can be given as:

$$\sigma_{rr} = k\,(\pi + 1 - \cos 2\theta)$$

$$\sigma_{\theta\theta} = k\,(\pi + 1 + \cos 2\theta)$$

$$\sigma_{zz} = \sigma_m = k\,(1 + \pi)$$

$$\sigma_{r\theta} = k \sin 2\theta \qquad (4.16)$$

where, $\pi/4 \geq \theta \geq -\pi/4$. In Prandtl field the maximum hoop stress, $\sigma_{\theta\theta}$, occurs directly ahead of the crack ($\theta = 0$):

$$\sigma_{rr} = k\,\pi$$

$$\sigma_{\theta\theta} = k\,(\pi + 2)$$

$$\sigma_{zz} = \sigma_m = k\,(1 + \pi)$$

$$\sigma_{r\theta} = 0 \tag{4.17}$$

The hoop stress $(2+\pi)\sigma_0/\sqrt{3}$ is the greatest possible stress in an elastic perfectly-plastic material in mode I. However, Du and Hancock (1991) have shown that this stress, and the Prandtl field from which it is derived, only occurs when $T \geq +0.446\ \sigma_0$. Here T is the second term in the Williams (1957) expansion of the asymptotic elastic field

$$\sigma_{ij} = A_{ij}(\theta)r^{-1/2} + B_{ij}(\theta)r^{0} + C_{ij}(\theta)r^{1/2} + \cdots \tag{4.18}$$

Focusing on the terms that are non-zero at the tip, the far elastic field can be written as:

$$\sigma_{ij} = \frac{K}{\sqrt{2\pi r}} f_{ij}(\theta) + \begin{bmatrix} T & 0 \\ 0 & 0 \end{bmatrix} \qquad (i, j = 1, 2) \tag{4.19}$$

T corresponds to a uni-axial tensile or compressive stress parallel to the crack flanks. If T is zero or negative Du and Hancock (1991) have shown that within the plastic zone elastic wedges appear on the crack flanks as shown in Figure 4.4. As T/σ_0 becomes more negative (compressive) the stress ahead of crack decreases due to a decrease in the hydrostatic or mean stress, which O'Dowd and Shih (1991) have called Q. In this case the stresses directly ahead of the crack ($\theta = 0$) are written as:

$$\sigma_{rr} = k\,\pi + Q$$

$$\sigma_{\theta\theta} = k\,(\pi + 2) + Q$$

$$\sigma_{zz} = \sigma_m = k\,(1 + \pi) + Q$$

$$\sigma_{r\theta} = 0 \tag{4.20}$$

The stress field for incomplete crack tip plasticity (Du & Hancock 1991, Li & Hancock 1999) can be determined by assembling plastic and elastic sectors. The stresses within an elastic sector are given by a solution of Timoshenko & Goodier (1970) for a semi-infinite wedge loaded by constant surface tractions:

$$\sigma_{rr} = E_1 \sin 2\theta + E_2 \cos 2\theta + \tfrac{1}{2}(E_3\theta + E_4)$$

$$\sigma_{\theta\theta} = -E_1 \sin 2\theta - E_2 \cos 2\theta + \tfrac{1}{2}(E_3\theta + E_4)$$

$$\sigma_{r\theta} = E_1 \cos 2\theta - E_2 \sin 2\theta - E_3/4$$

$$\sigma_{zz} = \tfrac{1}{2}(E_3\theta + E_4) \tag{4.21}$$

The constants E_1, E_2, E_3 and E_4 are determined by the boundary conditions. Using this solution the elastic-plastic crack tip field has been discussed by Li & Hancock (1999). The asymptotic crack tip field is developed by assembling centred fan, constant stress and elastic sectors subject to conditions of equilibrium at the sector boundary. A particularly important condition applies to an elastic wedge located on the crack flanks:

$$\sigma_{\theta\theta} = \sigma_{r\theta} = 0,\ \theta = \pm\ \pi \tag{4.22}$$

Consider an elastic wedge AOB on the upper crack flank in cylindrical co-ordinate system (r,θ) centred at the crack tip as illustrated in Figure 4.5. The angular span of the elastic wedge is denoted by φ. γ is measured from the upper crack flank ($\theta = \pi$), such that $\theta = \pi - \gamma$. H and K denote the hoop and shear stresses on the elastic-plastic boundary OB. Following Timoshenko & Goodier (1970) the stresses within the elastic wedge can be given as:

$$\sigma_{rr} = -2P(\cos 2\gamma + 1) - 2Q(2\gamma + \sin 2\gamma)$$

$$\sigma_{\theta\theta} = 2P(\cos 2\gamma - 1) + 2Q(\sin 2\gamma - 2\gamma)$$

$$\sigma_{r\theta} = 2P\sin 2\gamma - 2Q(\cos 2\gamma - 1) \tag{4.23}$$

where, P and Q are constants. At $\gamma = \varphi$, $\sigma_{\theta\theta} = H$ and $\sigma_{r\theta} = K$. Substituting in Equations 4.23, gives constants P and Q as:

$$P = \frac{H(\cos 2\varphi - 1) + K(\sin 2\varphi - 2\varphi)}{4(1 - \cos 2\varphi - \varphi\sin 2\varphi)}$$

$$Q = \frac{H\sin 2\varphi - K(\cos 2\varphi - 1)}{4(1 - \cos 2\varphi - \varphi\sin 2\varphi)} \tag{4.24}$$

The stresses within the plastic sectors can also be solved using the boundary conditions on the elastic-plastic boundary OB. If the elastic sector is followed by a centred fan, the shear stress on the boundary, K, equals the yield stress in shear, k. Using Hencky equilibrium equations the stress field within the fan can be given as:

$$\sigma_{rr} = \sigma_{\theta\theta} = \sigma_{zz} = \sigma_m = 2k(\pi - \varphi - \theta) - H$$

$$\sigma_{r\theta} = k \tag{4.25}$$

For a constant stress sector adjoining the centred fan, the stress field can be given as:

$$\sigma_{rr} = k(-\cos 2\theta - 2\varphi + \frac{3\pi}{2}) - H$$

$$\sigma_{\theta\theta} = k(\cos 2\theta - 2\varphi + \frac{3\pi}{2}) - H$$

$$\sigma_{r\theta} = k\sin 2\theta$$

$$\sigma_{zz} = \sigma_{m} = k(\frac{3\pi}{2} - 2\varphi) - H \qquad (4.26)$$

where, $\pi/4 \leq \varphi \leq 3\pi/4$. Following Du and Hancock (1991), the elastic sector on the crack flank is followed by a centred fan which leads to a constant stress sector directly ahead of crack. At any sector boundary involving a fan, $\sigma_{r\theta} = k$, and $\sigma_{rr} = \sigma_{\theta\theta} = \sigma_{zz} = \sigma_{m}$. Therefore, at the boundary between elastic sector and fan, $\sigma_{r\theta} = K = k$, and $\sigma_{rr} = \sigma_{\theta\theta}$. Applying these boundary conditions to Equations 4.23 to solve for constants P and Q, and then by Equations 4.24, H and K can be given as:

$$H = \frac{2\varphi k\cos 2\varphi - k\sin 2\varphi}{1 - \cos 2\varphi}$$

$$K = k \qquad (4.27)$$

Then, for an specific value of φ the stresses in the different sectors can be solved and the sectors are assembled accordingly.

4.1.2 Plane strain mixed mode crack tip fields

Slip line fields for mixed mode (I/II) loading have been discussed by Shih (1974). The mixed mode (I/II) slip line field illustrated in Figure 4.6, shows a statically admissible field in which plasticity fully surrounds the crack tip and assuming full continuity of stresses through out the slip line field. The sector boundary *of* makes an angle, α with the upper crack flank ($\theta = \pi$) such that, $\theta_{of} = \pi - \alpha$. The angular position of sector boundary *oe*, $\theta_{oe} = (3\pi/4 + \gamma)$, and δ is the rotation of the constant stress diamond *cod* from the symmetry axis due to applied mode II loading, where α, γ and δ are related by: $\gamma = -\pi/4 - \alpha$, $\delta = -1/2 - \alpha$, and $\pi/4 \leq \alpha \leq 3\pi/8 - ¼$. The cylindrical stresses in the constant stress sector *aob* adjacent to the lower crack flank can be given as:

$$\sigma_{rr} = k\ (1 + \cos 2\theta)$$

$$\sigma_{\theta\theta} = k\ (1 - \cos 2\theta)$$

$$\sigma_{r\theta} = -\ k\ \sin 2\theta \qquad (4.28)$$

Using the Hencky equilibrium equations (Hencky, 1923) the stresses for the sectors can be solved consecutively. In the centred fan *boc* the stresses are:

$$\sigma_{rr} = \sigma_{\theta\theta} = k\ (1 + 3\pi/2 + 2\theta)$$

$$\sigma_{r\theta} = -\ k \qquad (4.29)$$

The stresses in the constant stress diamond *cod* can be given as:

$$\sigma_{rr} = k\ [(1 + \pi + 2\delta) - \sin(\pi/2 + 2\delta - 2\theta)]$$

$$\sigma_{\theta\theta} = k\ [(1 + \pi + 2\delta) + \sin(\pi/2 + 2\delta - 2\theta)]$$

$$\sigma_{r\theta} = k \cos(\pi/2 + 2\delta - 2\theta) \qquad (4.30)$$

In the centred fan *doe* the stresses are:

$$\sigma_{rr} = \sigma_{\theta\theta} = k\ (1 + 3\pi/2 + 2\theta - 4\delta)$$

$$\sigma_{r\theta} = k \qquad (4.31)$$

The stresses in the constant stress sector *eof* can be written as:

$$\sigma_{rr} = k\ [(1 + 4\delta - 2\gamma) + \cos(2\gamma - 2\theta)]$$

$$\sigma_{\theta\theta} = k\ [(1 + 4\delta - 2\gamma) - \cos(2\gamma - 2\theta)]$$

$$\sigma_{r\theta} = k \sin(2\gamma - 2\theta) \qquad (4.32)$$

In the centred fan *fog* the stresses can be given as:

$$\sigma_{rr} = \sigma_{\theta\theta} = -\ k\ (1 + 3\pi/2 + 2\theta)$$

$$\sigma_{r\theta} = -\ k \qquad (4.33)$$

Finally, the stresses in the constant stress triangle *goh* adjacent to the upper crack flank can be given as:

$$\sigma_{rr} = -\ k\ (1 + \cos 2\theta)$$

$$\sigma_{\theta\theta} = -\ k\ (1 - \cos 2\theta)$$

$$\sigma_{r\theta} = k \sin 2\theta \qquad (4.34)$$

Li and Hancock (1999) have discussed mixed mode (I/II) slip line fields in which plasticity does not fully surround the crack tip, and an elastic wedge appears on the upper crack flank. Following Shih (1974) the ratio of tension to shear can be expressed in terms of a mixity. The ratio of tension to shear in the remote elastic field is defined as elastic or far field mixity, which can be given as:

$$M_{el} = \frac{2}{\pi}\tan^{-1}\left(\frac{K_I}{K_{II}}\right) = \frac{2}{\pi}\tan^{-1}\left\{\lim_{r\to\infty}\frac{\sigma_{\theta\theta}(r,\theta=0)}{\sigma_{r\theta}(r,\theta=0)}\right\} \qquad (4.35)$$

The ratio of tension to shear directly ahead of crack is defined as plastic or near field mixity where plasticity occurs at the crack tip:

$$M_p = \frac{2}{\pi}\tan^{-1}\left\{\lim_{r\to 0}\frac{\sigma_{\theta\theta}(r,\theta=0)}{\sigma_{r\theta}(r,\theta=0)}\right\} \qquad (4.36)$$

Two mixed mode slip line fields (Li & Hancock, 1999) of different mixities are illustrated in Figure 4.7. In type I field, the plastic part below the symmetry axis consists of a constant stress sector, a fan, and a part of a constant stress sector. Type II field occurs for a relatively lower value of mixity, where the same part (below the symmetry axis) consists of two constant stress sectors, a fan, and a portion of a fan. In the both cases, φ is the angular span of the elastic wedge at the upper crack flank, α is the angular span of the centred fan *boc* in the fully plastic side, and δ is the angle which the sector boundary *od* makes with the symmetry axis. Then for type I field the plastic mixity can be given as:

$$M_p = \frac{2}{\pi}\tan^{-1}\left\{\frac{\cos 2\alpha - 1 - 2\alpha}{-\sin 2\alpha}\right\} \tag{4.37}$$

$$M_p = \frac{2}{\pi}\tan^{-1}\left\{\frac{[\sin 2\delta + 2(\pi-\delta)](1-\cos 2\varphi) - 2\varphi + \sin 2\varphi}{\cos 2\delta(1-\cos 2\varphi)}\right\} \tag{4.38}$$

where, $\alpha \geq \pi/4$ and $\alpha - \delta = \pi/4$. For type II field the mixity can be written as:

$$M_p = -\frac{2}{\pi}\tan^{-1}\left\{\frac{\pi}{2} - 4\alpha - 1\right\} \tag{4.39}$$

$$M_p = \frac{2}{\pi}\tan^{-1}\left\{2\pi - \frac{2\varphi - \sin 2\varphi}{1-\cos 2\varphi}\right\} \tag{4.40}$$

where, $\alpha \leq \pi/4$, and $\alpha + \delta = \pi/4$. The stresses for the fields can be solved by using the equilibrium equations for the plastic sectors and the wedge solution for the elastic sector, and the sectors can be assembled accordingly if the plastic mixities are known.

The mixed mode I/II fields discussed by Li and Hancock (1999), shown in Figure 4.7, consist of five sectors. Starting from the lower crack flank, the sectors can be given as: constant stress sector, fan, constant stress sector, fan and finally elastic sector on the upper crack flank. Zhu and Chao (2001) have presented six sector fields for mixed mode I/II loading as the modification of five sector solution, where a constant stress sector has been included between the fan and the elastic sector on the upper crack flank. A six sector crack tip field is shown schematically in Figure 4.8, where the sector angles are defined as θ_1, θ_2, θ_3, θ_4 and θ_5. In Figure 4.8, $\theta_1 = -3\pi/4$ and $\theta_2 = \theta_3 - \pi/2$. Three unknown angles θ_3, θ_4 and θ_5 can be determined by solving the equations:

$$\frac{T_\pi}{k} = -\frac{\cos(\theta_5 - 2\theta_4)}{\sin\theta_5} - 1$$

$$4\left(\theta_3 - \frac{\pi}{4}\right) = \left(2\theta_4 - \frac{3\pi}{2} - 1\right) - (\pi - \theta_5)\frac{\cos 2\theta_4}{\sin^2\theta_5} - \frac{\cos(\theta_5 - 2\theta_4)}{\sin\theta_5}$$

$$\frac{T_p}{k} = \left(2\theta_3 - 1 - \frac{\pi}{2}\right) + \sin 2\theta_3 \qquad \sigma_{r\theta}(\theta = 0) < k$$

$$\frac{T_p}{k} = 4\theta_3 - \pi \qquad \sigma_{r\theta}(\theta = 0) = k \tag{4.41}$$

where, the parameters T_π and T_p can be given as:

$$2T_\pi = \sigma_{rr}(\theta = \pi) - \sigma^p_{rr}(\theta = \pi)$$

$$T_p = \sigma_{\theta\theta}(\theta = 0) - \sigma^p_{\theta\theta}(\theta = 0) \qquad \sigma_{r\theta}(\theta = 0) < k$$

$$T_p = \sigma_{\theta\theta}(\theta = 0) - k\left(1 + \frac{3\pi}{2}\right) \qquad \sigma_{r\theta}(\theta = 0) = k \tag{4.42}$$

where, $\sigma^p_{rr}(\theta = \pi)$ and $\sigma^p_{\theta\theta}(\theta = 0)$ are the stress components in the Prandtl field and $\sigma_{rr}(\theta = \pi)$ and $\sigma_{\theta\theta}(\theta = 0)$ are the stress components given by the mixed mode I/II finite element result. Following Zhu and Chao (2001), the stresses for the six sectors can be given as:

Constant stress sector AOB:

$$\sigma_{rr} = k(1 + \cos 2\theta)$$

$$\sigma_{\theta\theta} = k(1 - \cos 2\theta)$$

$$\sigma_{r\theta} = -k \sin 2\theta \tag{4.43}$$

Fan sector BOC:

$$\sigma_{rr} = \sigma_{\theta\theta} = k(1 + 3\pi/2 + 2\theta)$$

$$\sigma_{r\theta} = -k \tag{4.44}$$

Constant stress sector COD:

$$\sigma_{rr} = k(1 + \pi/2 + 2\theta_3) + k \sin 2(\theta - \theta_3)$$

$$\sigma_{\theta\theta} = k(1 + \pi/2 + 2\theta_3) - k \sin 2(\theta - \theta_3)$$

$$\sigma_{r\theta} = k \cos 2(\theta - \theta_3) \tag{4.45}$$

Fan sector DOE:

$$\sigma_{rr} = \sigma_{\theta\theta} = k(1 + \pi/2 + 4\theta_3 - 2\theta)$$

$$\sigma_{r\theta} = k \tag{4.46}$$

Constant stress sector EOF:

$$\sigma_{rr} = k(1 + \pi/2 + 4\theta_3 - 2\theta_4) + k \sin 2(\theta - \theta_4)$$

$$\sigma_{\theta\theta} = k(1 + \pi/2 + 4\theta_3 - 2\theta_4) - k \sin 2(\theta - \theta_4)$$

$$\sigma_{r\theta} = k \cos 2(\theta - \theta_4) \tag{4.47}$$

Elastic sector FOG:

$$\sigma_{rr} = -k \frac{\cos(\theta_5 - 2\theta_4)}{\sin\theta_5}(1 + \cos 2\theta) - k \frac{\cos 2\theta_4}{1 - \cos 2\theta_5}\{2(\pi - \theta) - \sin 2\theta\}$$

$$\sigma_{\theta\theta} = -k \frac{\cos(\theta_5 - 2\theta_4)}{\sin\theta_5}(1 - \cos 2\theta) - k \frac{\cos 2\theta_4}{1 - \cos 2\theta_5}\{2(\pi - \theta) + \sin 2\theta\}$$

$$\sigma_{r\theta} = k \frac{\cos(\theta_5 - 2\theta_4)}{\sin\theta_5}\sin 2\theta - k \frac{\cos 2\theta_4}{1 - \cos 2\theta_5}(1 - \cos 2\theta) \tag{4.48}$$

For the this solution, Zhu and Chao (2001) have defined the plastic mixity, M_p, which can be related to the sector angle θ_3 as:

$$M_p = \frac{2}{\pi}\tan^{-1}\left\{\frac{1 + \pi/2 + 2\theta_3 + \sin 2\theta_3}{\cos 2\theta_3}\right\} \qquad 0 \le \theta_3 \le \pi/4$$

$$M_p = \frac{2}{\pi}\tan^{-1}\left\{1 + \frac{\pi}{2} + 4\theta_3\right\} \qquad -1/2 \le \theta_3 \le 0 \tag{4.49}$$

4.2 Plane stress slip line fields

Plane stress crack tip fields for elastic-perfectly plastic materials can be represented in terms of slip line fields using theory introduced by Hill (1950). The slip lines are the characteristics of the equilibrium equations. Depending upon the combination of the principal stresses satisfying the plane stress yield criterion, the equilibrium equations can be hyperbolic, parabolic, or elliptic. The resulting slip lines may be real and distinct, real and coincident, or imaginary depending on the nature of the equilibrium equations. For the hyperbolic equilibrium equations, the slip lines are non-orthogonal, but make equal angles with one or other of the two principal directions. Thus the principal directions bisect the angles between two slip lines as illustrated in Figure 4.9. The two non-orthogonal families of slip lines are inclined at $\pm(\pi/4 + \lambda/2)$ to the maximum principal direction, where, $\sin\lambda = (\sigma_1 + \sigma_2) / 3(\sigma_1 - \sigma_2)$ and $\sigma_1 > \sigma_2$.

Under parabolic conditions, the angle between the two sets of lines becomes zero, leaving a single set of coincident slip lines (Hill 1952, Hodge 1951) corresponding to the numerically smaller principal direction.

To discuss crack tip plasticity in plane stress, consider a cylindrical co-ordinate system (r,θ) centred at the crack tip such that the crack lies along $\theta = \pm\pi$. The von Mises yield criterion in plane stress can be given as:

$$\sigma_e^2 = \sigma_{rr}^2 + \sigma_{\theta\theta}^2 - \sigma_{rr}\sigma_{\theta\theta} + 3\sigma_{r\theta}^2 = \sigma_0^2 \qquad (4.50)$$

Rice (1982) has shown that for an incompressible material undergoing plastic deformation, the assumption that the crack tip stresses are finite plus the plane stress condition allows the asymptotic equilibrium equation to be written as:

$$\frac{\partial(\sigma_{11} + \sigma_{22})}{\partial\theta} s_{rr} = 0 \qquad (4.51)$$

where, σ_{11} and σ_{22} are the Cartesian stresses and s_{rr} is the radial stress deviator in the cylindrical co-ordinate system. Equation 4.51 has two simple solutions:

$$\frac{\partial(\sigma_{11} + \sigma_{22})}{\partial\theta} = 0,\ s_{rr} \neq 0 \qquad (4.52)$$

or,

$$s_{rr} = 0,\ \frac{\partial(\sigma_{11} + \sigma_{22})}{\partial\theta} \neq 0 \qquad (4.53)$$

One solution given by Equation 4.52 corresponds to a constant stress sector in which the Cartesian stresses σ_{11}, σ_{22} and σ_{12} do not vary with the angle, and consequently the mean stress, σ_m, is constant throughout the sector. This sector consists of two non-orthogonal families of straight slip lines.

The second solution given by Equation 4.53 corresponds to a curved fan sector in which the radial stress deviator, $s_{rr} = 0$. The cylindrical stresses for this sector can be given as:

$$\sigma_{\theta\theta} = 2\sigma_{rr} = \pm 2k\cos(\theta - \phi)$$

$$\sigma_{r\theta} = \pm k\sin(\theta - \phi) \qquad (4.54)$$

where, k is the yield stress in shear and ϕ is the angle at which the curved lines are asymptotic. The curved fan sector consists of a set of radial straight lines and a set of curves with the equation of the form:

$$r^2\sin(\theta - \phi) = \text{constant} \qquad (4.55)$$

At $\theta = \phi$ the equilibrium equations become parabolic and give use to a single set of slip lines.

4.2.1 Plane stress mode I crack tip fields

A possible plane stress mode I slip line field has been discussed by Hutchinson (1968) on the assumption that the plasticity surrounds the crack tip at all angles. In this case the equilibrium equations require a discontinuity in radial stress such that the traction free conditions occur on the crack flanks ($\theta = \pm\,\pi$) and the yield condition is satisfied at all angles. The allowable discontinuity in radial stress, $(\sigma_{rr}^{+} - \sigma_{rr}^{-})$ across the sector boundary can be given by applying the yield criterion:

$$\sigma_{rr}^{+} - \sigma_{rr}^{-} = (4 - 3\sigma_{\theta\theta}^{2} - 12\sigma_{r\theta}^{2})^{\frac{1}{2}} \tag{4.56}$$

The Hutchinson plane stress mode I field is shown in Figure 4.10. The cylindrical stresses within the constant stress sector AOB can be given as:

$$\sigma_{rr} = -\,\frac{\sqrt{3}}{2}\,k\,(1 + \cos 2\theta)$$

$$\sigma_{\theta\theta} = -\,\frac{\sqrt{3}}{2}\,k\,(1 - \cos 2\theta)$$

$$\sigma_{r\theta} = \frac{\sqrt{3}}{2}\,k\,\sin 2\theta \tag{4.57}$$

OB is the radial line of discontinuity which makes an angle, $\theta_{OB} = 151.4^{0}$ with the crack plane. The stresses within the constant stress sector BOC can be written as:

$$\sigma_{rr} = \frac{\sqrt{3}}{4}\,k\,(-\,1 + 3\cos 2\theta_{OB}) + \frac{\sqrt{3}}{4}\,k\,(1 + \cos 2\theta_{OB})\cos 2(\theta - \theta_{OB}) + \frac{\sqrt{3}}{2}\,k\,\sin 2\theta_{OB}\,\sin 2(\theta - \theta_{OB})$$

$$\sigma_{\theta\theta} = -\,\sigma_{rr} + \frac{\sqrt{3}}{2}\,k\,(-\,1 + 3\cos 2\theta_{OB})$$

$$\sigma_{r\theta} = -\,\frac{\sqrt{3}}{4}\,k\,(1 + \cos 2\theta_{OB})\sin 2(\theta - \theta_{OB}) + \frac{\sqrt{3}}{2}\,k\,\sin 2\theta_{OB}\cos 2(\theta - \theta_{OB}) \tag{4.58}$$

OC is the sector boundary between the constant stress sector BOC and curved fan sector COD, which makes an angle, $\theta_{OC} = 79.7^{0}$ with the crack plane. Finally following Hill (1952), the stresses within the curved fan sector COD can be given as:

$$\sigma_{rr} = k\cos\theta$$

$$\sigma_{\theta\theta} = 2k\cos\theta$$

$$\sigma_{r\theta} = k \sin\theta \tag{4.59}$$

Dong & Pan (1990) have discussed a modification of this plane stress mode I slip line field as shown in Figure 4.11, where plasticity surrounds the crack tip at all angles, but differs slightly from Hutchinson (1968) field. This field exhibits a very small constant stress sector directly ahead of the crack with a span of 5.22^0, although no major variation in stress fields is apparent. The spans of the sectors in this field are very close to that of the Hutchinson field.

Sham and Hancock (1999) have discussed plane stress mode I slip line field with incomplete crack tip plasticity where the problem of stress discontinuity has been avoided. This field consists of a curved fan sector ahead of the crack complemented by elastic sectors to the crack flanks as shown schematically in Figure 4.12. AOB is the elastic sector on the upper crack flank. The elastic-plastic boundary OB makes an angle θ_{OB} with the crack plane which is to be determined. Applying traction free boundary conditions on the upper crack flank to the solution of Timoshenko & Goodier (1970), the stresses in the elastic sector AOB can be given as:

$$\sigma_{rr} = A\left(2\theta - 2\pi + \sin 2\theta\right) + B\left(1 + \cos 2\theta\right)$$

$$\sigma_{\theta\theta} = A\left(2\theta - 2\pi - \sin 2\theta\right) + B\left(1 - \cos 2\theta\right)$$

$$\sigma_{r\theta} = A\left(\cos 2\theta - 1\right) - B\sin 2\theta \tag{4.60}$$

Following Hill (1952) the stresses within the curved fan sector BOC ahead of the crack can be given as:

$$\sigma_{rr} = k \cos\theta$$

$$\sigma_{\theta\theta} = 2k \cos\theta$$

$$\sigma_{r\theta} = k \sin\theta \tag{4.61}$$

Equilibrium equations require continuity of traction across any sector boundary. Continuity of all stresses across the sector boundary OB is assumed. Equating Equations 4.60 & 4.61 on the sector boundary OB gives a set of three equations:

$$A\left(2\theta - 2\pi + \sin 2\theta\right) + B\left(1 + \cos 2\theta\right) = k \cos \theta$$

$$A\left(2\theta - 2\pi - \sin 2\theta\right) + B\left(1 - \cos 2\theta\right) = 2k \cos \theta$$

$$A\left(\cos 2\theta - 1\right) - B\sin 2\theta = k \sin \theta \tag{4.62}$$

Solving Equations 4.62 for θ gives:

$$(\pi - \theta) \tan \theta - 2 = 0 \tag{4.63}$$

Substituting $\theta = \theta_{OB}$ in Equation 4.63 gives:

$$(\pi - \theta_{OB}) \tan \theta_{OB} - 2 = 0 \quad (4.64)$$

where, $\pi > \theta_{OB} > 0$. The value of θ_{OB} obtained from Equation 4.64 is 39.126^0. Applying mode I symmetry condition, the angle of elastic-plastic boundary OC with the crack plane, $\theta_{OC} = - \theta_{OB}$ $(- \pi < - \theta_{OB} < 0)$.

The cylindrical stresses within the elastic sector AOB and fan sector BOC have been given by Equations 4.60 & 4.61 respectively. The stresses within the elastic sector COD at the lower crack flank can be given as:

$$\sigma_{rr} = A(2\theta + 2\pi + \sin 2\theta) + B(1 + \cos 2\theta)$$

$$\sigma_{\theta\theta} = A(2\theta + 2\pi - \sin 2\theta) + B(1 - \cos 2\theta)$$

$$\sigma_{r\theta} = A(\cos 2\theta - 1) - B\sin 2\theta \quad (4.65)$$

The constants A and B can then be calculated from traction continuity across the sector boundary OC. Comparison of the analytic and computational solutions supports the form of field suggested by Sham and Hancock (1999).

4.2.2 Plane stress mixed mode crack tip fields

A statically admissible plane stress near mode I slip line field has been discussed by Shih (1973). This field consists of five constant stress sectors and two curved fan sectors with six sector boundaries as shown schematically in Figure 4.13. The field shows discontinuities in radial stress across the sector boundaries OB and OH. The angular positions of the six sector boundaries are defined as θ_1, θ_2, θ_3, θ_4, θ_5 and θ_6 and two asymptotic angles ϕ_1 and ϕ_2 associated with the curved fan sectors DOE and FOG respectively. In solving the field Shih obtained six equations from the traction free boundary conditions and traction continuity across the sector boundaries. The additional equation needed to solve the field satisfactorily was not found. Consequently, Shih varied the angles θ_1 and θ_6 corresponding to lines of discontinuity OB and OH respectively, keeping the angle BOH constant to obtain a family of statically admissible mixed mode fields. It was observed that with increasing mode II loading discontinuity across line OB decreases with decreasing θ_1 and finally vanishes at $\theta_1 = 125.26^0$, where discontinuity across line OH still remains at $\theta_6 = -177.22^0$ just below the lower crack flank as shown in Figure 4.14. With further increasing mode II loading, the discontinuity across OH vanishes and OH merges with lower crack flank in near mode II. At this stage a curved fan sector develops at 125.26^0 as shown by BOC in Figure 4.14. It can be noted that during the entire transition from mode I to mode II the crack line ahead of the crack lies within the curved fan sector.

Dong & Pan (1990) have discussed a modification of the plane stress mixed mode field discussed by Shih. In solving the problem Dong & Pan have derived the missing seventh equation in near mode I and near mode II. They have shown that during the very early stage of transition from mode I to mode II, the crack line ahead of crack lies within a constant stress sector which differs from the Shih field. They also found that in near mode II when discontinuity across OB (Figures 4.13, 4.14) vanishes at $\theta_1 = 125.26^0$, the discontinuity across OH exists at $\theta_6 = -175.16^0$, which also slightly differs from the Shih field. In this field the discontinuity across OH exists until a pure mode II field is achieved.

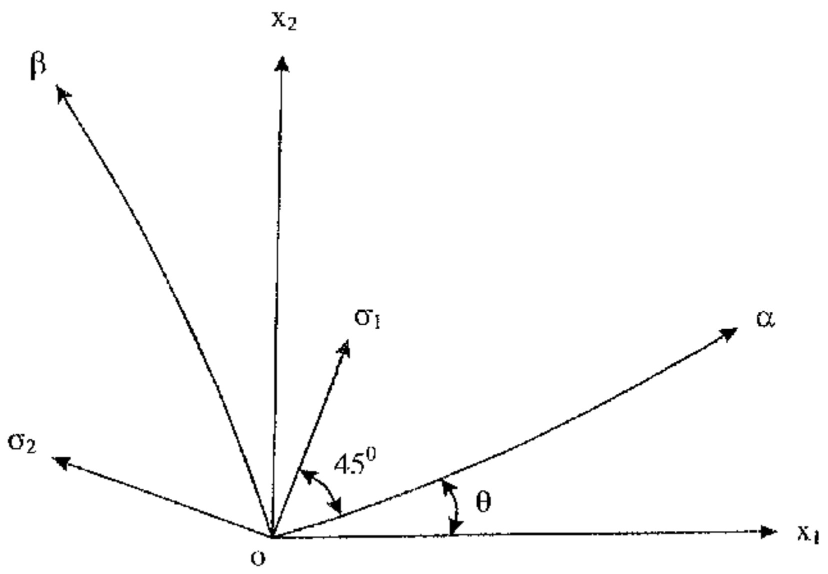

Figure 4.1: Orientation of α and β lines in the co-ordinate system.

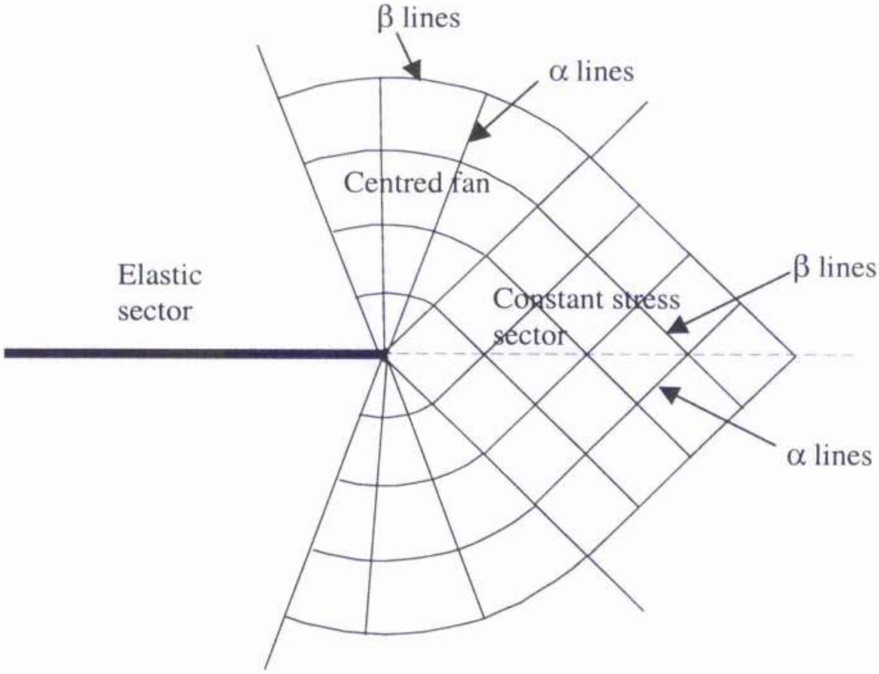

Figure 4.2: Slip line field indicating α and β lines in constant stress and centred fan sectors.

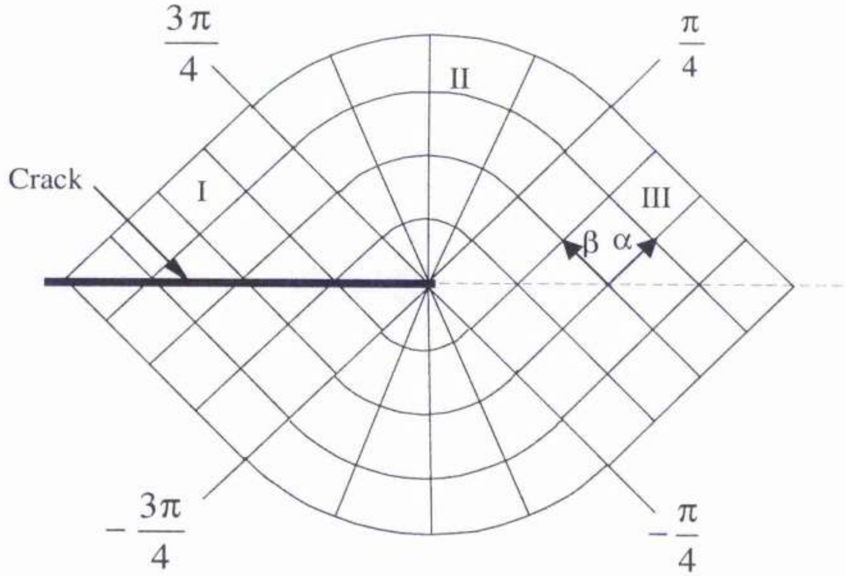

Figure 4.3: The Prandtl slip line field.

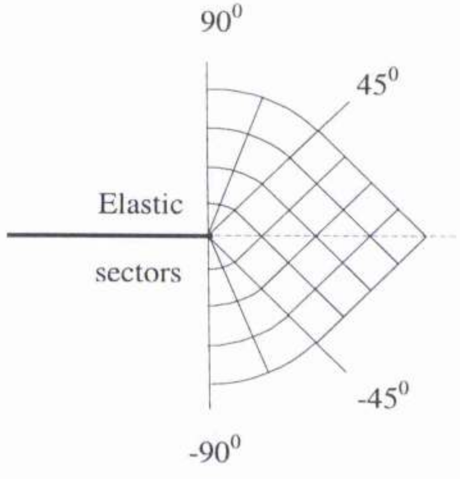

$T/\sigma_0 = -0.5$

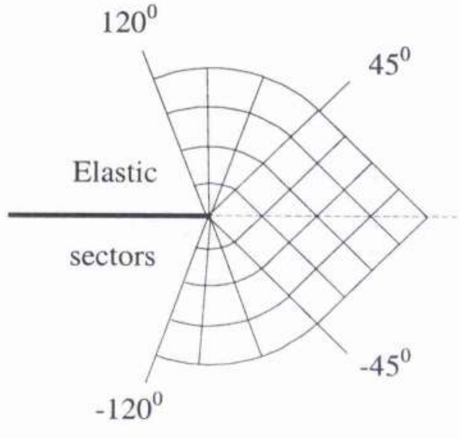

$T/\sigma_0 = 0$

Figure 4.4: Mode I slip line fields with elastic sectors on the crack flanks.

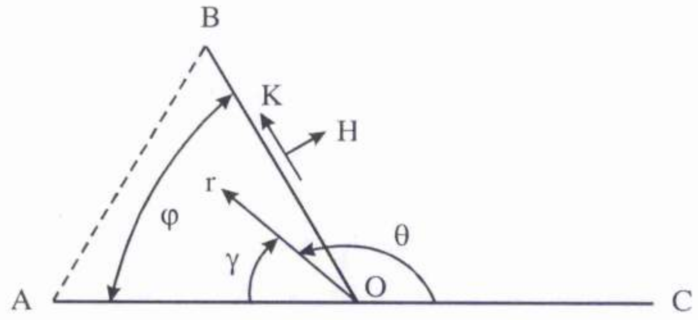

Figure 4.5: Elastic wedge on the crack flank.

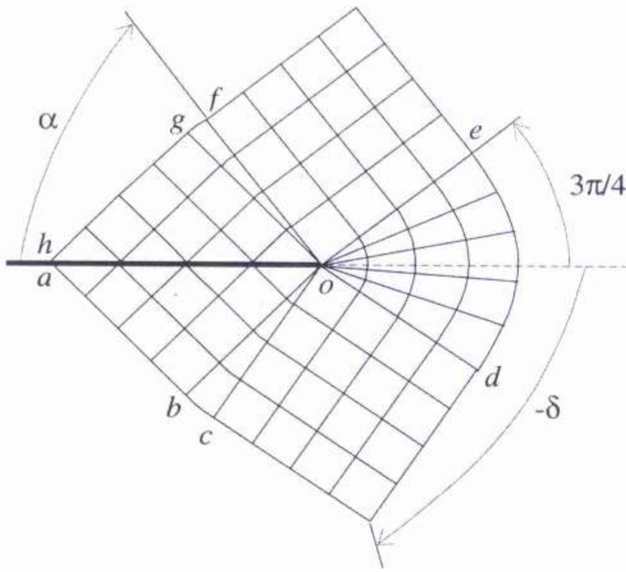

Figure 4.6: Mixed mode slip line field, plane strain.

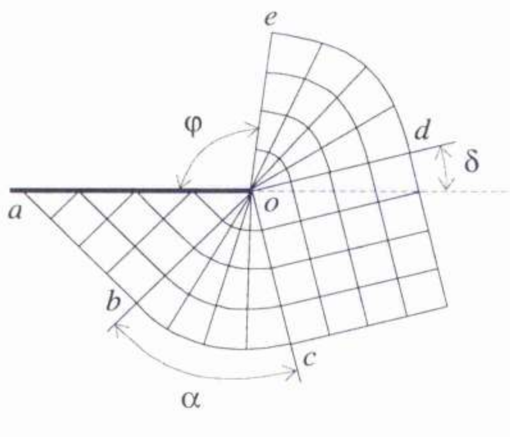

Type I

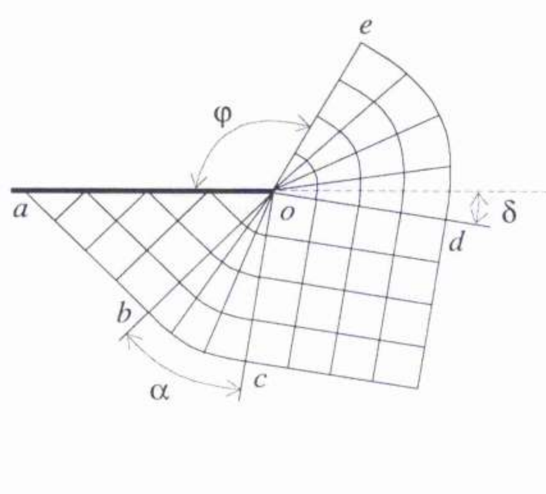

Type II

Figure 4.7: Mixed mode slip line fields with elastic sectors on the upper crack flanks.

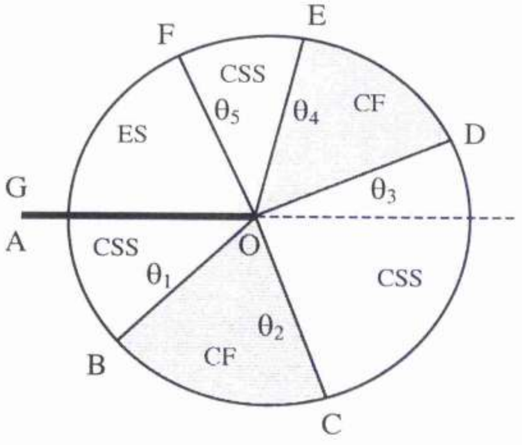

Figure 4.8: Zhu and Chao (2001) six sector crack tip field.

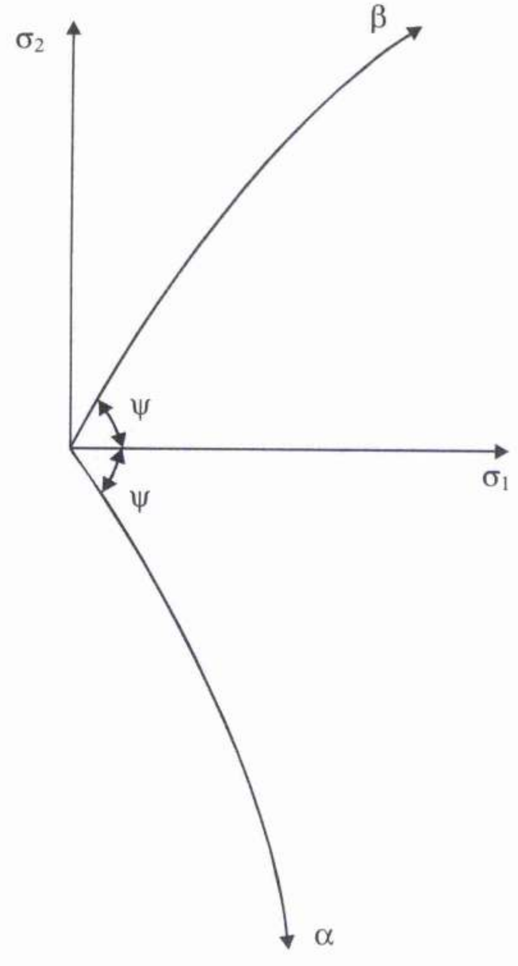

Figure 4.9: Non-orthogonal slip lines (α, β) for plane stress.

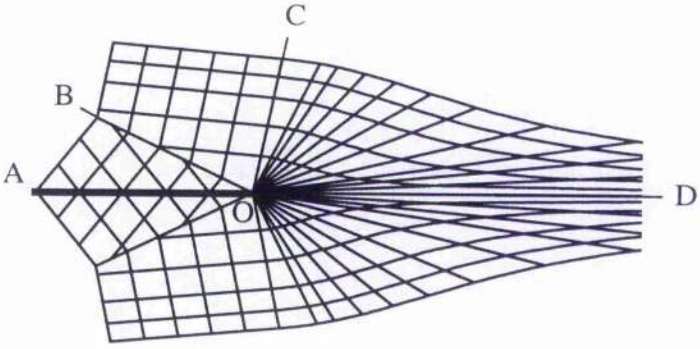

Figure 4.10: Hutchinson mode I slip line field, plane stress.

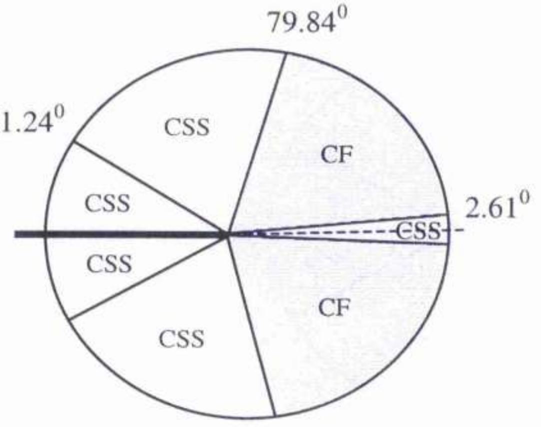

Figure 4.11: Dong & Pan mode I slip line field shown schematically.

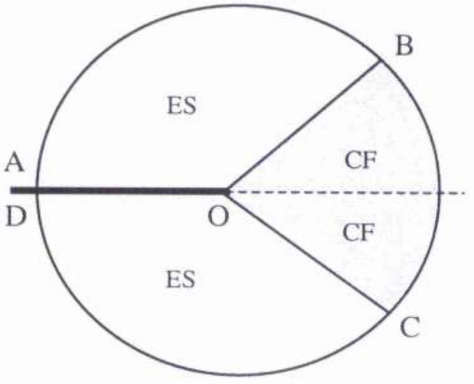

Figure 4.12: Sham & Hancock mode I slip line field shown schematically.

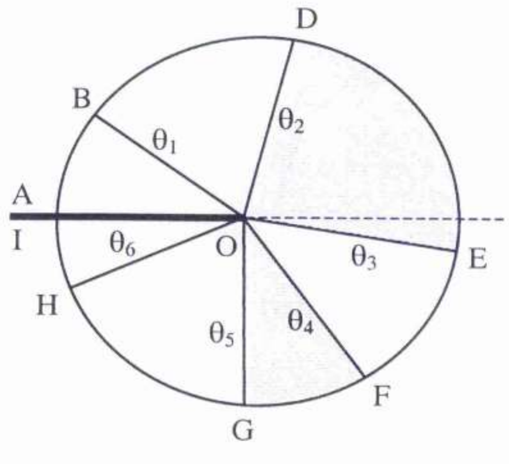

Figure 4.13: Shih plane stress near mode I slip line field shown schematically.

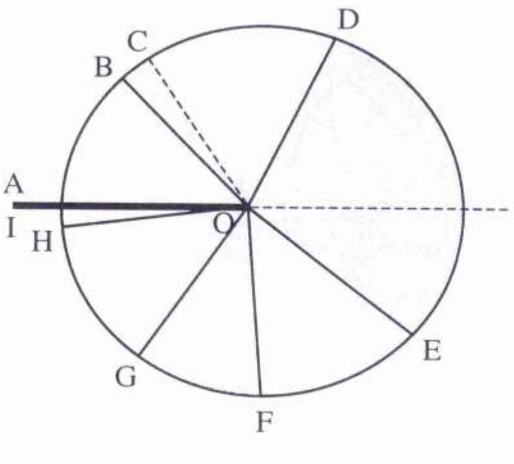

Figure 4.14: Shih plane stress near mode II slip line field shown schematically.

Chapter 5 Crack propagation and toughness in mixed mode loading

5.1 Criteria for crack propagation

Several criteria have been proposed to describe the direction of crack propagation in brittle materials under mixed mode I/II loading. The Maximum Hoop Stress (Erdogan and Sih, 1963) and the Maximum Strain Energy Release Rate (Hussain et al., 1974) criteria are most widely accepted. Both criteria are based on LEFM, and predict closely similar directions of crack propagation. In the Maximum Hoop Stress criterion, the crack is assumed to propagate in the direction perpendicular to the direction of the maximum hoop stress ($\sigma_{\theta\theta}$), or equivalently in the direction of zero shear stress. The Maximum Strain Energy Release Rate criterion suggests that crack propagates in a direction in which the stain energy release rate is maximum. The direction of maximum strain energy release rate can be determined in numerical calculations by using an extension of the virtual crack extension method of Parks (1974). In ductile material plasticity occurs at the crack tip and the criteria based on LEFM should be modified to consider crack tip plasticity.

Extensive analytical, numerical and experimental investigations have been undertaken to examine the behaviour of cracks under mixed mode (I/II) loading (Shih, 1974, Ghosal et al. 1994, Maccagno et al., 1991). The experimental work has examined the effect of mixed mode (I/II) loading on fracture toughness of materials showing brittle (cleavage) and ductile fracture behaviour. In mixed mode (I/II) fracture, Maccagno and Knott (1989) have defined an equivalent crack angle, β_{eq}, which gives the relative amount of mode I and mode II loading as:

$$\beta_{eq} = \tan^{-1}\left(\frac{K_I}{K_{II}}\right) \tag{5.1}$$

With this notation, pure mode I and mode II loadings correspond to equivalent crack angles 90^0 and 0^0 respectively. For mixed mode (I/II) loading, $90^0 > \beta_{eq} > 0^0$.

5.2 Cleavage (brittle) fracture

During cleavage cracks propagate along low index crystallographic planes following a transgranular path. Although cleavage may occur under macroscopically elastic conditions it is associated with local plasticity and possibly ductile crack extension. Maccagno and Knott (1991) have investigated cleavage fracture behaviour of steel under mixed mode (I/II) loading at -196^0 C. The experimental technique used edge-cracked bend bar specimens with symmetric four-point loading for mode I and anti-symmetric four-point loading (Gao et al., 1979) for mixed mode (I/II) and mode II. Tests were performed on four grades of steels: En3B mild steel, 1Cr-1Mo-0.3V structural steel, HY130 pressure vessel steel and C-Mn steel submerged arc weld. The directions of crack propagation obtained from their investigation were consistent with the Maximum Hoop Stress criterion of Erdogan and Sih (1963). It was observed that in all cases under pure mode I loading, the crack propagated along the direction of the original crack, which corresponds to a fracture angle, $\theta_0 = 0^0$. Under mixed mode (I/II) loading, the crack advances in a direction other than $\theta_0 = 0^0$, and with increasing mode II loading, the fracture angle, θ_0, increases. Figure 5.1 illustrates the directions of crack propagation under different mixed mode (I/II) loadings in large grain 1Cr-1Mo-0.3V steel specimens (Maccagno & Knott, 1991). From the experimental data, Maccagno & Knott (1991) compared the fracture angle, θ_0, with that predicted by Maximum Hoop Stress criterion as shown in Figure 5.2. The experimental results agree well with the theoretical prediction. Gao et al. (1979) and Yokobori et al. (1983) also investigated brittle fracture under mixed mode (I/II) loading using similar materials. Gao et al. used 1.3Cr-0.5Mo-0.1V steel specimens with anti-symmetric four-point bend loading, and Yokobori et al. used 0.04% C mild steel tubes under remotely applied tension and torsion, and show similar results as illustrated in Figure 5.3.

Manoharan et al. (1989a, 1989b) and Graves (1992) have shown that under mixed mode (I/III) loading the fracture toughness of a brittle material increases with increasing mode III loading. Using aluminium alloys, Kamat & Hirth (1995a) have shown that mixed mode I/II and I/III have similar effects on fracture toughness. It was observed (Kamat & Hirth,1995a) that fracture toughness of the aluminium alloy, 2034 Al(1.08 wt% Mn) corresponding to pure mode I decreases slightly in near mode I as the mode II (or mode III) loading applied, subsequently the toughness does not vary further with increasing mode II (or mode III) loading as shown in Figure 5.4.

5.3 Ductile fracture

In ductile materials the crack extends due to nucleation, growth and coalescence of micro-voids, which form at inclusions and second phase particles by interface de-cohesion or particle cracking. The voids then grow by plastic strain and hydrostatic stress and finally coalesce with the blunting crack tip. In ductile materials crack initiation and advance in mixed mode (I/II) can occur in the direction of maximum shear rather than the direction normal to the maximum hoop stress (Bhattacharjee and Knott, 1994). Bhattacharjee and Knott (1993) have shown experimentally that in ductile crack growth under mixed mode (I/II) loading the shear mode dominates over the opening mode and crack initiation and advance are due to shear. Figure 5.5 shows two similar specimens tested under similar mode I/II ratios at -100^0 C (brittle region) and at 20^0 C (ductile region). In the brittle specimen the crack propagates following the Maximum Hoop Stress criterion, whereas, in the ductile specimen the crack advances in the original direction following the maximum shear path.

Experimental studies (Bhattacharjee et al., 1994, Tohgo et al., 1988) have shown that under mixed mode (I/II) loading in ductile materials part of the crack tip blunts and the other part sharpens due to a competition between hydrostatic stress and equivalent plastic strain. Analytical (Shih, 1974) and numerical (Ghosal et al., 1994, 1996) investigations have shown that the hydrostatic stress directly ahead of the crack in mode I loading decreases as mode II loading applied, and this is accompanied by an increase in equivalent plastic strain at the crack tip. Budden (1988) and Saka et al. (1986) have shown by mixed mode (I/II) blunting analysis that the crack tip blunts depending upon the initial crack tip profile. Budden modelled the crack tip with sharp corners, and Saka et al. used a crack with circular tip. The changes of crack tip profiles shown by Budden and Saka et al. are illustrated in Figure 5.6. Aoki et al. (1987) have investigated deformation of a smooth crack tip under mixed mode (I/II) loading by finite element analysis. They have reported that crack initiation may occur either from the blunted side or from the sharpened side of the crack tip depending upon the ratio of mode I & II. With mode I/II ratios higher than 0.6, void volume fraction and equivalent plastic strain are higher at the blunted side, which may result in crack initiation from the blunted side. On the other hand, with mode I/II ratios less than 0.6, the void volume fraction and equivalent plastic strain are higher at the sharpened side, which may result in crack initiation from the sharpened side following the direction of maximum shear. Bhattacharjee and Knott (1994) have shown experimentally that even for mode I/II ratios much higher than 0.6, i.e., with a mode I/II ratio 3.15, crack initiation may occur from the sharpened side of the crack tip. Figure 5.7 shows the changes in notch tip profiles in HY 100 steel specimens (Bhattacharjee and Knott, 1994) at different load values under mode I/II ratio 1.57.

Under mixed mode (I/II) loading, the fracture toughness for ductile materials decreases with increasing mode II loading. Kamat and Hirth (1995a) experimentally have shown the effects of mixed mode I/II and I/III on fracture toughness of aluminium alloy 2034 Al (<0.1 wt% Mn) and found a similar variation of toughness under the two mixed modes as shown in Figure 5.8.

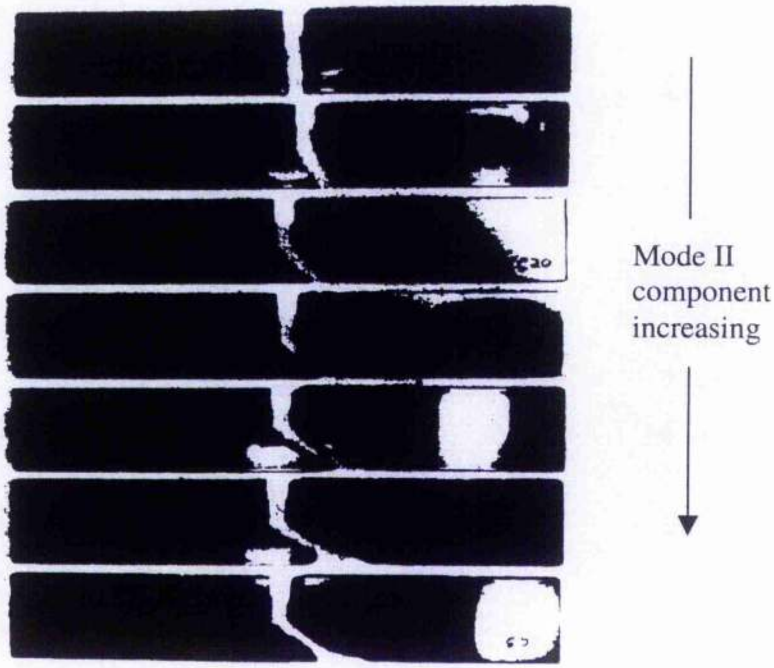

Figure 5.1: Direction of crack propagation under mixed mode (I/II) loading in large grain 1Cr-1Mo-0.3V steel specimens (Maccagno & Knott, 1991).

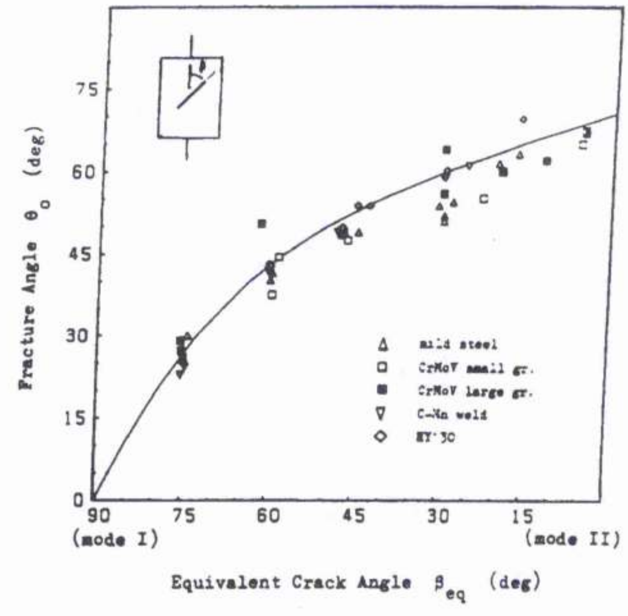

Figure 5.2: Comparison of experimental and theoretical fracture angles (Maccagno & Knott, 1991).

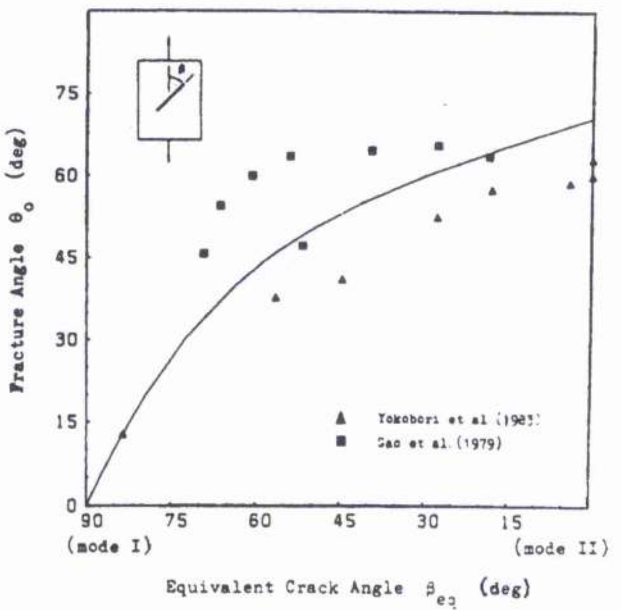

Figure 5.3: Comparison of experimental fracture angles (Gao et al., 1979, Yokobori et al., 1983) with theoretical prediction (Maccagno & Knott, 1991).

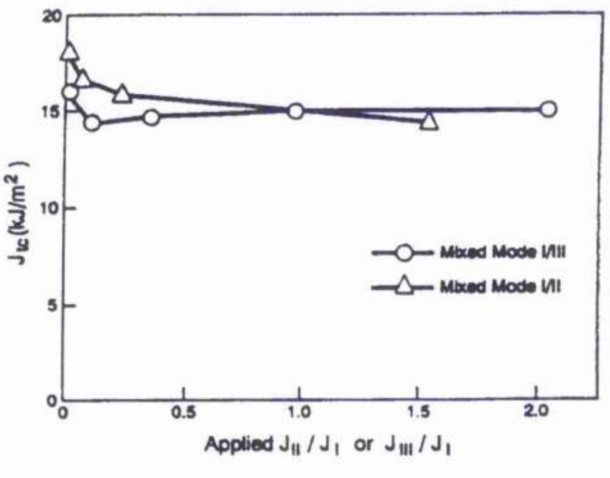

Figure 5.4: Effect of mixed mode (I/II, I/III) loading on fracture toughness, J_{tc} of the aluminium alloy, 2034 Al (1.08 wt% Mn) (Kamat & Hirth, 1995).

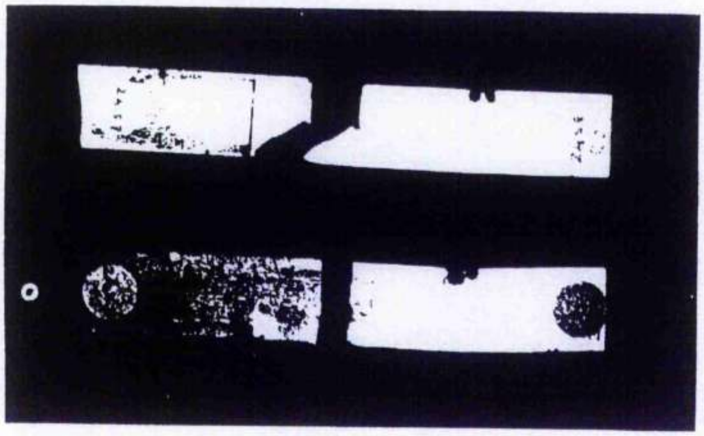

Figure 5.5: Specimens showing brittle (top) and ductile (bottom) fracture (Bhattacharjee & Knott, 1993).

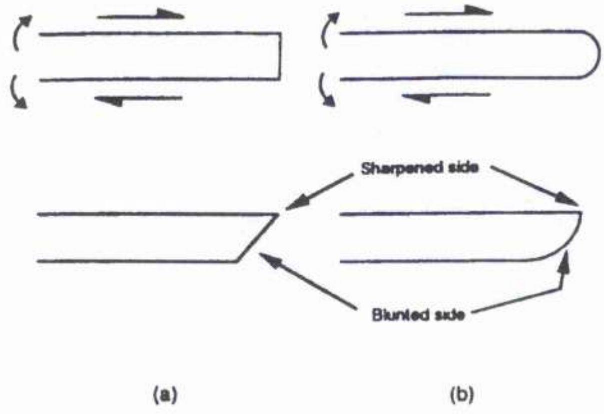

Figure 5.6: Change in crack tip profile due to (a) Budden (1988) and (b) Saka et al. (1986) (Bhattacharjee & Knott, 1994).

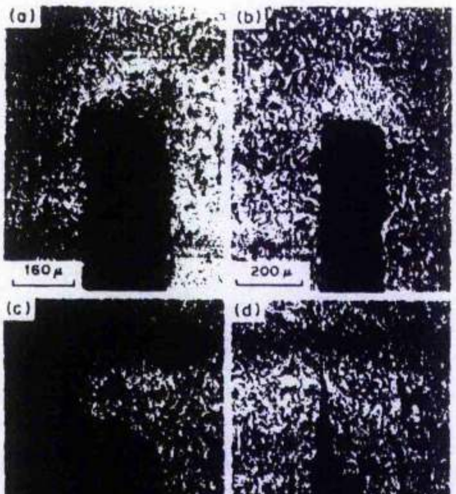

Figure 5.7: Change in notch tip profile with load in HY 100 steel specimens under mixed mode ($K_I/K_{II} = 1.57$) (Bhattacharjee & Knott, 1994).

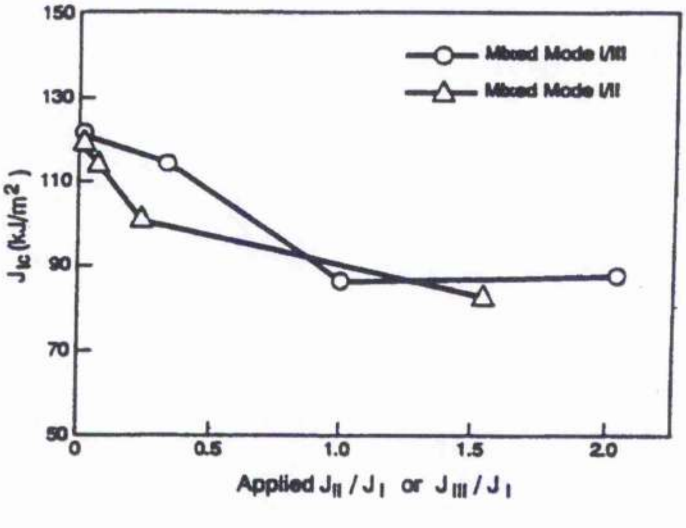

Figure 5.8: Effect of mixed mode (I/II, I/III) loading on fracture toughness, J_{Ic} of the aluminium alloy, 2034 Al (<0.1 wt% Mn) (Kamat & Hirth, 1995).

Chapter 6 Numerical methods

6.1 Boundary layer formulations

The concept of a boundary layer formulation was introduced by Rice and Tracey (1973) to investigate elastic-plastic crack tip fields. Interest is focused on the small region close to a crack tip where plastic deformation takes place. Instead of modelling the complete structure, a circular region centred on the crack tip is considered. The boundary conditions for the model are based on the first term (boundary layer formulation) or first and second terms (modified boundary layer formulation) of the Williams expansion (Williams, 1957). Displacements corresponding to the asymptotic elastic field for mode I and mode II loading and T-stress are applied on the remote boundary of the model. The Cartesian displacements u_1 and u_2 are given by:

$$u_1 = u_1^{K_I} + u_1^{K_{II}} + u_1^T$$

$$u_2 = u_2^{K_I} + u_2^{K_{II}} + u_2^T \tag{6.1}$$

where, $u_1^{K_I}$ and $u_2^{K_I}$ are Cartesian displacements for mode I, $u_1^{K_{II}}$ and $u_2^{K_{II}}$ are Cartesian displacements for mode II and u_1^T and u_2^T are displacements for the T-stress. The displacements for mode I and II are given as:

$$u_1^{K_I} = \frac{K_I}{2G}\left(\frac{r}{2\pi}\right)^{\frac{1}{2}}\left(\cos\frac{\theta}{2}\left(\kappa - 1 + 2\sin^2\frac{\theta}{2}\right)\right)$$

$$u_2^{K_I} = \frac{K_I}{2G}\left(\frac{r}{2\pi}\right)^{\frac{1}{2}}\left(\sin\frac{\theta}{2}\left(\kappa + 1 - 2\cos^2\frac{\theta}{2}\right)\right)$$

$$u_1^{K_{II}} = \frac{K_{II}}{2G}\left(\frac{r}{2\pi}\right)^{\frac{1}{2}}\left(\sin\frac{\theta}{2}\left(\kappa + 1 + 2\cos^2\frac{\theta}{2}\right)\right)$$

$$u_2^{K_{II}} = \frac{K_{II}}{2G}\left(\frac{r}{2\pi}\right)^{\frac{1}{2}}\left(-\cos\frac{\theta}{2}\left(\kappa - 1 - 2\sin^2\frac{\theta}{2}\right)\right) \tag{6.2}$$

where, K_I and K_{II} are applied stress intensity factors, r is the distance from the crack tip, $\kappa = (3 - 4\nu)$ for plane strain and $\kappa = (3 - \nu)/(1 + \nu)$ for plane stress, ν is Poisson's ratio and G is the shear modulus. The displacements corresponding to the T-stress in plane strain and plane stress can be given as:

$$u_1^T = \frac{T\left(1 - \nu^2\right) r \cos\theta}{E}$$

$$u_2^T = -\frac{T\nu(1+\nu)r\sin\theta}{E}, \text{ for plane strain} \tag{6.3}$$

and

$$u_1^T = \frac{Tr\cos\theta}{E}$$

$$u_2^T = -\frac{\nu Tr\sin\theta}{E}, \text{ for plane stress} \tag{6.4}$$

where, r is the distance from the crack tip, E is modulus of elasticity, ν is Poisson's ratio. The displacements were calculated using a spread sheet in Microsoft Excel and pasted into an ABAQUS (Hibbitt, Karlsson and Sorensen, 1998) input deck.

Plane strain problems have been investigated under mode I, mixed mode I/II and mode II loadings with K_I/K_{II} ratios: ∞, 2, 1, ½ and 0, and at three levels of T-stress: $T = -0.5\sigma_0$, 0 and $+0.5\sigma_0$, where σ_0 is the uni-axial yield strength. Plane stress problems have been investigated under mode I, mixed mode I/II and mode II loadings with K_I/K_{II} ratios: ∞, 1, ½, 0.45, ¼ and 0, and at T = 0. The plane stress mode I problem has also been investigated at $T = \pm 0.5\sigma_0$ to determine the effect of the T-stress on crack tip plastic zone..

The mesh used for numerical analysis is shown in Figure 6.1. The mesh is based on 24 rings of 24 second order iso-parametric hybrid elements highly focused at the crack tip. The crack tip is modelled by 49 initially coincident but independent nodes. Displacement boundary conditions are applied on the outer nodes of the mesh. Plasticity was restricted to a small fraction of the mesh radius to represent contained yielding.

Finite element analysis was performed using finite element code ABAQUS (Hibbitt, Karlsson and Sorensen, 1998). The material response is taken to be elastic-perfectly plastic. The uni-axial stress-strain relations are given by the equations:

$$\sigma = E\varepsilon, \quad \varepsilon < \sigma_0/E$$

$$\sigma = \sigma_0, \quad \varepsilon \geq \sigma_0/E \tag{6.5}$$

where, σ is the uni-axial stress, E is modulus of elasticity, ε is strain and σ_0 is the uni-axial yield strength. The plastic response of the material was modelled as isotropic and almost incompressible elastic material using a Poisson's ratio of 0.49. In uni-axial tension plastic deformation is assumed to occur at a constant stress, σ_0, such that there is no strain hardening, as illustrated schematically in Figure 6.2. This response is known as elastic-perfectly plastic. Under the near incompressible conditions associated with plastic flow the use of reduced integration hybrid elements, and small departure from perfect incompressibility help to avoid mesh-locking problems.

To generalise the uni-axial material response to multi-axial states of stress the von Mises yield criterion was used with an associated flow rule and incremental plasticity within a framework of small displacement gradient theory of deformation. A modulus of elasticity of 2×10^{11} Pa and a yield strength, 2×10^{8} Pa were used in the analysis, although non-dimensional results are always presented.

Output data were written to an abaqus.rpt file using post processing programs fullfan3.go and fullfanodd3.go given in Appendix I which were used in conjunction with the ABAQUS post-processor ABAQUS Post (Hibbitt, Karlsson and Sorensen, 1998). The radial distances and Cartesian stresses at different angles surrounding the crack tip were obtained from the abaqus.rpt file. The data were obtained at 7.5^0 intervals starting from crack plane to 180^0 and -180^0. The data were then arranged in matrix form using the Matlab programs fullfan3.m and fullfanodd3.m given in Appendix II and the stresses were extrapolated to the crack tip in Cartesian form. The asymptotic stresses are then transformed to polar co-ordinate system. The data from output files were plotted as angle versus stresses using Microsoft Excel.

J-integrals were determined surrounding the crack tip by using the CONTOURS parameter in *CONTOUR INTEGRAL option in the ABAQUS input file. The evaluation of the J-integral is based on a modification of the virtual crack extension method of Parks (1974) due to Li, Shih & Needleman (1985). In ABAQUS model each ring of elements surrounding the crack tip is considered as a contour. To evaluate J-integral, ABAQUS automatically identifies the elements of each ring from the node set defined by *NSET option using NSET = TIP parameter in ABAQUS input file. Four J-integral contours were used at the crack tip to maintain accuracy of result and obtained in ABAQUS data file.

6.2 Determination of slip line fields from numerical results

Slip line fields were determined from the asymptotic stresses in plane strain and plane stress. The crack tip field is initially divided into elastic and plastic sectors. The angular span over which yield criterion is not satisfied defines the elastic sector, and the sector over which the yield criterion is satisfied defines the plastic sector. In plane strain slip line fields, the crack tip plastic sector can only comprise constant stress and centred fan sectors. In constant stress sectors, the mean stress, σ_m, does not vary with angle. In centred fan sectors shear stress, $\sigma_{r\theta}$, equals the yield stress in shear, k, while the mean stress, σ_m, varies linearly with the angle. This allows the angular span of elastic sectors, constant stress sectors and centred fans to be identified from the numerical results to an accuracy, which is limited by the angular mesh refinement.

In plane stress slip line fields, the crack tip plastic sector is also divided into constant stress and curved fan sectors. In constant stress sectors, the mean stress, σ_m, does not vary with angle. In curved fan sectors, the radial stress deviator, s_{rr} is zero, or equivalently, $\sigma_{\theta\theta} = 2\sigma_{rr}$. The angle at which shear stress, $\sigma_{r\theta} = 0$, defines the asymptotic angle, ϕ. This information again allows asymptotic slip line fields to be constructed from numerical data in plane stress.

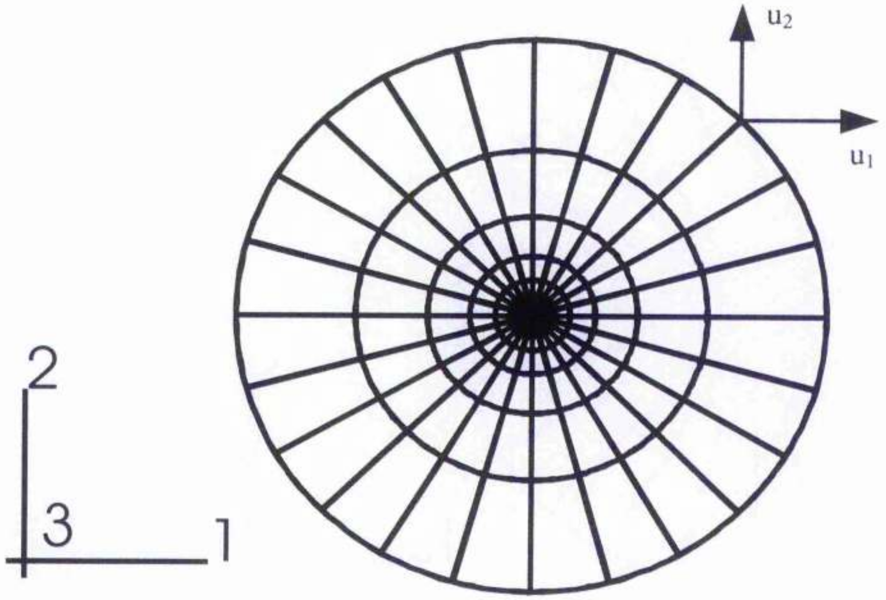

Figure 6.1: Mesh used in boundary layer formulation.

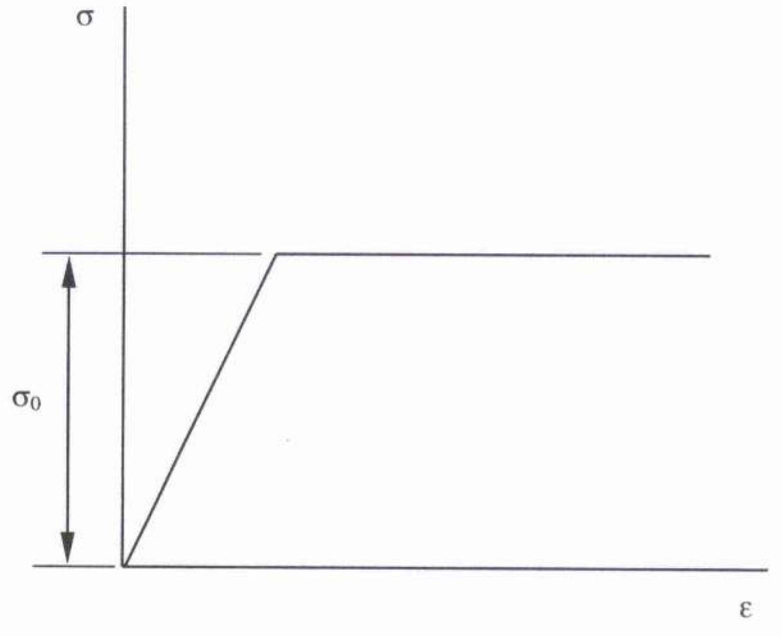

Figure 6.2: Stress-strain curve for elastic-perfectly plastic material.

Chapter 7 Results

7.1 Plane strain mixed mode (I/II) crack tip fields in perfect plasticity

7.1.1 Plastic zones

In plane strain, the effect of the T-stress on plastic zone in mode I, mixed mode I/II and mode II loading has been investigated at three levels of T-stress: T=0 and $T=\pm 0.5\sigma_0$. The plastic zones are shown in Figures 7.1 to 7.5. In mode I loading a compressive T-stress enlarges both wings of the plastic zone and causes the plastic lobes to swing forward. The tensile T stress has little effect on the plastic zone size but causes the plastic lobes to swing backward as shown in Figure 7.1. These results are consistent with those reported by Du & Hancock (1991).

Under mixed mode loading ($K_I/K_{II}=2$), a compressive T-stress enlarges the forward lobe of the plastic zone, whereas a positive T-stress increases the trailing lobe causing it to merge with the crack flank, as shown in Figure 7.2.

Under mixed mode loading ($K_I/K_{II}=1$), both positive and negative T-stresses increase the size of the plastic zone as shown in Figure 7.3. In this case a compressive T-stress causes the part of the plastic zone in the positive quadrant to increase in size and to swing upward but decreases the size of the lobe in the negative quadrant. A tensile T-stress decreases the positive part of the plastic zone and causes it to swing downward, but it enlarges the positive part.

In the case of $K_I/K_{II}=1/2$, both positive and negative T-stresses increase the plastic zone size, but compressive T-stress cause the plastic zone to move upward and in contrast tensile T-stress cause the forward part of the plastic zone to swing downward as illustrated in Figure 7.4.

In pure mode II loading the plastic zone shape shown in Figure 7.5 is symmetric about the crack plane, as the stress field must be anti-symmetric. A T-stress destroys this symmetry. A compressive T-stress causes an enlarged lobe to develop in the area above the symmetry axis, while a tensile T stress enlarges the lobe in the area below the symmetry axis.

7.1.2 Asymptotic stress fields

The asymptotic stresses have been determined numerically for mode I, II and mixed mode I/II loading with and without T-stresses. The angular variation of stresses at the crack tip are shown in Figures 7.6a to 7.20b. The effect of T-stress on the plastic mixity is shown in Figure 7.26 and Table 7.1. Elastic and plastic mixities have been discussed in Section 4.1.2. The effect of T-stress on the mode I and mixed mode I/II fields is essentially to change the hoop stress (or equivalently the mean stress) directly ahead of the crack. In mixed mode fields, a tensile T-stress increases the hoop stress ahead of the crack and increases plastic mixity, whereas a compressive T-stress causes the hoop stress and plastic mixity to decrease. Under mode I, the shear stress ahead of the crack is defined to be zero and the effect of T-stress is only to increase or decrease the hoop stress (or equivalently the mean stress) directly ahead of the crack depending upon tensile or compressive T-stress. The mode I stress fields ($T=-0.5\sigma_0$, 0, $+0.5\sigma_0$) are shown in Figures 7.6a to 7.8b, and the mixed mode I/II fields are shown in Figures 7.9a to 7.17b. Mode II loading gives anti-symmetric stress field, where the hoop stress ahead of the crack is zero. In this case a compressive T-stress gives rise to a compressive hoop stress directly ahead of crack, which results in a negative plastic mixity. On the other hand, a tensile T-stress gives rise to a tensile hoop stress ahead of crack, which corresponds to a positive plastic mixity. The mode II stress fields are given in Figures 7.18a to 7.20b.

The crack tip fields (mode I, II and mixed mode I/II, and $T=-0.5\sigma_0$, 0, $+0.5\sigma_0$) have been represented in terms of slip line fields which are shown in Figures 7.21 to 7.25. The slip line fields have been constructed from numerical results as discussed in Section 6.2. The critical angles of the slip line fields are given in Table 7.2. The mode I slip line fields ($T=-0.5\sigma_0$, 0, $+0.5\sigma_0$) are shown in Figure 7.21. Under mode I, a tensile T-stress gives rise to the Prandtl field, where plasticity fully surrounds the crack tip. For T=0, field consists of a constant stress diamond ahead of the crack and two fan sectors, complemented by elastic sectors to the crack flanks. A compressive T-stress decreases the angular span of the fan sectors, and thus the angular spans of the elastic wedges on the crack flanks increase. The mixed mode I/II slip line fields are shown in Figures 7.22 to 7.24. Under mixed mode I/II loading the constant stress diamond ahead of the crack rotates with increasing mode II loading and plasticity eventually breaks through to the lower crack flank. Compressive T-stress causes the constant stress diamond to rotate more compared to T=0 field. Tensile T-stress has little effect on the rotation. Under mode II loading, plasticity surrounds the crack tip at all angles, where T-stress has very little effect on the slip line field. The mode II slip line fields ($T=-0.5\sigma_0$, 0, $+0.5\sigma_0$) are shown in Figure 7.25.

7.1.3 Loading

The level of loading may be measured in the remote field by the applied stress intensity factors K_I and K_{II}. These can be combined to give a remotely applied strain energy release rate, G, or equivalent J:

$$G = J = \frac{K_I^2}{E'} + \frac{K_{II}^2}{E'} \tag{7.1}$$

where $E' = E$ for plane stress, and $E' = E/(1-\nu^2)$ for plane strain. Under conditions of non-linear or linear elasticity J is expected to be path independent, so that values of J measured in the local field near the crack tip correspond to the remotely applied J. However, under conditions of incremental plasticity, in which limited amounts of local unloading may occur, the local and remotely measured J-values may differ (Zywicz & Parks, 1989). The local value of J was measured by the routine provided by ABAQUS (Hibbitt, Karlsson and Sorensen, 1998). This is based on a modification of the virtual crack extension method of Parks(1974) due to Li, Shih & Needleman (1985). The ratio of the local to remote values of J are given in Table 7.3. The trend of the results is that the negative values of T tend to increase the ratio of local to remote J and positive T stresses to decrease it.

7.2 Plane stress mixed mode (I/II) crack tip fields in perfect plasticity

Plane stress mode I, mode II and mixed mode I/II crack tip fields have been investigated analytically and numerically, and represented in-terms of slip line fields. Analytical solutions were obtained by assembling the constant stress, fan and elastic sectors subject to boundary conditions and continuity of tractions across the sector boundaries. Slip line theory (Hill, 1950) was used to solve the plastic sectors (constant stress and fan sectors) and the solutions for elastic sectors were given by using the semi-infinite wedge solution of Timoshenko and Goodier (1970). Numerical solutions were obtained by using boundary layer formulation introduced by Rice and Tracey (1973).

The asymptotic crack tip stresses for plane stress mode I, II and mixed mode I/II are shown in Figures 7.27a to 7.32c. The data points in the graphs represent the numerical results, and the solid lines represent the analytical results. The analytical solutions show good agreement with the numerical results. Under mixed mode I/II loading the hoop stress (or equivalently the mean stress) ahead of the crack corresponding to mode I loading decreases with increasing mode II loading, which results in decreasing plastic mixity. The elastic and plastic mixities for the different combinations of loading are shown in Figure 7.39 and Table 7.4. Mode I stresses are shown in Figures 7.27a to 7.27c. Mixed mode fields are shown in Figures 7.28a to 7.31c. Finally mode II loading gives rise to an anti-symmetric crack tip field, in which the hoop stress (or equivalently the mean stress) ahead of the crack is defined to be zero. Mode II stresses are shown in Figures 7.32a to 7.32c.

The slip line fields have been determined from numerical data as discussed in Section 6.2. The slip line fields for mode I, II and mixed mode I/II loading are shown in Figures 7.33 to 7.38. The critical angles of the slip line fields are shown in Table 7.5. The mode I slip line field shown in Figure 7.33, consists of a curved fan sector ahead of the crack, which ranges from -39.126^0 to $+39.126^0$ and is complemented by elastic sectors to the crack flanks. The mode I plane stress slip line field has been discussed in detail by Sham and Hancock (1999). Under mixed mode I/II loading the curved fan sector ahead of the crack rotates. Figure 7.34 shows the slip line field under mixed mode, $K_I/K_{II}=1$, where the curved fan sector rotates and the span of the fan increases, while still retaining elastic sectors on the crack flanks. The corresponding stress fields are shown in Figures 7.28a to 7.28c. With increasing mode II loading plasticity breaks through to one crack flank and then to the other. The slip line field for mixed mode, $K_I/K_{II}=1/2$, is shown in Figure 7.35. Here plasticity breaks through to the upper crack flank, where a constant stress sector develops. The stress fields for this loading are shown in Figure 7.29a to 7.29c. The slip line field for mixed mode, $K_I/K_{II}=0.45$ is shown in Figure 7.36. Here plasticity breaks through to lower crack flank, where a constant stress sector develops. The corresponding stress fields are shown in Figures 7.30a to 7.30c. Under mixed mode, $K_I/K_{II}=1/4$, plasticity surrounds the crack tip at all angles and curved fan sectors emerge at $\pm 125.3^0$ separating two constant stress regions. The field consists of 4 constant stress sectors and 3 curved fan sectors as shown in Figure 7.37. The corresponding stress fields are shown in Figures 7.31a to 7.31c. Finally, mode II slip line field is shown in Figure 7.38, where plasticity surrounds the crack tip at all angles. Mode II field consists of 4 constant stress sectors and 3 curved fan sectors.

The effect of the T-stress on the crack tip plastic zone under mode I loading has been investigated at T=0 and $T = \pm 0.5\sigma_0$. The plastic zones are shown in Figure 7.40. Both tensile and compressive T-stresses enlarge the plastic zone. It can be noted that the tensile T-stress (Figure 7.40c) does not have much effect on the shape of the plastic zone, where the compressive T-stress (Figure 7.40a) has. A compressive T-stress rotates the wings of the plastic zone towards the crack flanks.

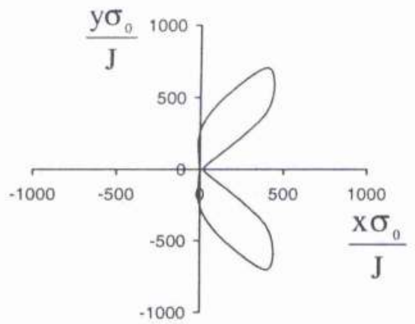

a) $T=-0.5\sigma_0$

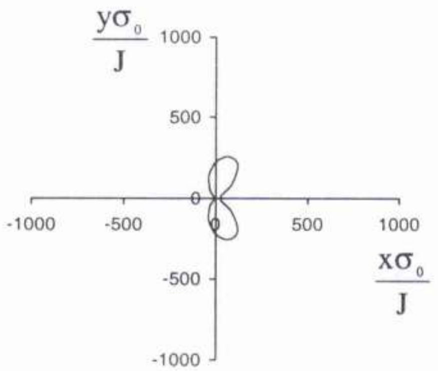

b) $T=0$

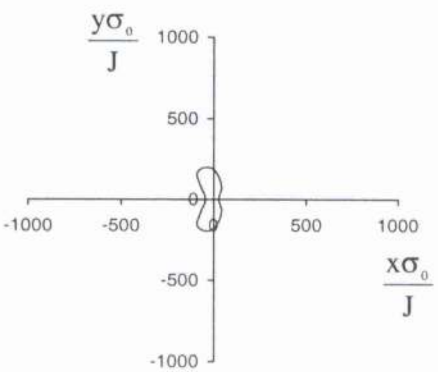

c) $T=+0.5\sigma_0$

Figure 7.1: Effect of T-stress on crack tip plastic zone under mode I loading, plane strain.

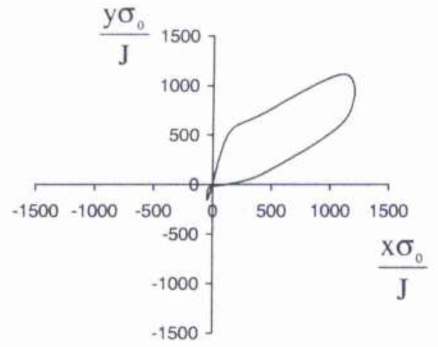

a) T=-0.5σ_0

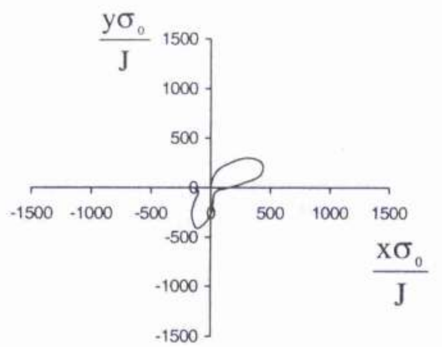

b) T=0

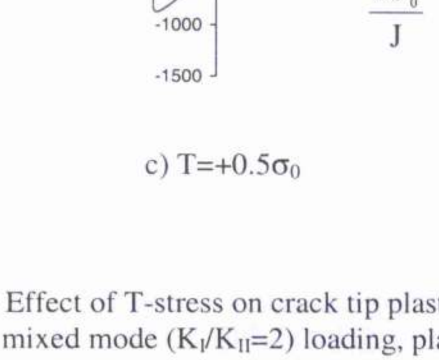

c) T=+0.5σ_0

Figure 7.2: Effect of T-stress on crack tip plastic zone under mixed mode (K_I/K_{II}=2) loading, plane strain.

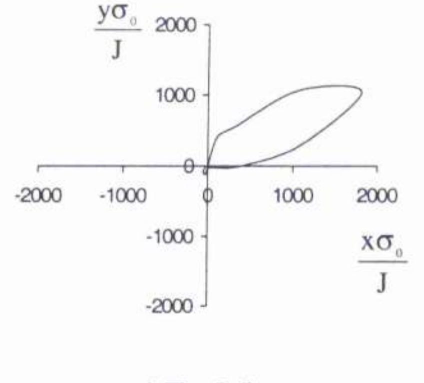

a) T=-0.5σ_0

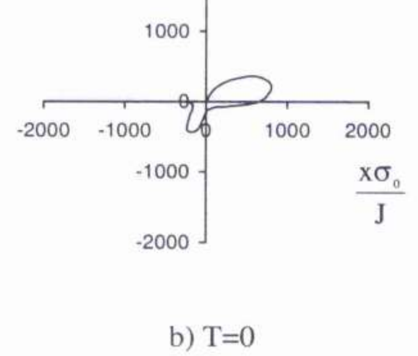

b) T=0

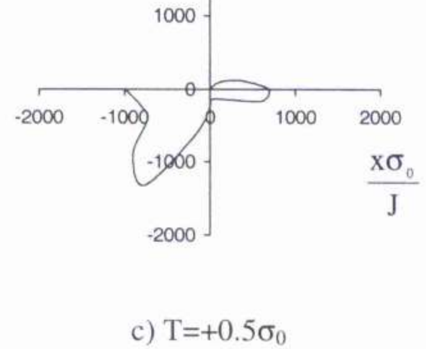

c) T=+0.5σ_0

Figure 7.3: Effect of T-stress on crack tip plastic zone under mixed mode (K_I/K_{II}=1) loading, plane strain.

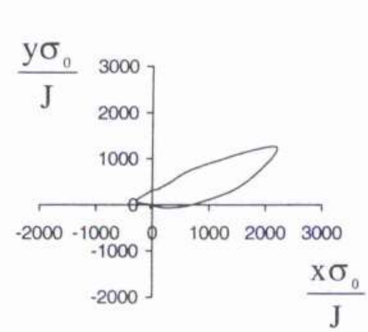

a) T=-0.5σ_0

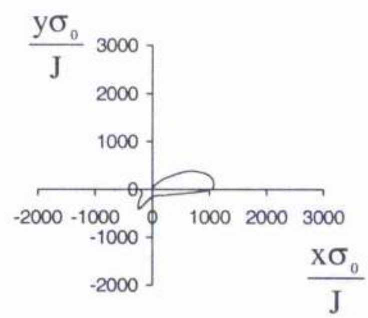

b) T=0

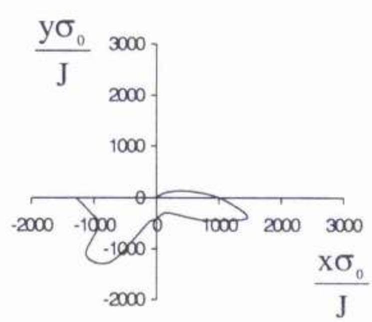

c) T=+0.5σ_0

Figure 7.4: Effect of T-stress on crack tip plastic zone under mixed mode (K_I/K_{II}=1/2) loading, plane strain.

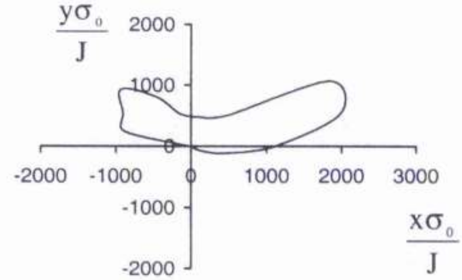

a) T=-0.5σ_0

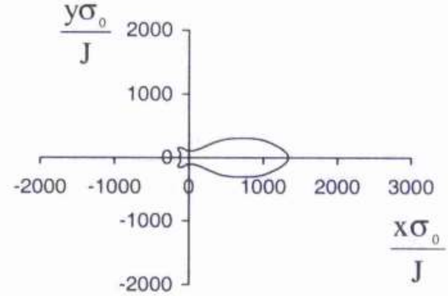

b) T=0

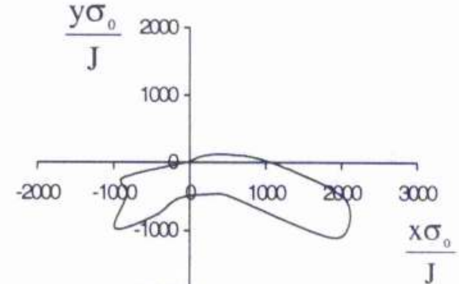

c) T=+0.5σ_0

Figure 7.5: Effect of T-stress on crack tip plastic zone under mode II loading, plane strain.

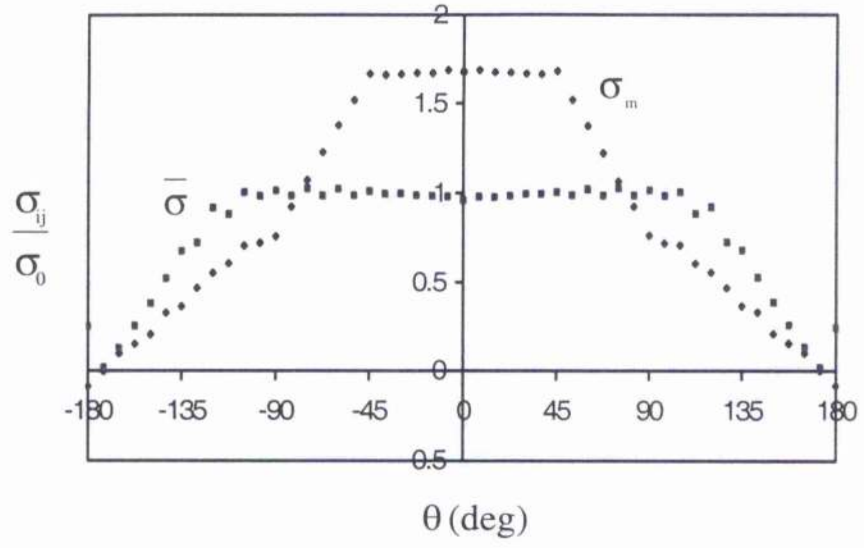

Figure 7.6a: Angular variation of stresses in mode I loading, plane strain, $T=-0.5\sigma_0$.

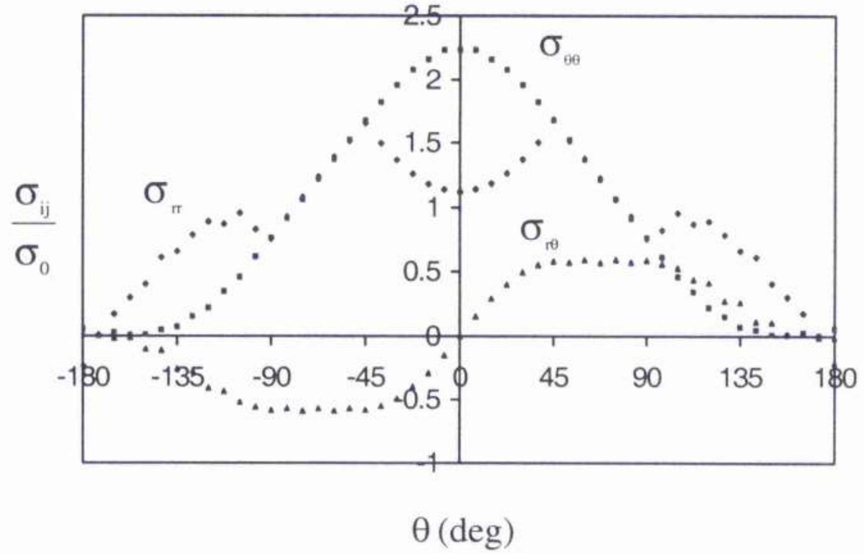

Figure 7.6b: Angular variation of stresses in mode I loading, plane strain, $T=-0.5\sigma_0$.

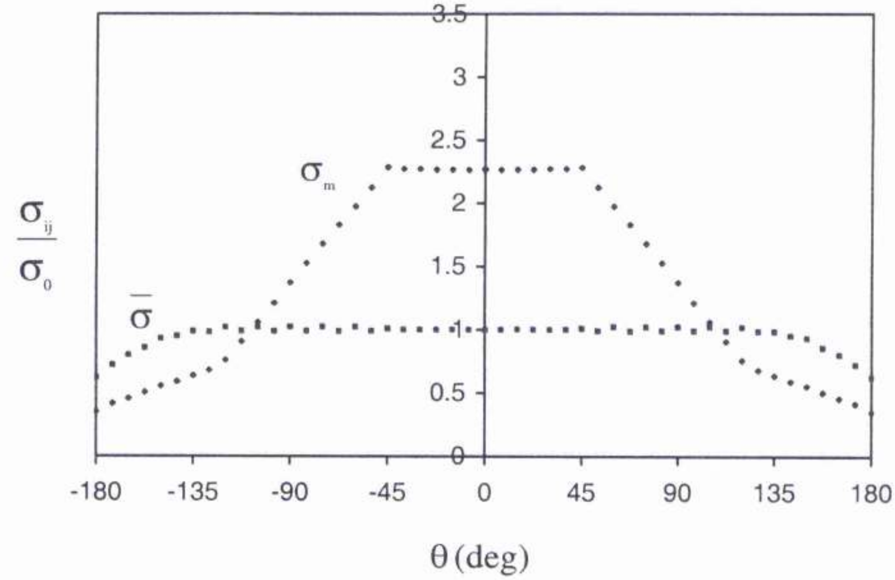

Figure 7.7a: Angular variation of stresses in mode I loading, plane strain, T=0.

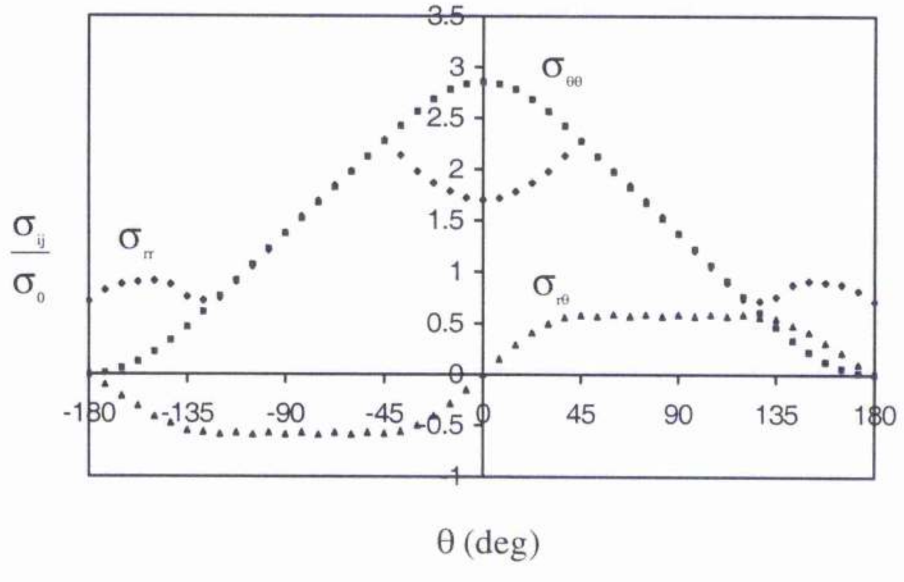

Figure 7.7b: Angular variation of stresses in mode I loading, plane strain, T=0.

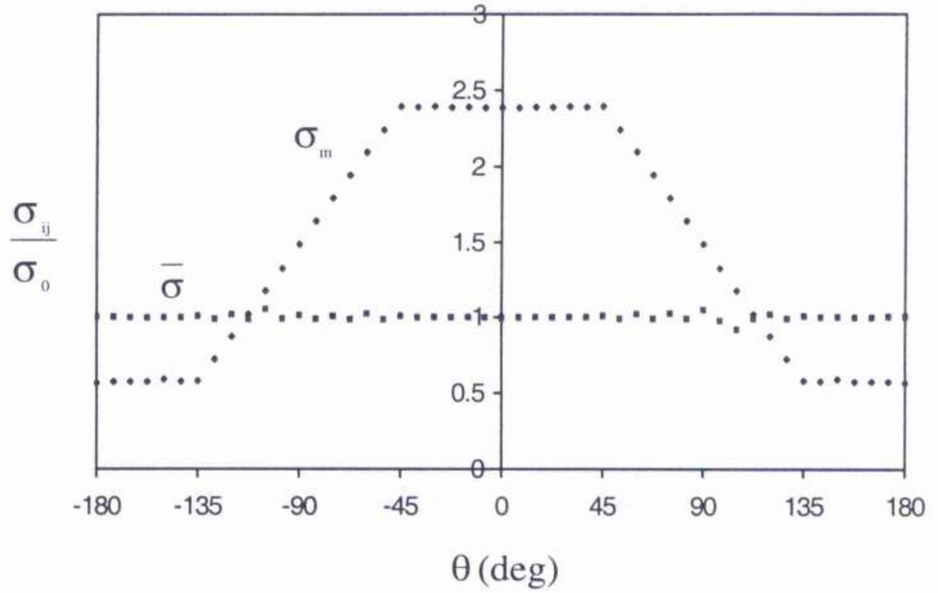

Figure 7.8a: Angular variation of stresses in mode I loading, plane strain, T=+0.5σ_0.

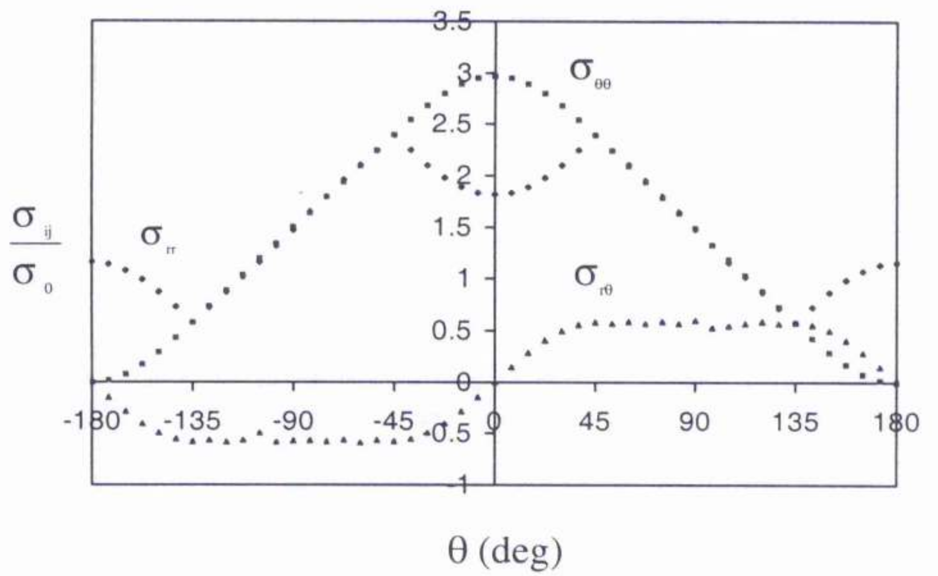

Figure 7.8b: Angular variation of stresses in mode I loading, plane strain, T=+0.5σ_0.

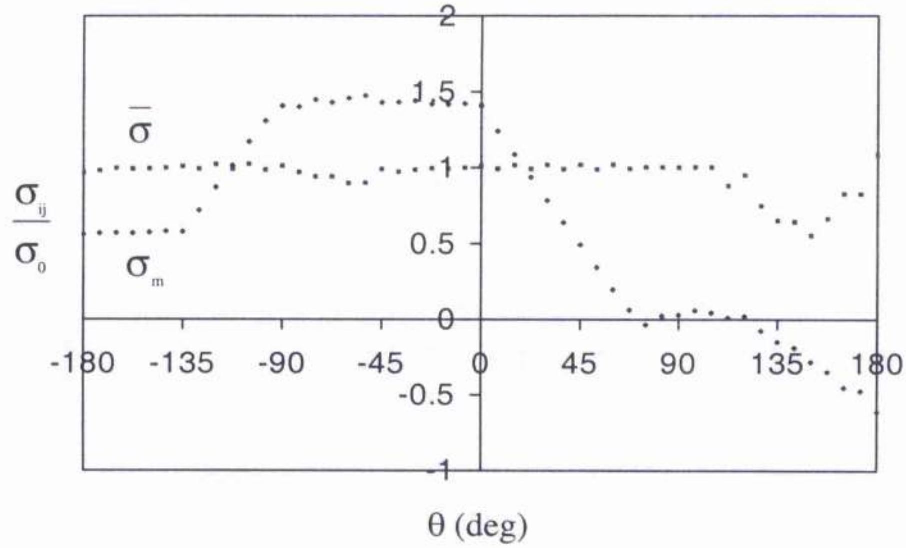

Figure 7.9a: Angular variation of stresses in mixed mode ($K_I/K_{II}=2$) loading, plane strain, $T=-0.5\sigma_0$.

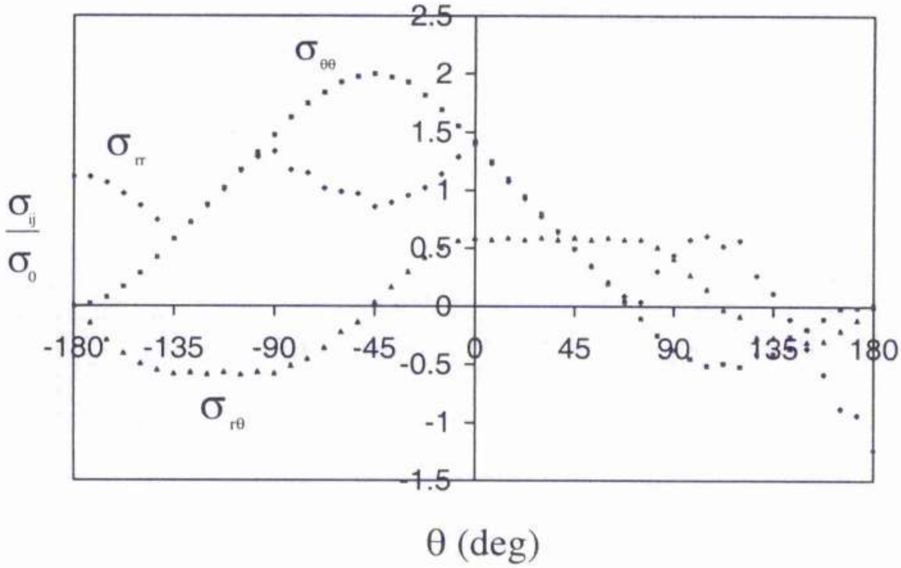

Figure 7.9b: Angular variation of stresses in mixed mode ($K_I/K_{II}=2$) loading, plane strain, $T=-0.5\sigma_0$.

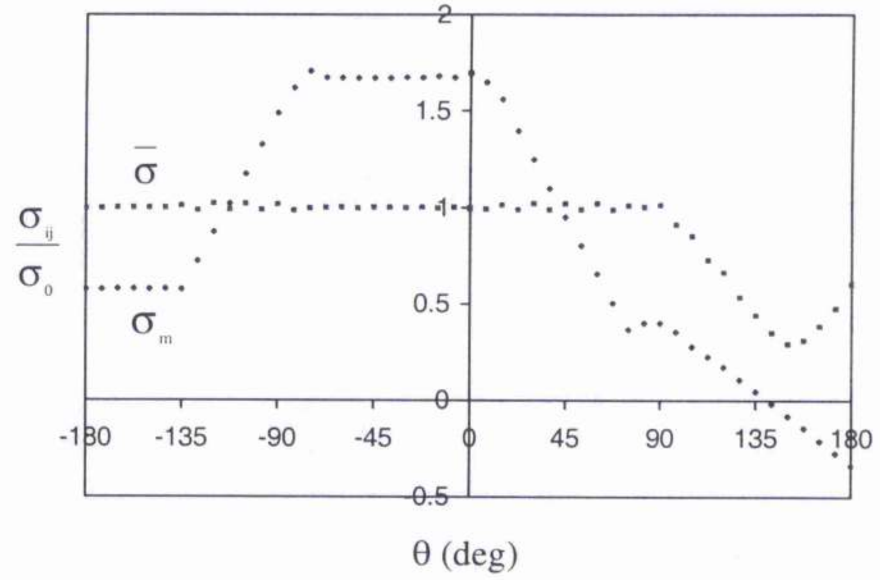

Figure 7.10a: Angular variation of stresses in mixed mode (K_I/K_{II}=2) loading, plane strain, T=0.

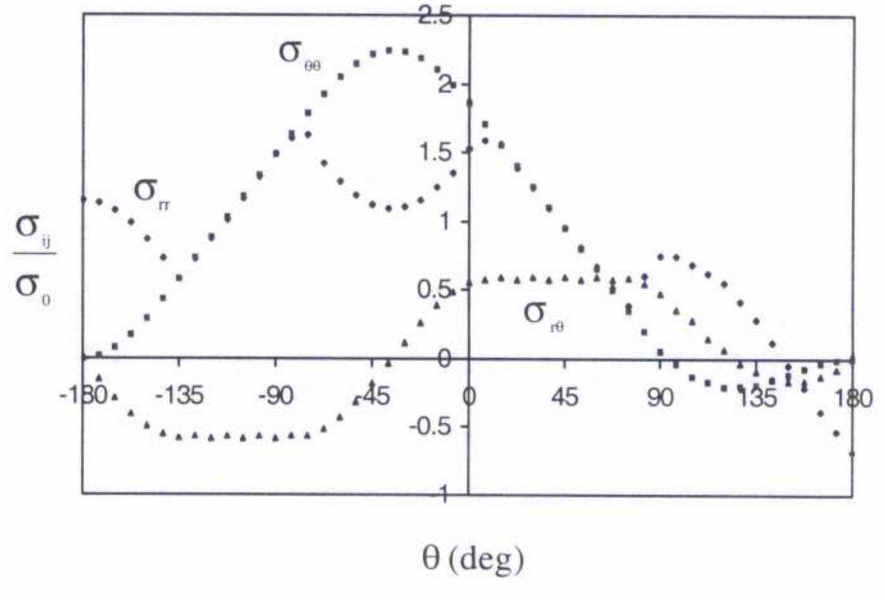

Figure 7.10b: Angular variation of stresses in mixed mode (K_I/K_{II}=2) loading, plane strain, T=0.

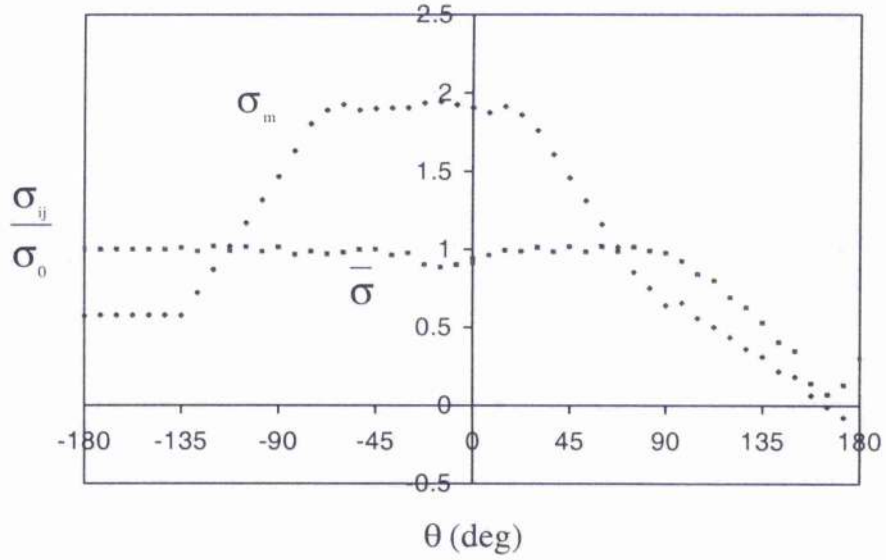

Figure 7.11a: Angular variation of stresses in mixed mode ($K_I/K_{II}=2$) loading, plane strain, $T=+0.5\sigma_o$.

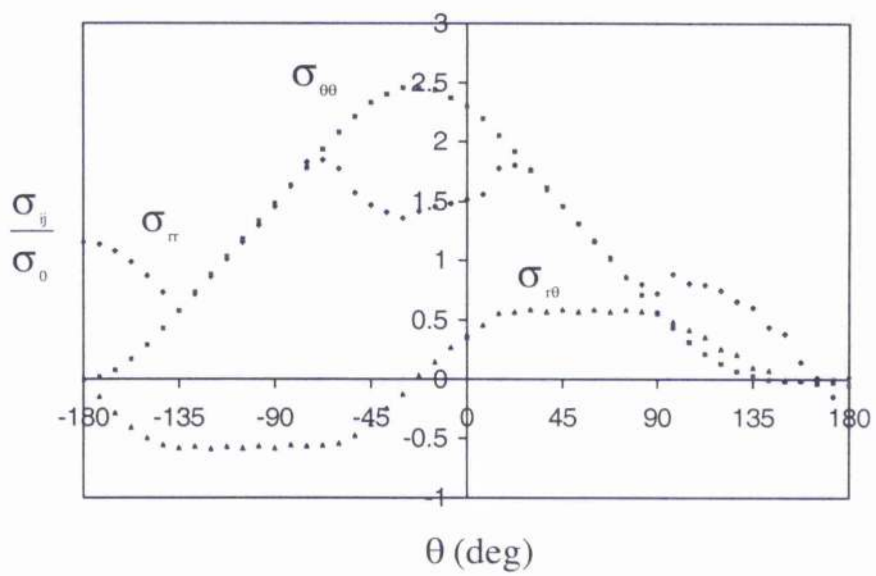

Figure 7.11b: Angular variation of stresses in mixed mode ($K_I/K_{II}=2$) loading, plane strain, $T=+0.5\sigma_o$.

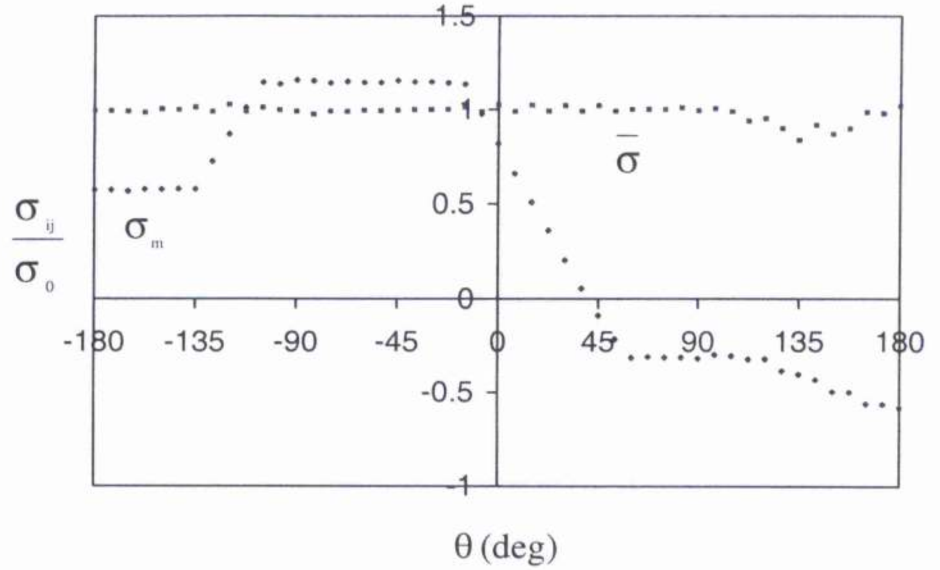

Figure 7.12a: Angular variation of stresses in mixed mode ($K_I/K_{II}=1$) loading, plane strain, $T=-0.5\sigma_0$.

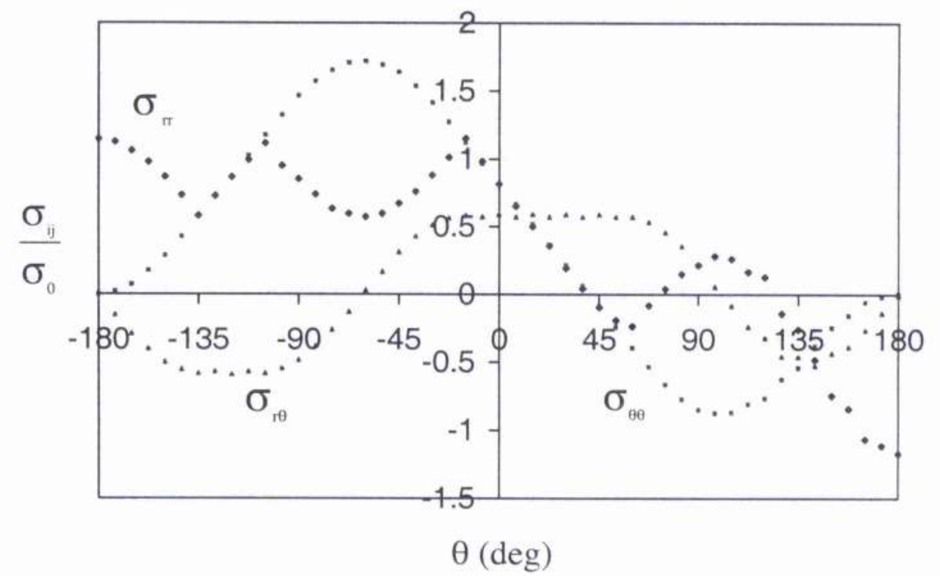

Figure 7.12b: Angular variation of stresses in mixed mode ($K_I/K_{II}=1$) loading, plane strain, $T=-0.5\sigma_0$.

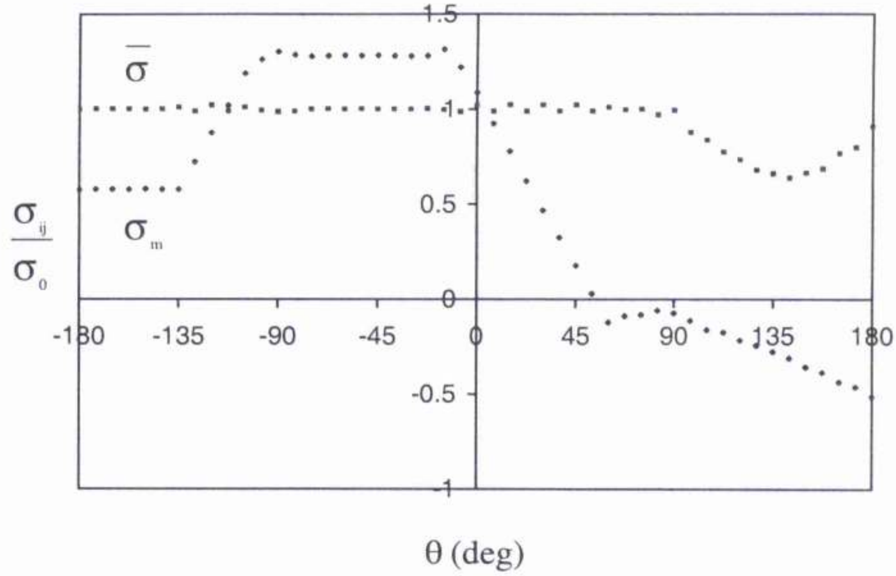

Figure 7.13a: Angular variation of stresses in mixed mode (K_I/K_{II}=1) loading, plane strain, T=0.

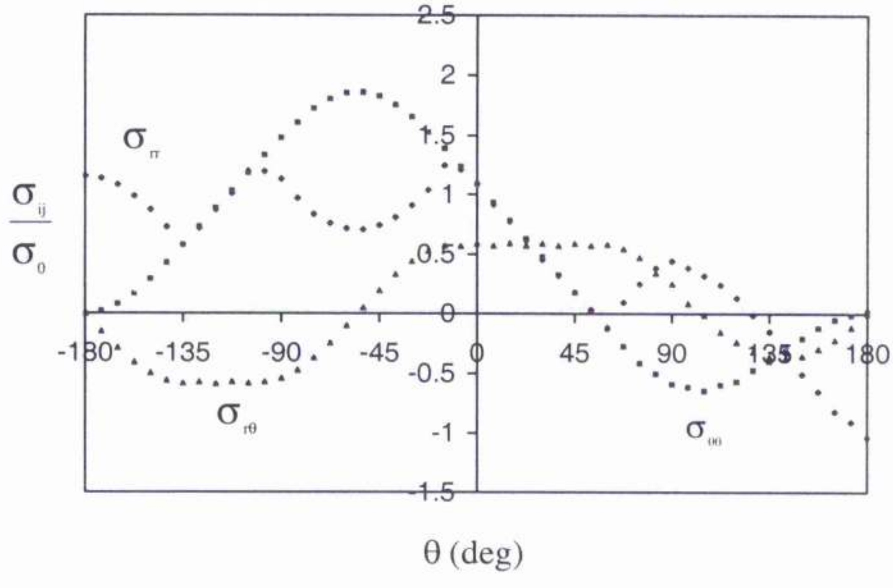

Figure 7.13b: Angular variation of stresses in mixed mode (K_I/K_{II}=1) loading, plane strain, T=0.

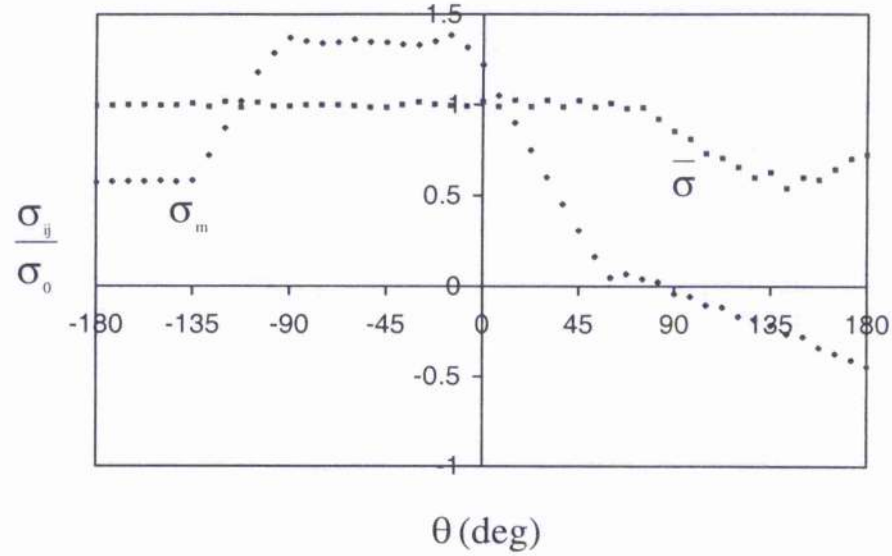

Figure 7.14a: Angular variation of stresses in mixed mode ($K_I/K_{II}=1$) loading, plane strain, $T=+0.5\sigma_0$.

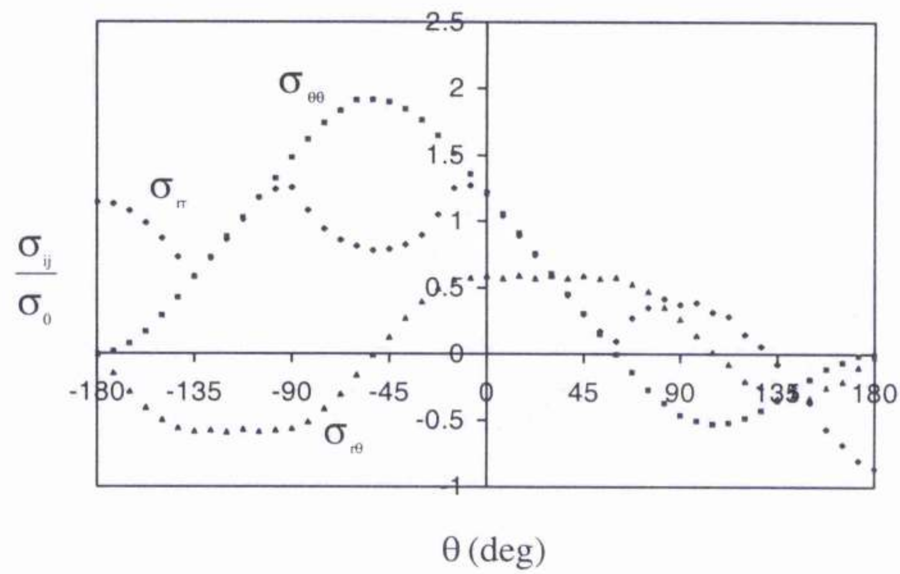

Figure 7.14b: Angular variation of stresses in mixed mode ($K_I/K_{II}=1$) loading, plane strain, $T=+0.5\sigma_0$.

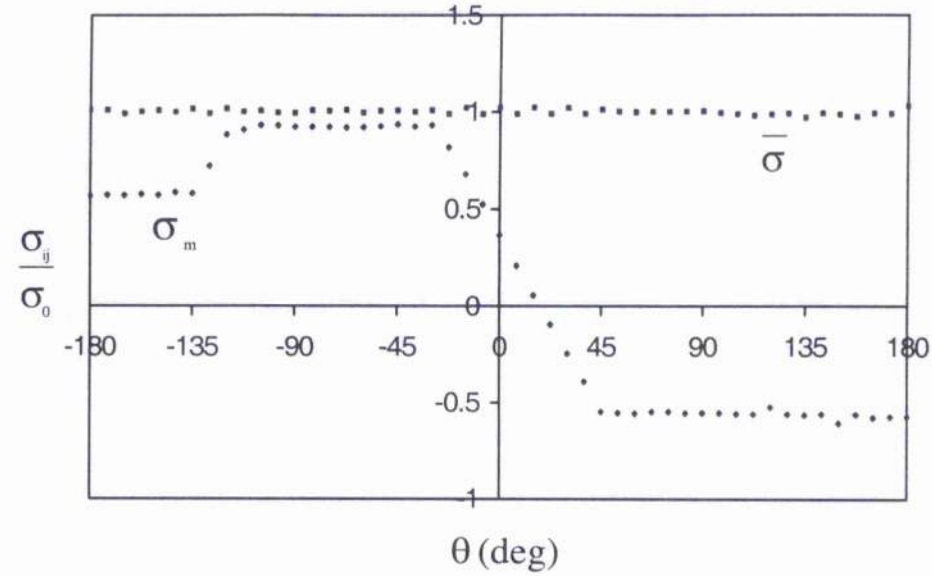

Figure 7.15a: Angular variation of stresses in mixed mode ($K_I/K_{II}=1/2$) loading, plane strain, $T=-0.5\sigma_0$.

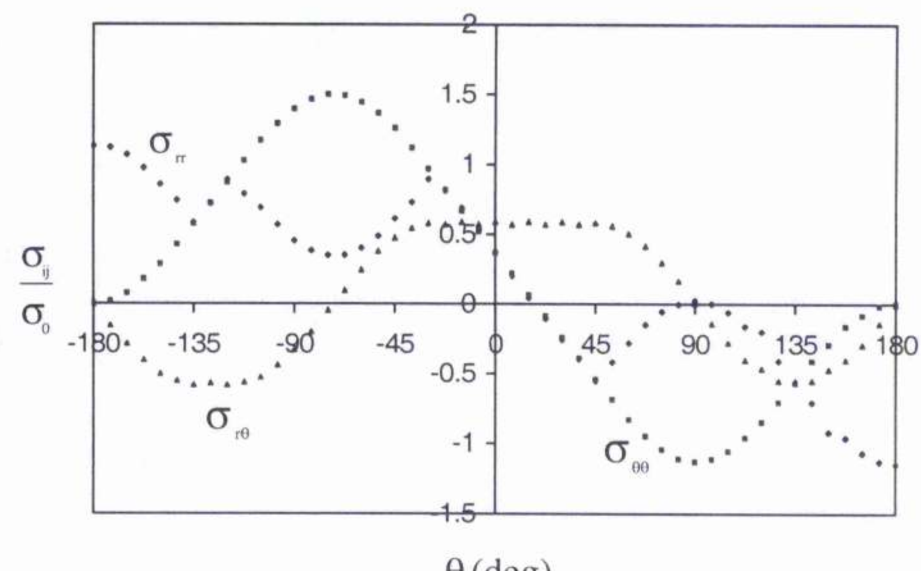

Figure 7.15b: Angular variation of stresses in mixed mode ($K_I/K_{II}=1/2$) loading, plane strain, $T=-0.5\sigma_0$.

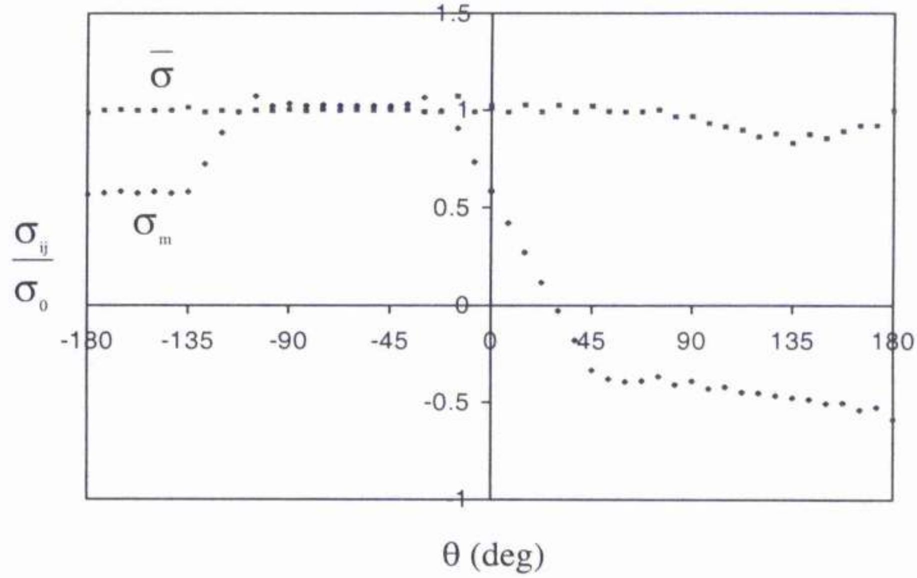

Figure 7.16a: Angular variation of stresses in mixed mode ($K_I/K_{II}=1/2$) loading, plane strain, T=0.

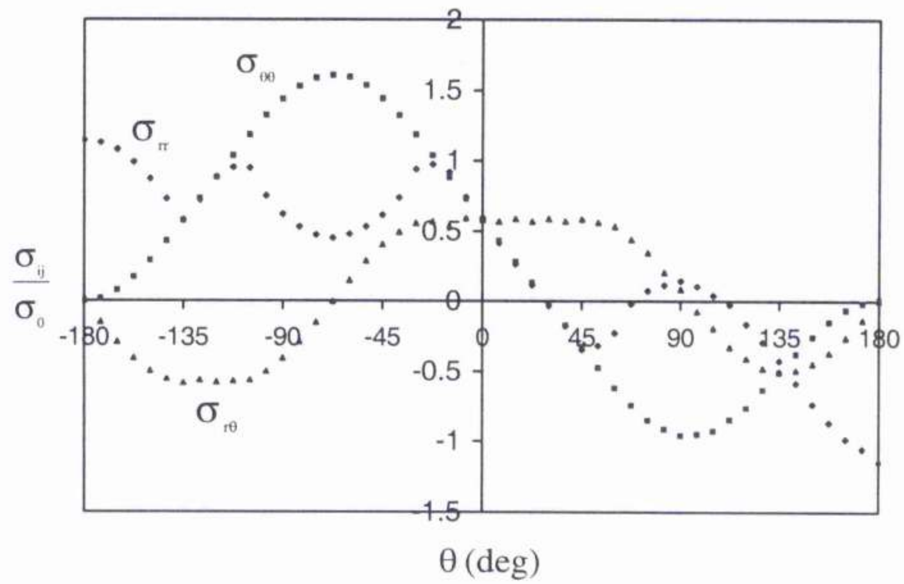

Figure 7.16b: Angular variation of stresses in mixed mode ($K_I/K_{II}=1/2$) loading, plane strain, T=0.

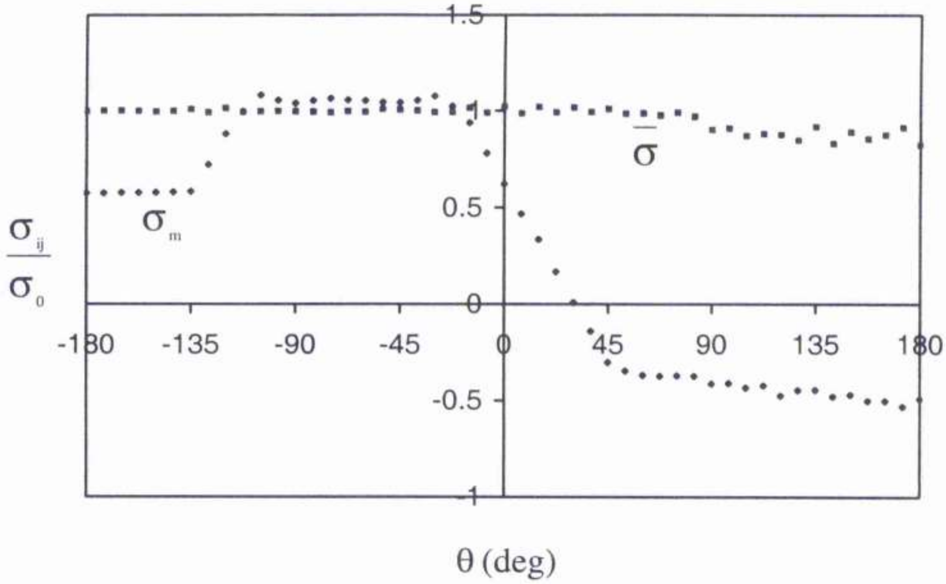

Figure 7.17a: Angular variation of stresses in mixed mode (K_I/K_{II}=1/2) loading, plane strain, T=+0.5σ_0.

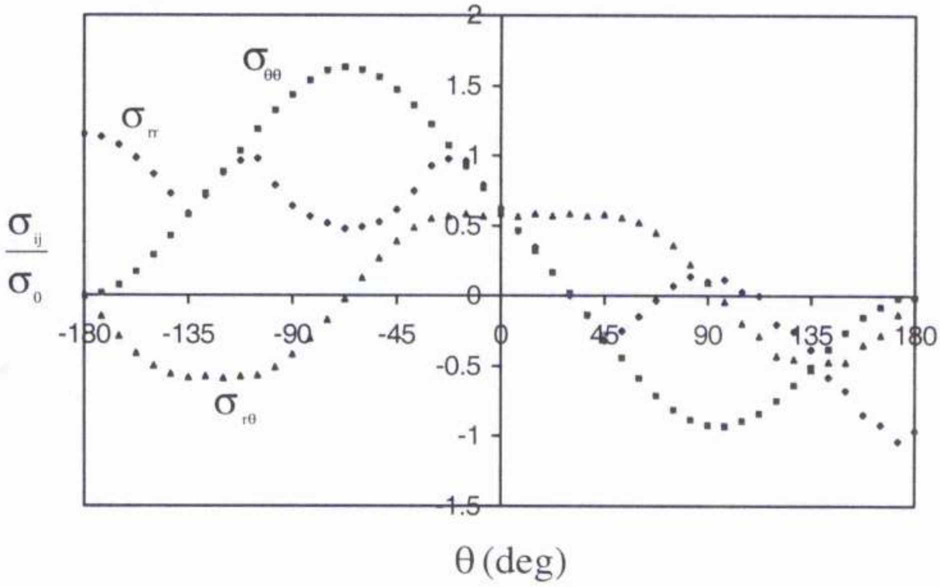

Figure 7.17b: Angular variation of stresses in mixed mode (K_I/K_{II}=1/2) loading, plane strain, T=+0.5σ_0.

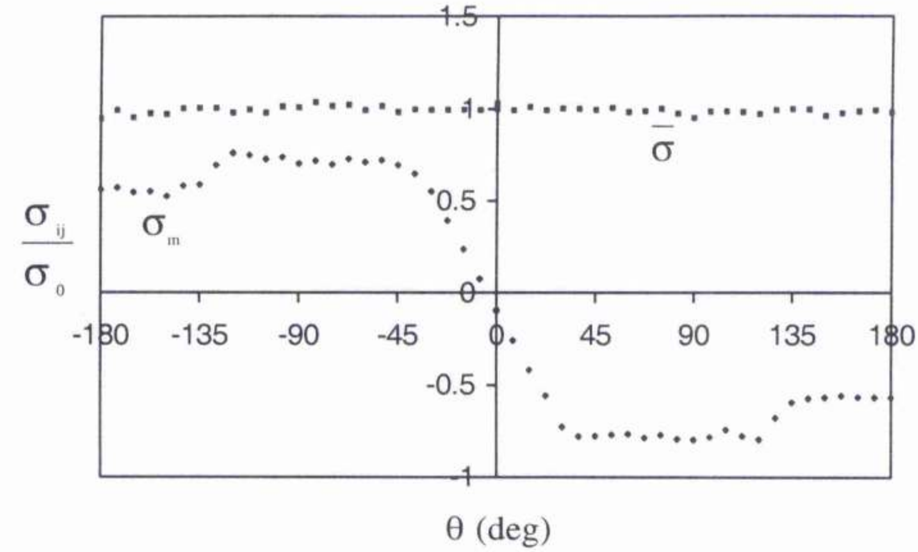

Figure 7.18a: Angular variation of stresses in mode II loading, plane strain, T=-0.5σ_0.

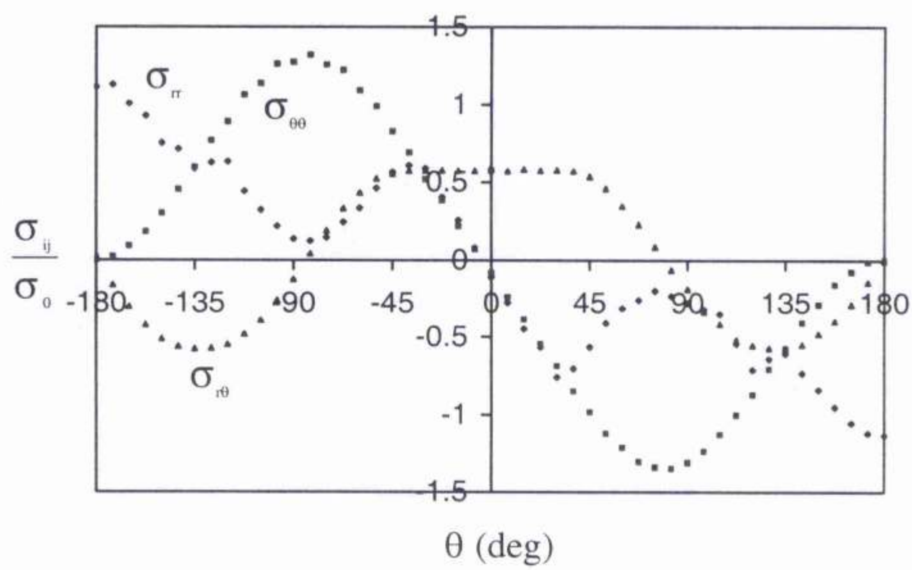

Figure 7.18b: Angular variation of stresses in mode II loading, plane strain, T=-0.5σ_0.

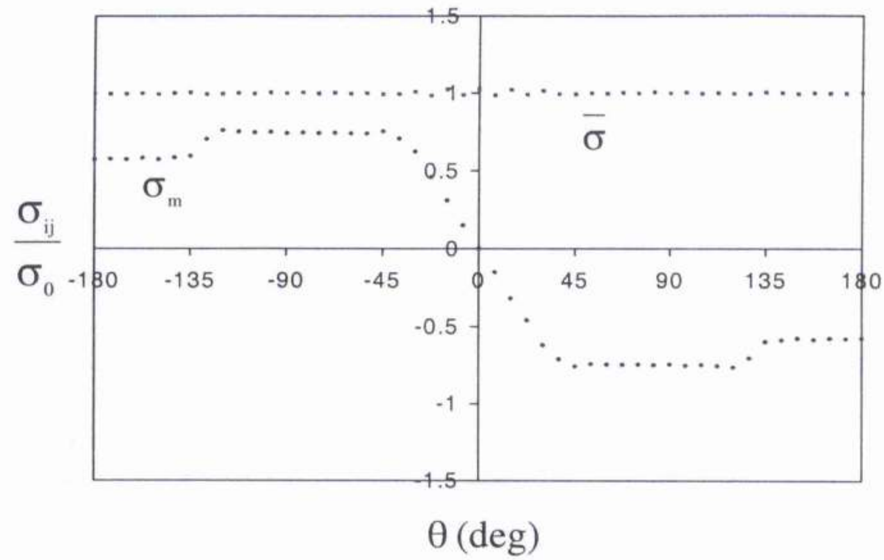

Figure 7.19a: Angular variation of stresses in mode II loading, plane strain, T=0.

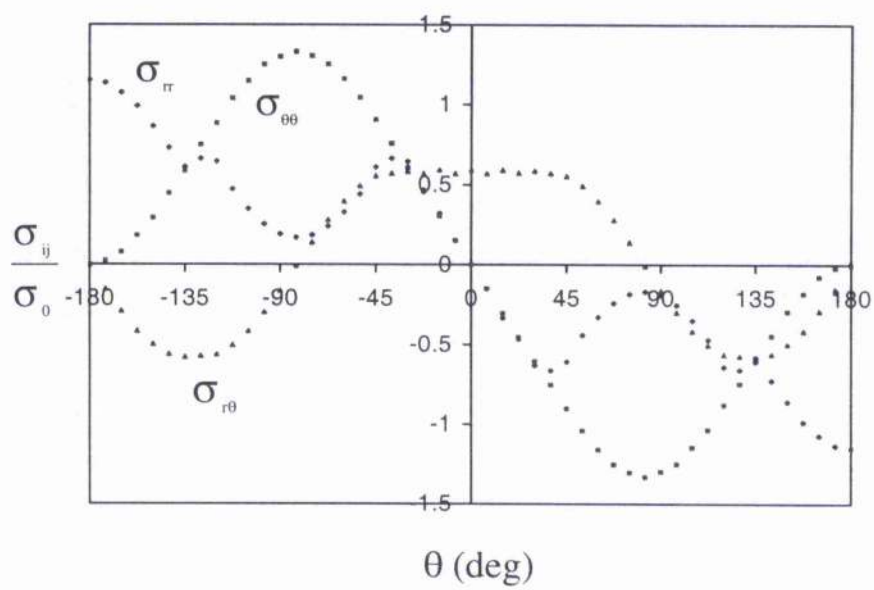

Figure 7.19b: Angular variation of stresses in mode II loading, plane strain, T=0.

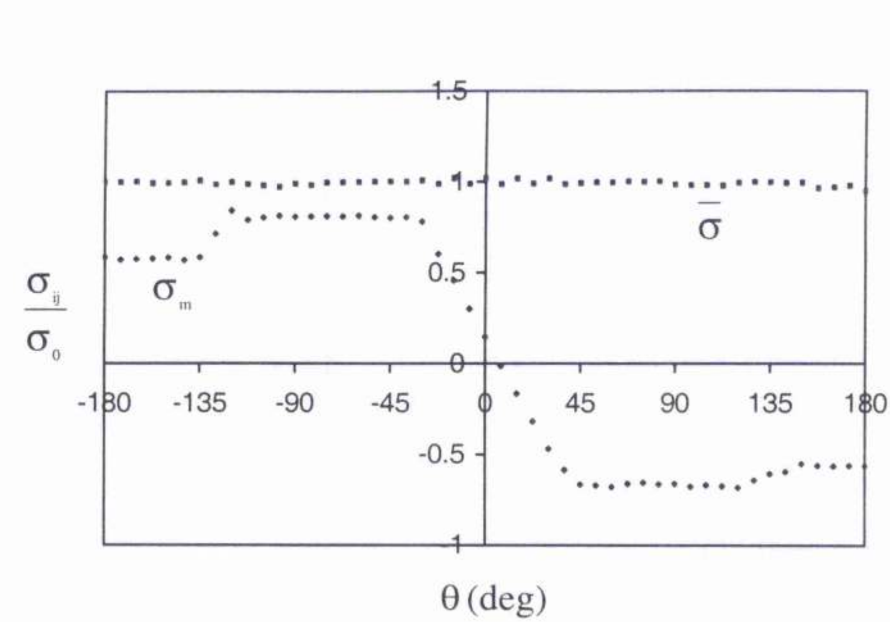

Figure 7.20a: Angular variation of stresses in mode II loading, plane strain, $T=+0.5\sigma_0$.

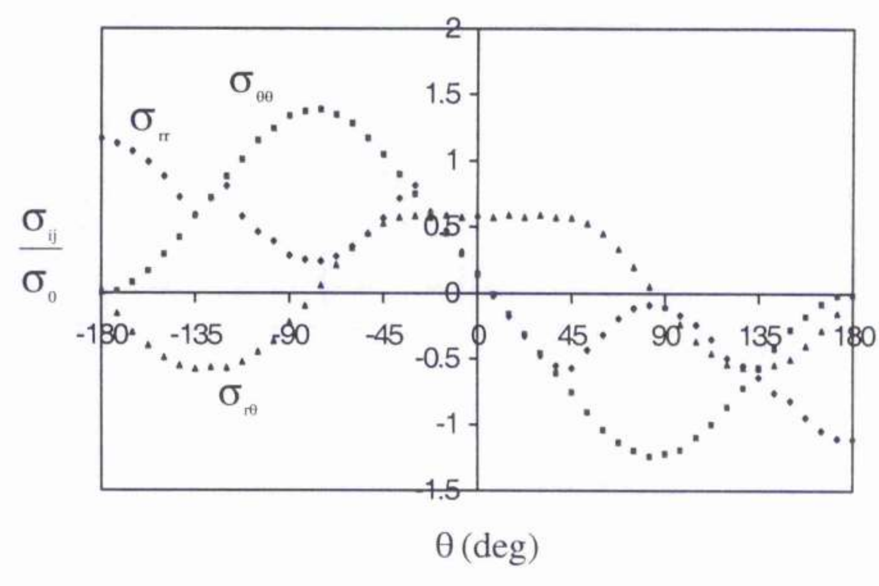

Figure 7.20b: Angular variation of stresses in mode II loading, plane strain, $T=+0.5\sigma_0$.

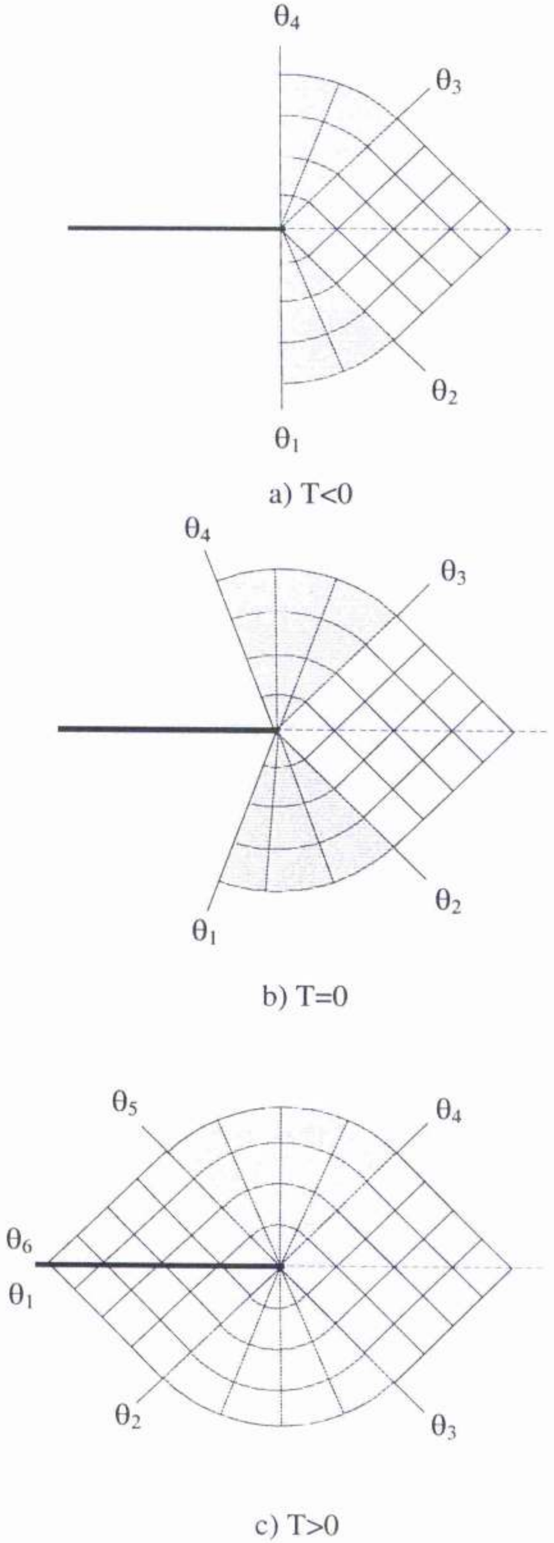

Figure 7.21: Slip line fields under mode I loading, plane strain.

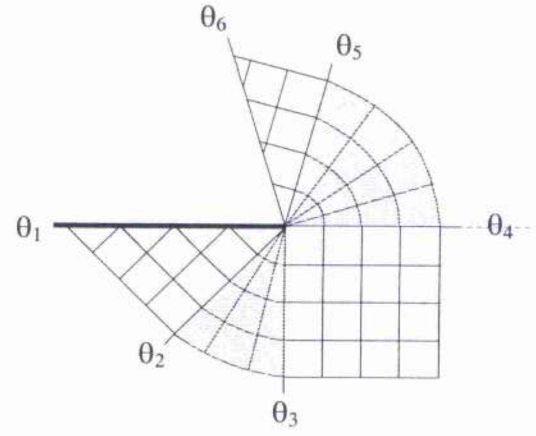

a) T<0

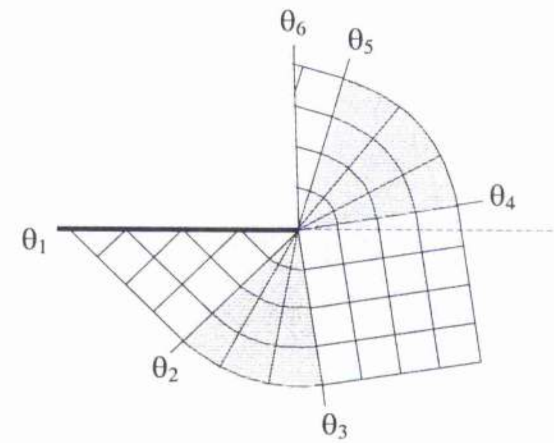

b) T=0

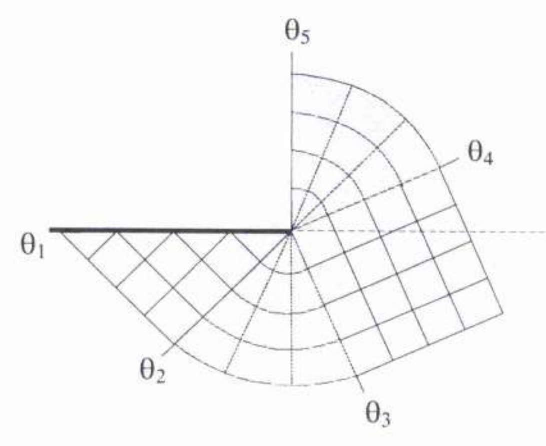

c) T>0

Figure 7.22: Slip line fields under mixed mode ($K_I/K_{II}=2$) loading, plane strain.

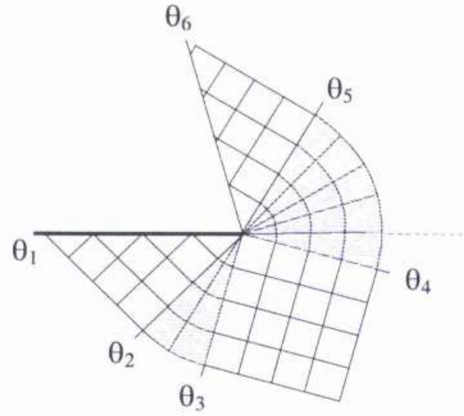

a) T<0

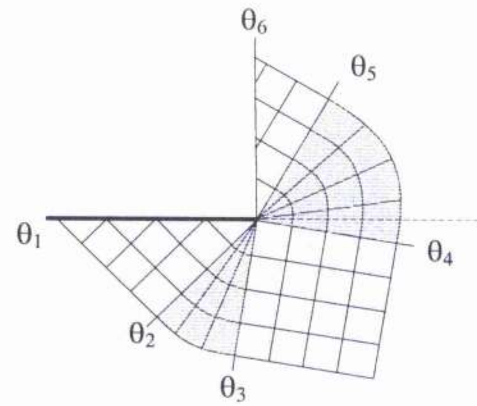

b) T=0

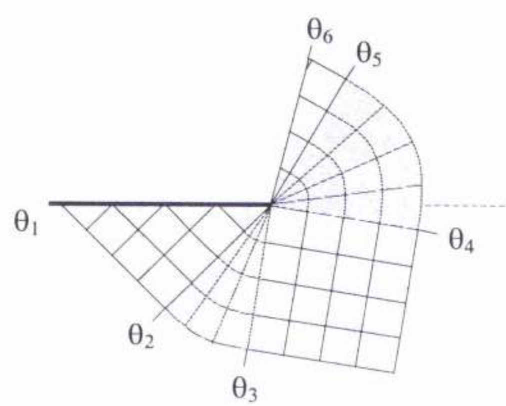

c) T>0

Figure 7.23: Slip line fields under mixed mode ($K_I/K_{II}=1$) loading, plane strain.

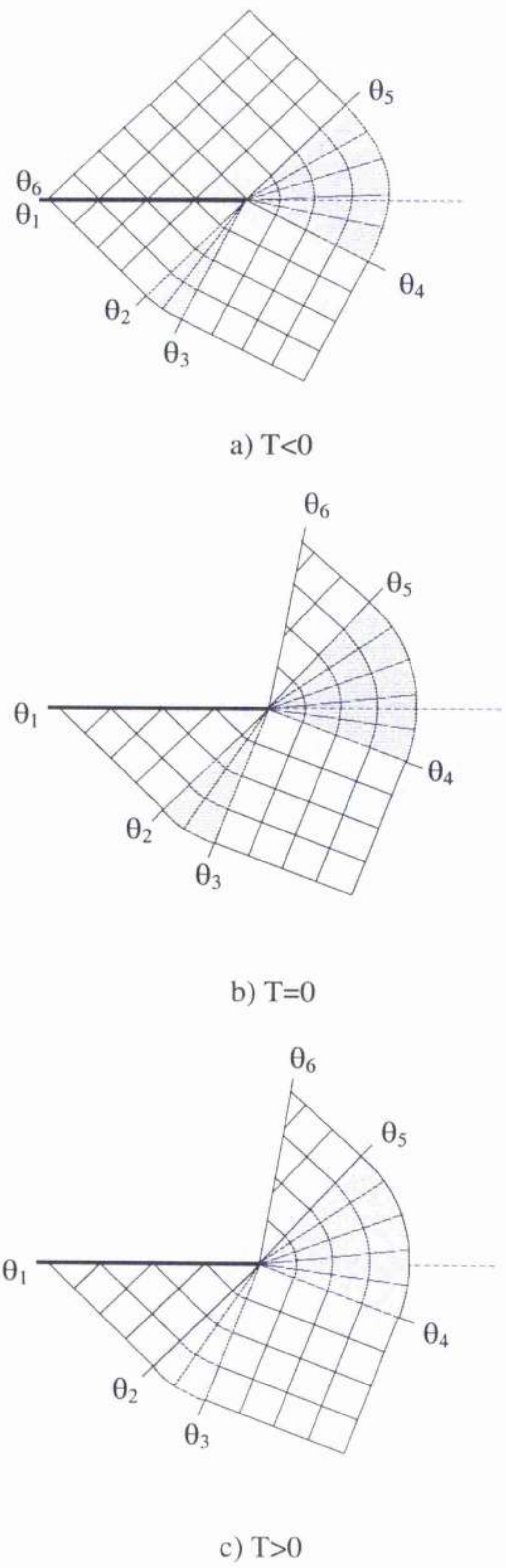

Figure 7.24: Slip line fields under mixed mode ($K_I/K_{II}=1/2$) loading, plane strain.

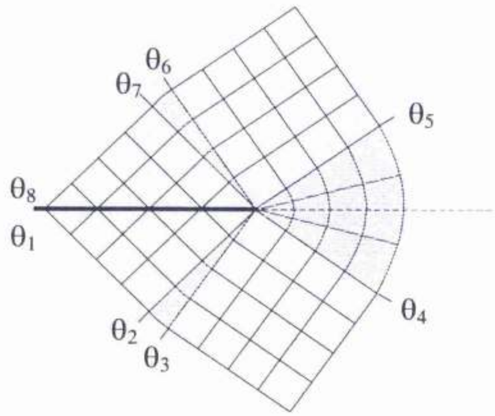

a) T<0

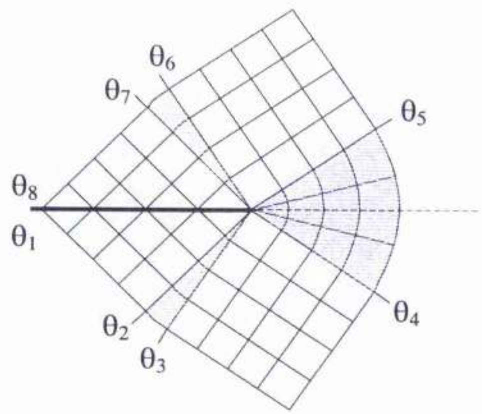

b) T=0

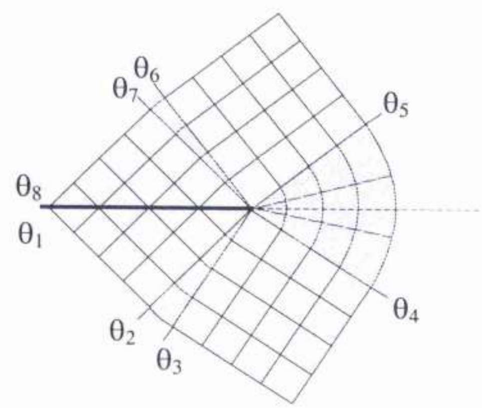

c) T>0

Figure 7.25: Slip line fields under mode II loading, plane strain.

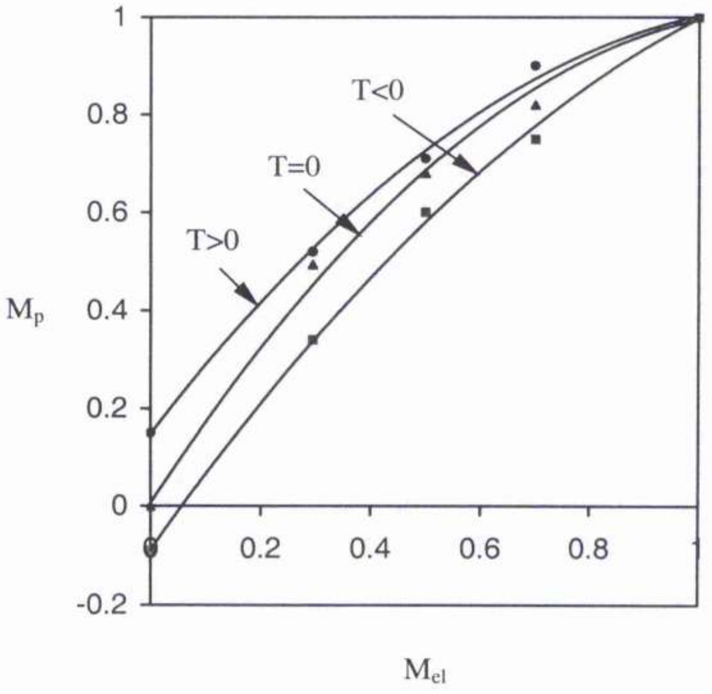

Figure 7.26: Elastic mixity (M_{el}) versus plastic mixity (M_p) in plane strain.

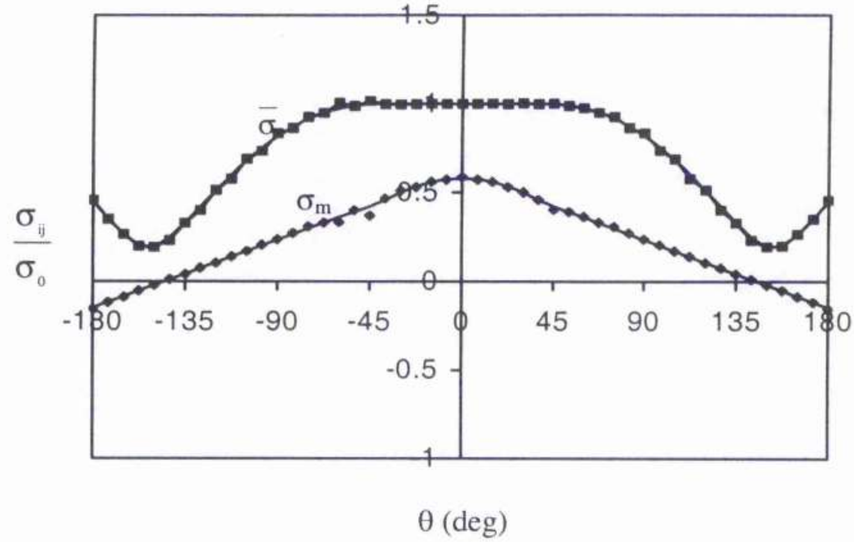

Figure 7.27a: Angular variation of stresses in mode I loading, plane stress, T=0.

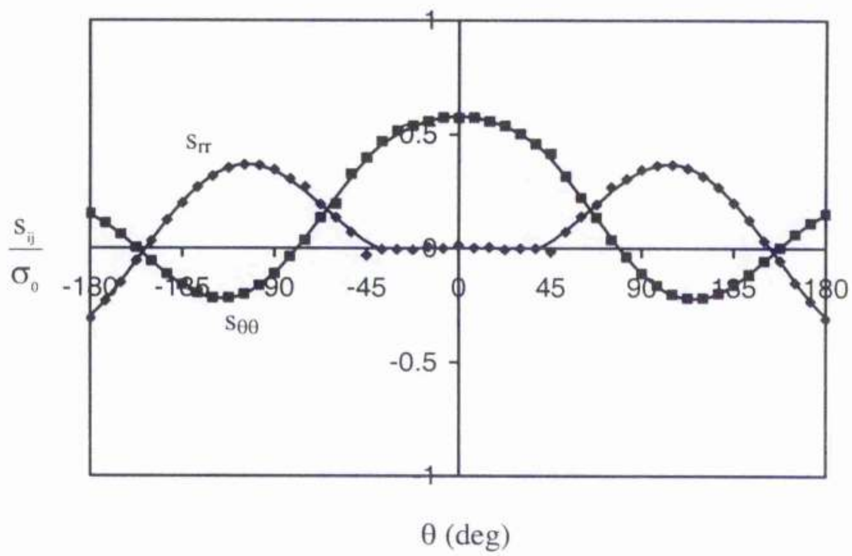

Figure 7.27b: Angular variation of deviatoric stresses in mode I loading, plane stress, T=0.

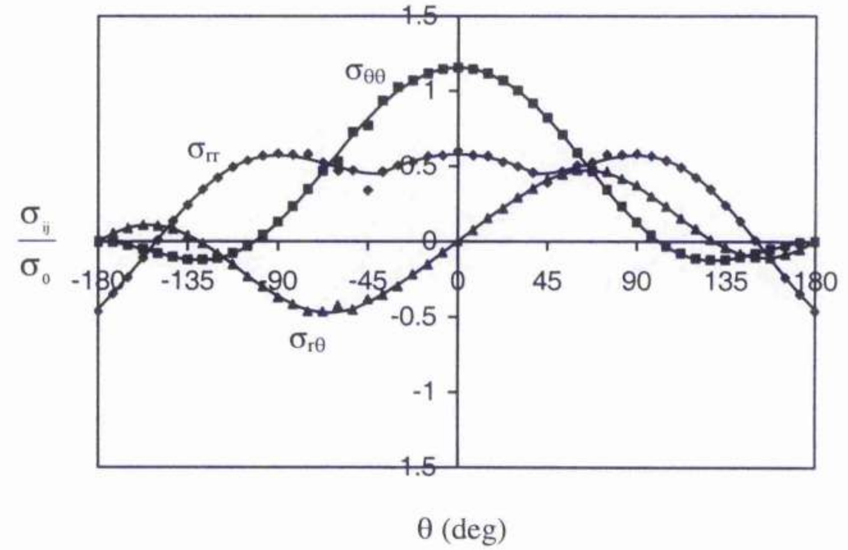

Figure 7.27c: Angular variation of stresses in mode I loading, plane stress, T=0.

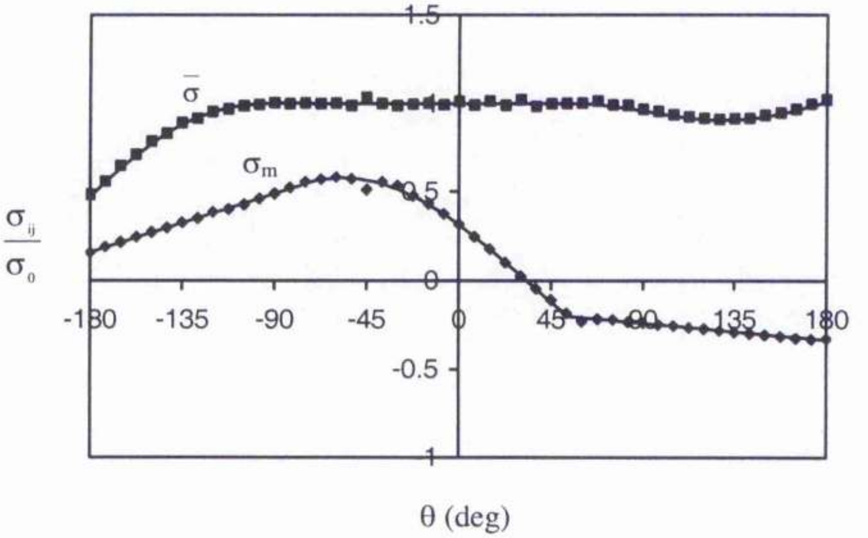

Figure 7.28a: Angular variation of stresses in mixed mode (K_I/K_{II}=1) loading, plane stress, T=0.

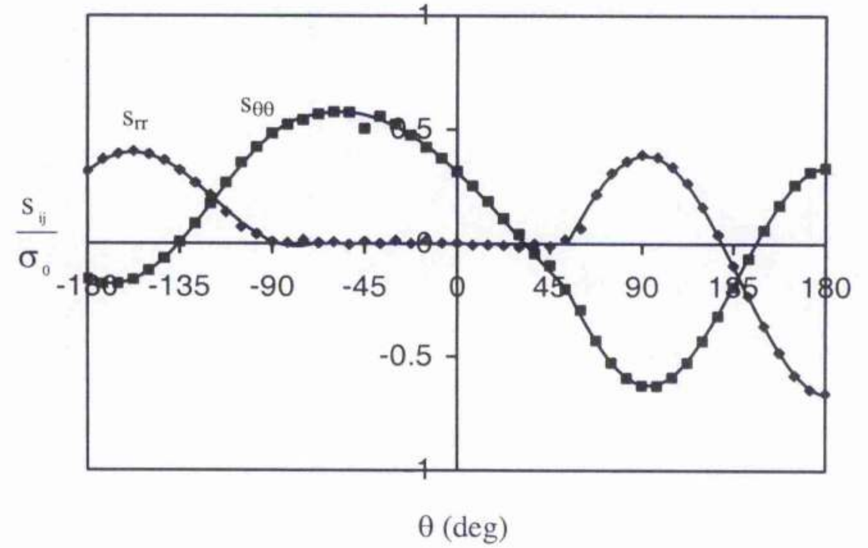

Figure 7.28b: Angular variation of deviatoric stresses in mixed mode (K_I/K_{II}=1) loading, plane stress, T=0.

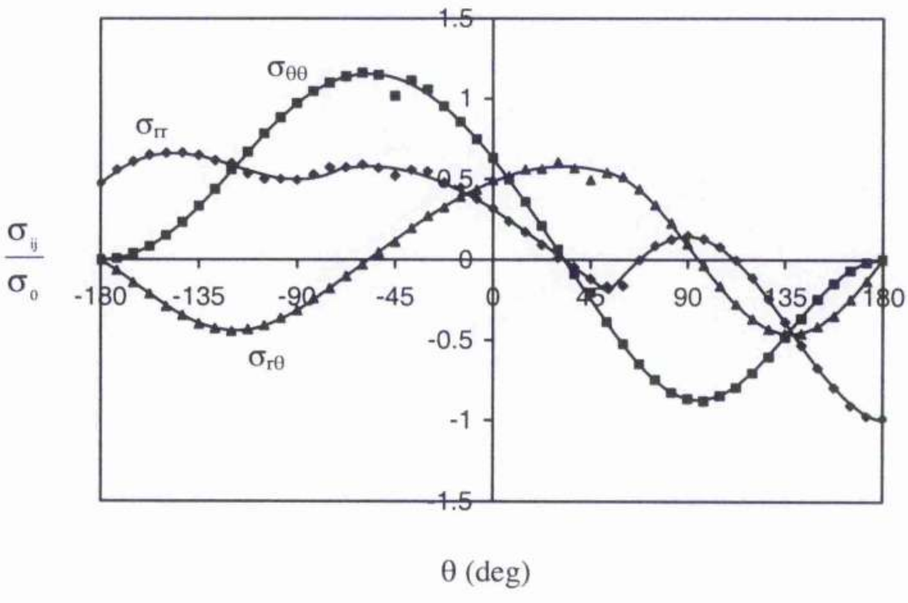

Figure 7.28c: Angular variation of stresses in mixed mode ($K_I/K_{II}=1$) loading, plane stress, T=0.

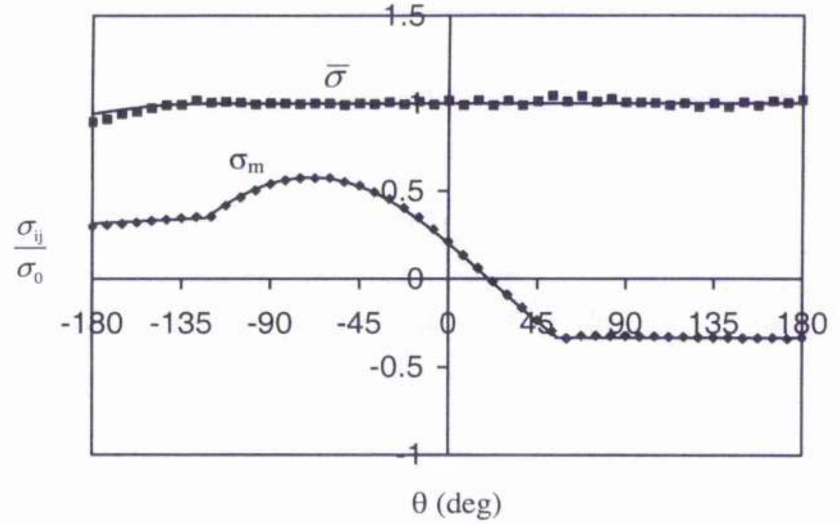

Figure 7.29a: Angular variation of stresses in mixed mode ($K_I/K_{II}=1/2$) loading, plane stress, T=0.

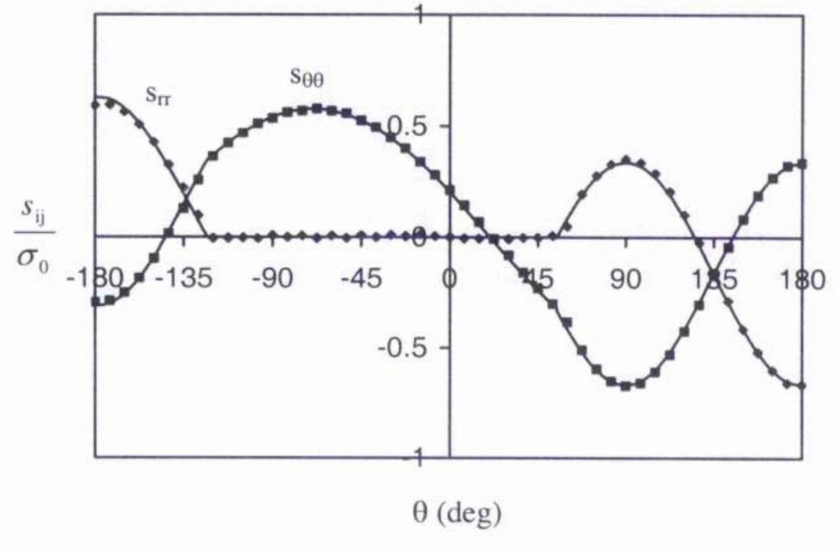

Figure 7.29b: Angular variation of deviatoric stresses in mixed mode ($K_I/K_{II}=1/2$) loading, plane stress, T=0.

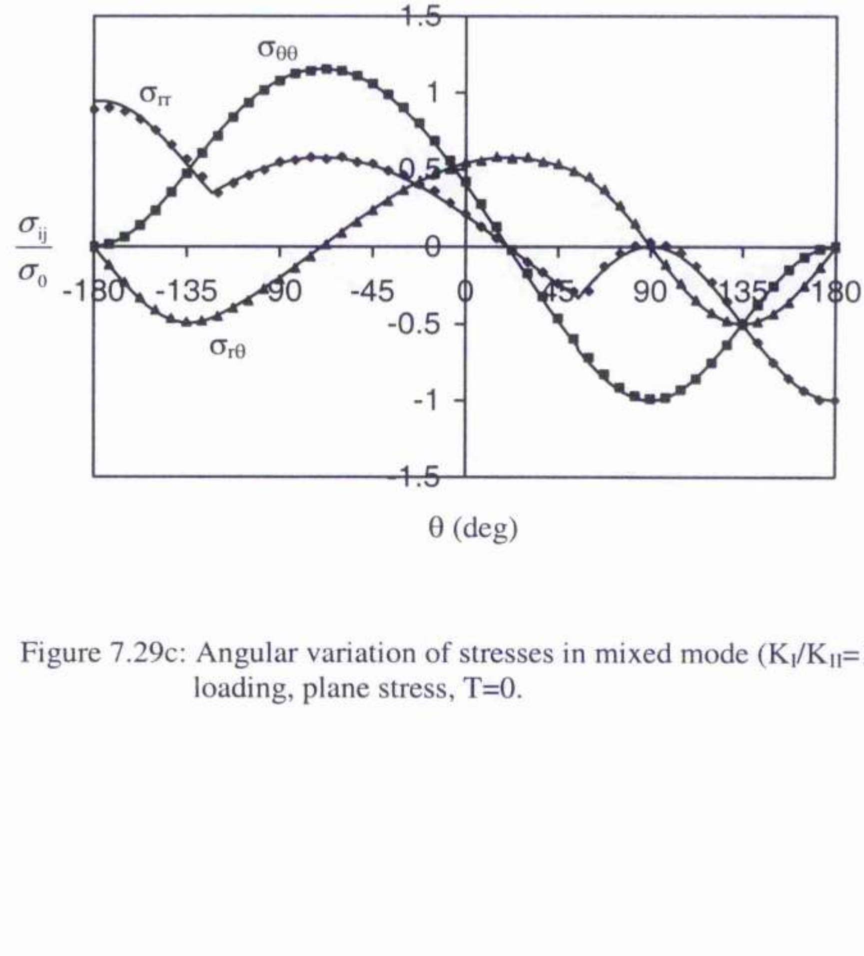

Figure 7.29c: Angular variation of stresses in mixed mode ($K_I/K_{II}=1/2$) loading, plane stress, T=0.

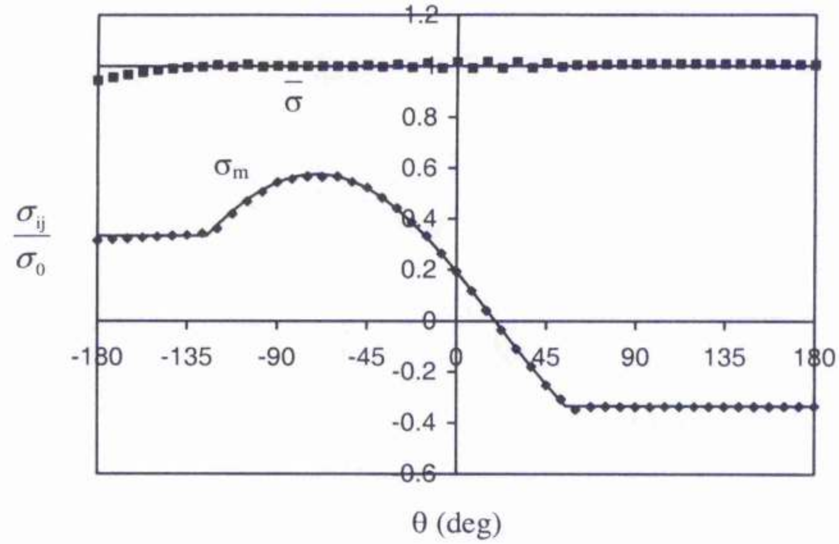

Figure 7.30a: Angular variation of stresses in mixed mode (K_I/K_{II}=0.45) loading, plane stress, T=0.

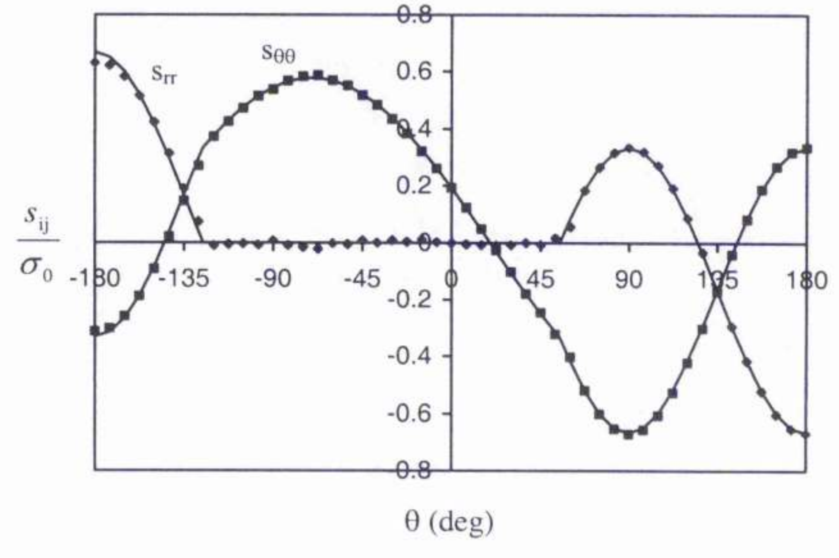

Figure 7.30b: Angular variation of deviatoric stresses in mixed mode (K_I/K_{II}=0.45) loading, plane stress, T=0.

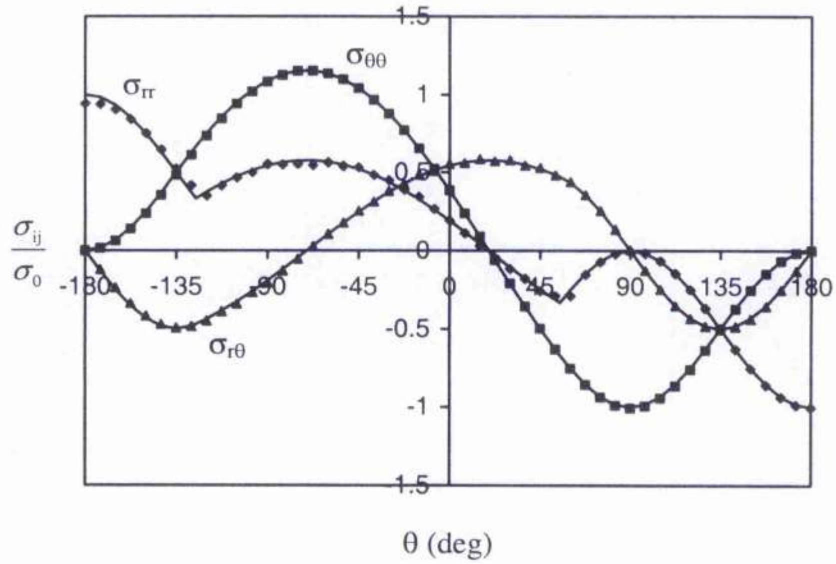

Figure 7.30c: Angular variation of stresses in mixed mode (K_I/K_{II}=0.45) loading, plane stress, T=0.

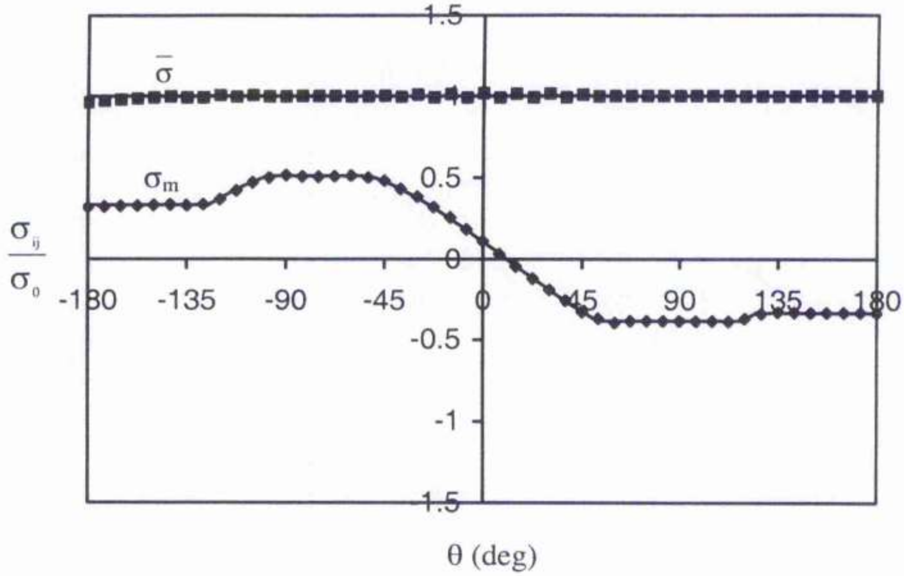

Figure 7.31a: Angular variation of stresses in mixed mode ($K_I/K_{II}=1/4$) loading, plane stress, T=0.

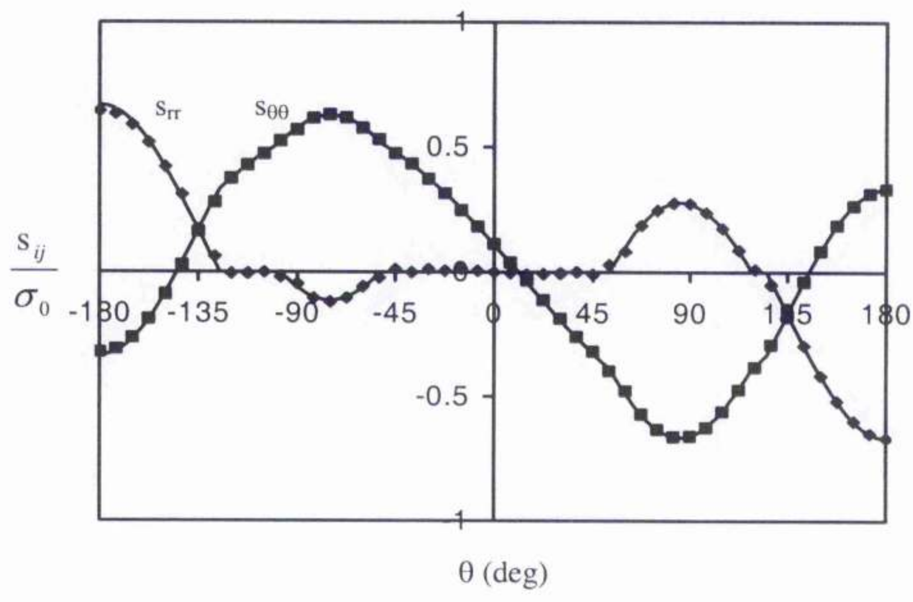

Figure 7.31b: Angular variation of deviatoric stresses in mixed mode ($K_I/K_{II}=1/4$) loading, plane stress, T=0.

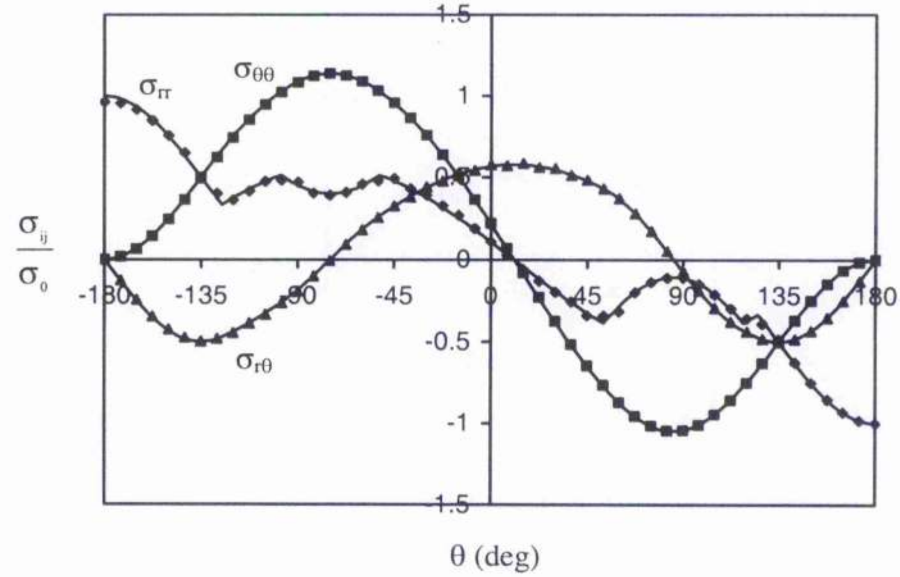

Figure 7.31c: Angular variation of stresses in mixed mode ($K_I/K_{II}=1/4$) loading, plane stress, T=0.

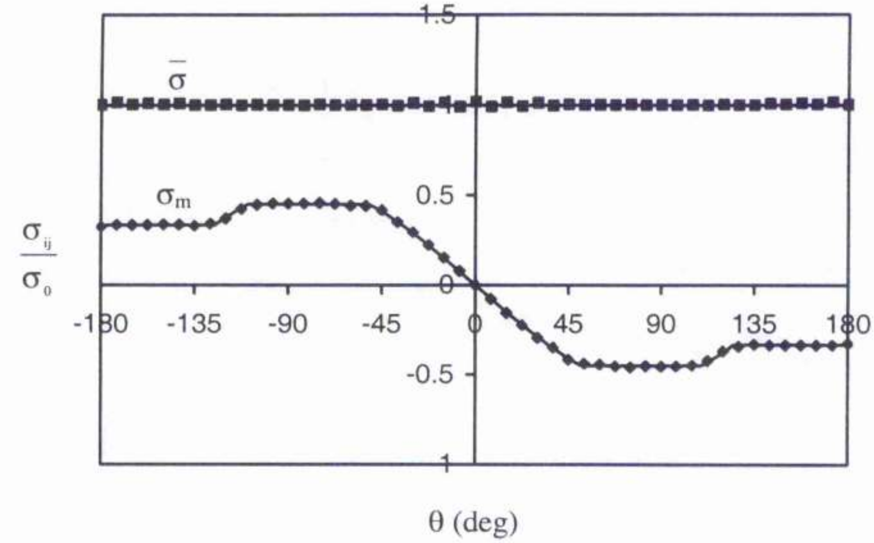

Figure 7.32a: Angular variation of stresses in mode II loading, plane stress, T=0.

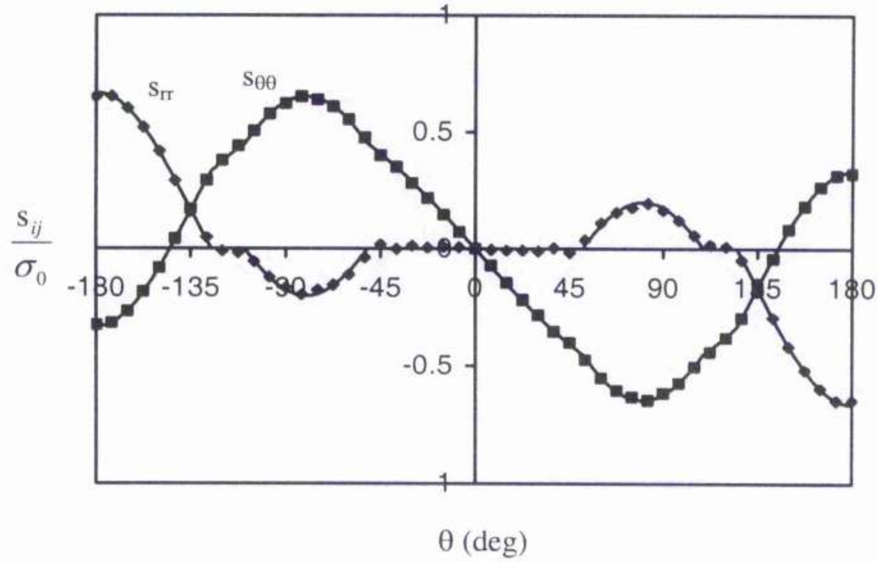

Figure 7.32b: Angular variation of deviatoric stresses in mode II loading, plane stress, T=0.

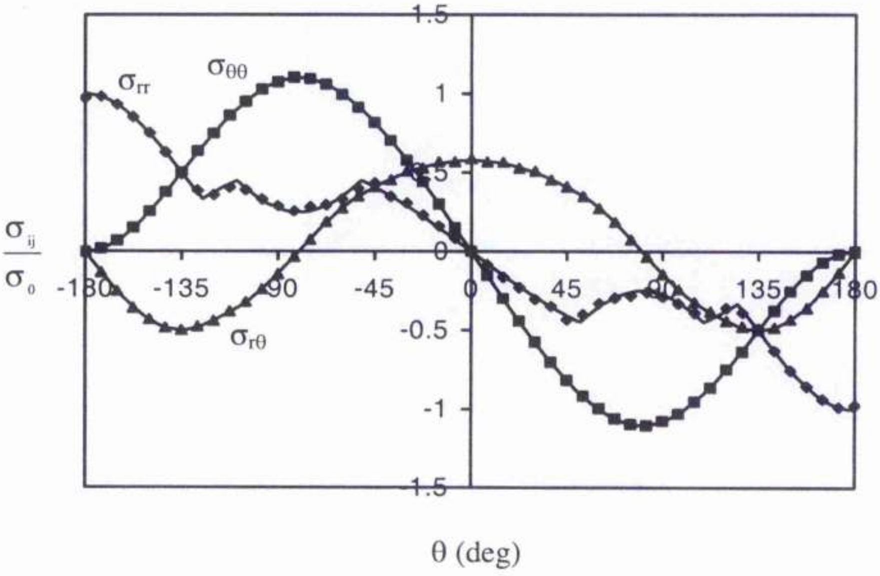

Figure 7.32c: Angular variation of stresses in mode II loading, plane stress, T=0.

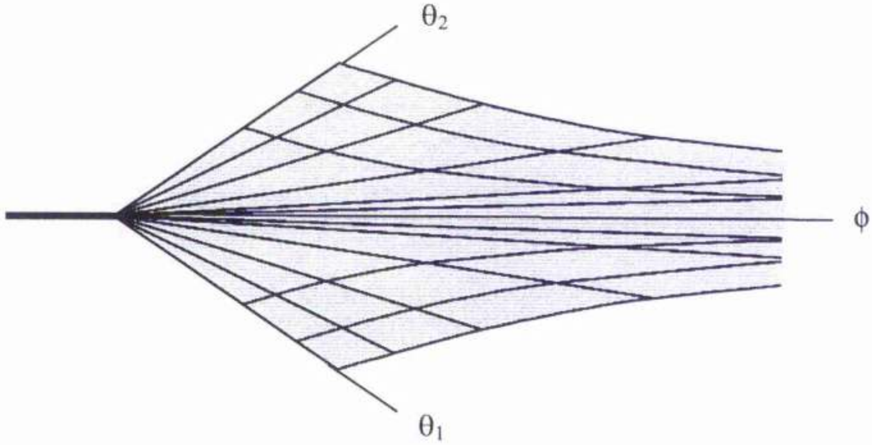

Figure 7.33: Slip line field at the crack tip under mode I loading, plane stress, T=0.

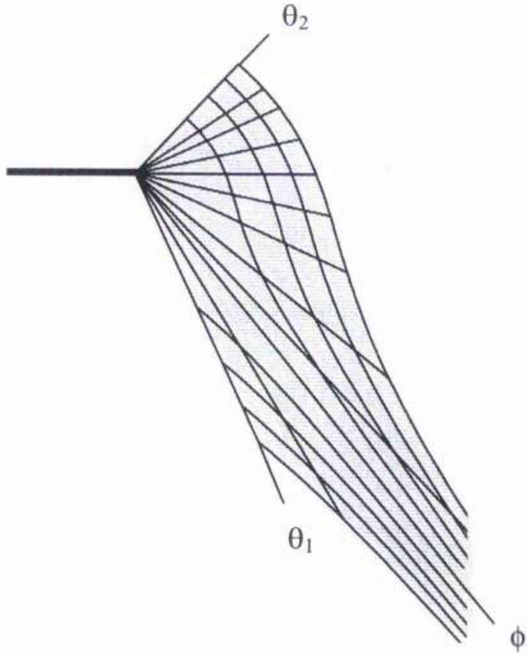

Figure 7.34: Slip line field at the crack tip under mixed mode ($K_I/K_{II}=1$) loading, plane stress, T=0.

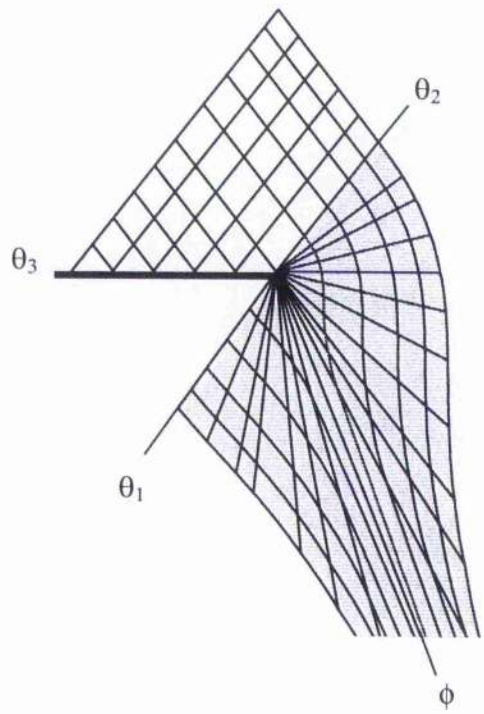

Figure 7.35: Slip line field at the crack tip under mixed mode ($K_I/K_{II}=1/2$) loading, plane stress, T=0.

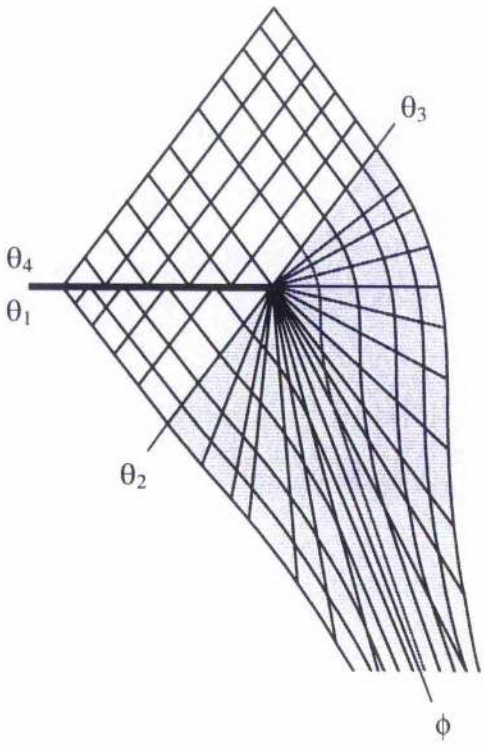

Figure 7.36: Slip line field at the crack tip under mixed mode (K_I/K_{II}=0.45) loading, plane stress, T=0.

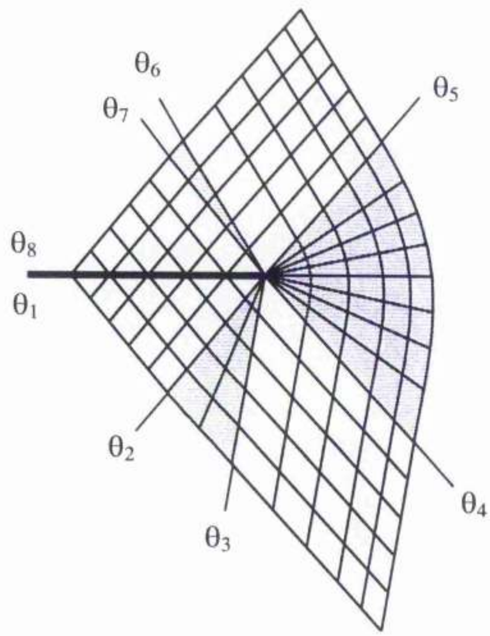

Figure 7.37: Slip line field at the crack tip under mixed mode
(K_I/K_{II}=1/4) loading, plane stress, T=0.

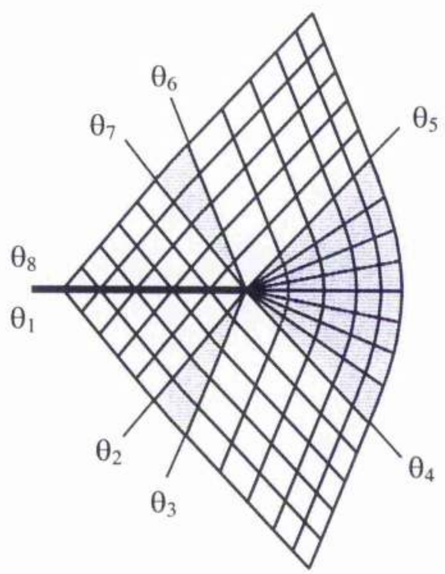

Figure 7.38: Slip line field at the crack tip under mode II loading, plane stress, T=0.

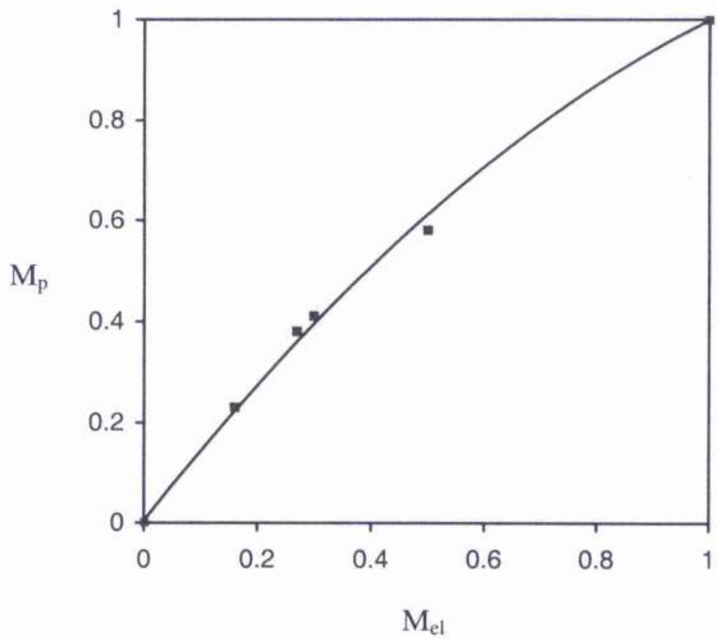

Figure 7.39: Elastic mixity (M_{el}) versus plastic mixity (M_p) in plane stress, T=0.

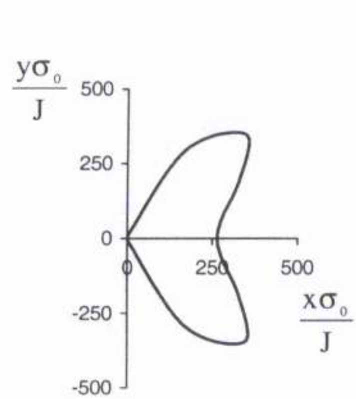

a) $T=-0.5\sigma_0$

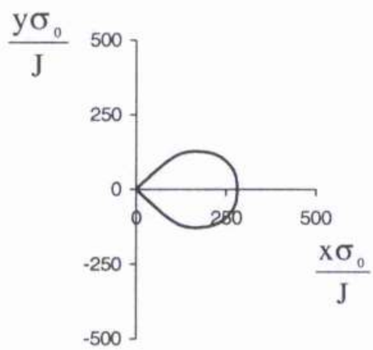

b) $T=0$

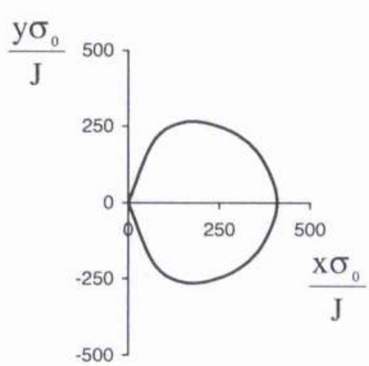

c) $T=+0.5\sigma_0$

Figure 7.40: Effect of T-stress on crack tip plastic zone under mode I loading, plane stress.

Loading mode	Elastic mixity (M_{el})	Plastic mixity (M_p)		
		$T=-0.5\sigma_0$	$T=0$	$T=+0.5\sigma_0$
K_I	1	1	1	1
$K_I/K_{II} = 2$	0.70	0.75	0.82	0.90
$K_I/K_{II} = 1$	0.50	0.60	0.68	0.71
$K_I/K_{II} = 1/2$	0.30	0.34	0.49	0.52
K_{II}	0	-0.09	0	0.15

Table 7.1: Elastic and plastic mixities, plane strain.

Loading mode	Mode of T-stress	Critical angle (anti-clockwise positive) in degree							
		θ_1	θ_2	θ_3	θ_4	θ_5	θ_6	θ_7	θ_8
K_I	T<0	-90	-45	+45	+90				
	T=0	-120	-45	+45	+120				
	T>0	-180	-135	-45	+45	+135	+180		
$K_I/K_{II}=2$	T<0	-180	-135	-90	0	+75	+107		
	T=0	-180	-135	-81	+9	+74	+92		
	T>0	-180	-135	-67	+23	+90			
$K_I/K_{II}=1$	T<0	-180	-135	-105	-15	+60	+107		
	T=0	-180	-135	-99	-9	+60	+91		
	T>0	-180	-135	-99	-9	+60	+76		
$K_I/K_{II}=1/2$	T<0	-180	-135	-117	-27	+45	+180		
	T=0	-180	-135	-111	-21	+48	+80		
	T>0	-180	-135	-111	-21	+48	+81		
K_{II}	T<0	-180	-135	-125	-35	+35	+125	+135	+180
	T=0	-180	-135	-124	-34	+34	+124	+135	+180
	T>0	-180	-135	-123	-33	+39	+129	+135	+180

Table 7.2: Critical angles on the slip line fields, plane strain.

Mode of loading	J_{local}/J_{remote} $(T=-0.5\sigma_0)$	J_{local}/J_{remote} $(T=0)$	J_{local}/J_{remote} $(T=+0.5\sigma_0)$
K_I	0.93	0.92	0.86
$K_I/K_{II}=2$	0.99	0.93	0.89
$K_I/K_{II}=1$	1.08	0.98	0.89
$K_I/K_{II}=1/2$	1.06	0.98	0.98
K_{II}	1.04	1	1.05

Table 7.3: J_{local}/J_{remote} ratios under mode I, II and mixed mode (I/II) loading, plane strain.

Loading mode	Elastic mixity (M_{el})	Plastic mixity (M_p)
K_I	1	1
$K_I/K_{II} = 1$	0.50	0.58
$K_I/K_{II} = 1/2$	0.30	0.41
$K_I/K_{II} = 0.45$	0.27	0.38
$K_I/K_{II} = 1/4$	0.16	0.23
K_{II}	0	0

Table 7.4: Elastic and plastic mixities in plane stress, T=0.

Loading mode	Critical angle (anti-clockwise positive) in degree							
	θ_1	θ_2	θ_3	θ_4	θ_5	θ_6	θ_7	θ_8
K_I	-39.126	39.126						
$K_I/K_{II}=1$	-69.6	53.34						
$K_I/K_{II}=1/2$	-122.87	54.7	180					
$K_I/K_{II}=0.45$	-180	-125.3	54.7	180				
$K_I/K_{II}=1/4$	-180	-125.3	-97.83	-51.92	52.77	118.6	125.3	180
K_{II}	-180	-125.3	-109.32	-51.21	51.21	109.32	125.3	180

Table 7.5: Critical angles on the slip line fields, plane stress, T=0.

Chapter 8 Plane stress analytical solutions

The concepts of plane strain and plane stress slip line fields and some of plane strain and plane stress mixed mode (I/II) slip line fields were introduced in Chapter 4. This Chapter develops the analytical solutions of the plane stress crack tip fields presented in Chapter 7. The structure of the asymptotic elastic-plastic crack tip fields can be determined by idealising the material response as elastic perfectly-plastic, which allows the use of slip line theory (Hill, 1950) both for plane stress and plane strain conditions. As discussed in Chapter 4 the plane stress asymptotic crack tip fields can be divided into elastic and plastic sectors. The region over which yield criterion is not satisfied defines the elastic sector and the region in which yield criterion is satisfied identifies the plastic sector. Rice (1982) has shown that under plane stress, with the assumption that the crack tip stresses are finite, plus the incompressibility condition and the yield criterion, allows the asymptotic equilibrium equation to provide two possible solutions for the plastic sector. These two solutions correspond to constant stress and curved fan sectors. In a constant stress sector mean stress, σ_m is constant. Within a constant stress sector the slip lines are straight and non-orthogonal. The angle between the slip lines can be determined by using the stress-strain relations in conjunction with the stress transformation equations to determine the angle between the lines of zero extension. In uniaxial tension or compression the slip lines are symmetrically disposed at $\pm 54.7^0$ and $\pm 125.3^0$ to the direction of uniaxial stress. In a curved fan sector the radial stress deviator, $s_{rr} = 0$ and $\sigma_{\theta\theta} = 2\sigma_{rr}$. This sector consists of a set of straight lines and a set of curves. The cylindrical stresses within a curved fan sector can be given as:

$$\sigma_{rr} = \pm\, k \cos(\theta - \phi)$$

$$\sigma_{\theta\theta} = \pm\, 2k \cos(\theta - \phi)$$

$$\sigma_{r\theta} = \pm\, k \sin(\theta - \phi) \qquad (8.1)$$

where, k is yield stress in shear and ϕ is the angle to which the curved lines are asymptotic. The stresses within an elastic sector can be given by the semi-infinite wedge solution of Timoshenko and Goodier (1970), subject to the requirement that the yield criterion is not violated:

$$\sigma_{rr} = A_1 \sin 2\theta + A_2 \cos 2\theta + (A_3\theta + A_4)/2$$

$$\sigma_{\theta\theta} = -A_1 \sin 2\theta - A_2 \cos 2\theta + (A_3\theta + A_4)/2$$

$$\sigma_{r\theta} = A_1 \cos 2\theta - A_2 \sin 2\theta - A_3/4 \qquad (8.2)$$

where, A_1, A_2, A_3 and A_4 are constants which are to be determined by the boundary conditions on the sector boundary. In the present work elastic sectors arise on the crack flanks ($\theta = \pm\pi$) where traction free conditions give the relations:

$$A_3 = 4\, A_1$$

$$A_4 = 2(A_2 \pm 2\pi A_1) \qquad (8.3)$$

The sectors can be assembled subject to the boundary conditions and continuity of tractions across the sector boundaries. Continuity of tractions does not in itself require continuity of stresses. Traction continuity requires $\sigma_{\theta\theta}$ and $\sigma_{r\theta}$ to be continuous across the sector boundaries, and an argument presented by Sham and Hancock (1999) shows that σ_{rr} must also be continuous on the boundary between an elastic sector and a centred fan, giving full continuity of all stress components. The boundary conditions require traction free conditions on the crack flanks and the loading is defined by ratio of tension to shear directly ahead of the crack. This is defined in terms of a plastic mixity M_p introduced by Shih (1974):

$$M_p = \frac{2}{\pi}\tan^{-1}\left(\frac{\sigma_{\theta\theta}}{\sigma_{r\theta}}\right) \tag{8.4}$$

Solutions are presented at the values of the plastic mixity listed Table 7.4. A near mode I field consist of a curved fan complemented by elastic sectors to the crack flanks. The method of solution for near mode-I fields starts by determining the asymptotic angle ϕ in the fan directly ahead of the crack for a defined plastic mixity. In the fields presented the plane directly ahead of the crack always lies in a curved fan sector in accord with the assumption of Shih (1974), but in contrast to the fields discussed by Dong and Pan (1990). This allows the relation between the asymptotic fan angle ϕ and the plastic mixity M_p to be written as:

$$\phi = \tan^{-1}\left(2\cot\left(\frac{\pi M_p}{2}\right)\right) \tag{8.5}$$

Continuity of stresses σ_{rr}, $\sigma_{\theta\theta}$ and $\sigma_{r\theta}$ across sector boundary between fan and elastic sector on the upper crack flank at θ_2 allows Equations 8.1 to be combined with Equations 8.2 and 8.3 to give three equations which can be solved simultaneously to define the sector boundary θ_2 and the two unknown constants A_1 and A_2. An identical argument gives the corresponding sector boundary θ_1 between the fan and the elastic sector on the lower flank. Finally it is necessary to check a posteriori that the stresses postulated in any elastic sectors do not violate the yield criterion.

The mode I fields shown in Figures 7.33 and 7.27a-c, discussed in detail by Sham and Hancock (1999), can be regarded as the limiting case of a near mode-I field. The field consists of a curved fan sector directly ahead of the crack in the angular range, $\theta = \pm 39.126^{\circ}$ complemented by elastic sectors extending to the crack flanks. Under mixed mode loading, the near mode I fields consist of a simple modification to this such that the curved fan rotates, but remains complemented by asymmetric elastic sectors to the crack flanks. As an example a mixed mode field corresponding to a remote ratio, $K_I/K_{II} = 1$ is shown in Figure 7.34. The field consists of a curved fan, which extends between 53.34° and -69.6°. The slip lines in the fan are asymptotic to the angle, $\phi = -57.17^{\circ}$ while elastic sectors extend to the crack flanks. The corresponding stress field is shown in Figures 7.28a-c.

A critical transitional field arises when the angle of the elastic wedge on the upper crack flank reaches 54.7° and the asymptotic angle $\phi = -70.53^{0}$, which corresponds to a plastic mixity, $M_p = 0.392$. The yield criterion is violated in any postulated elastic sector between the fan and the crack flanks, but the field can be completed by a constant stress sector extending from 54.7^0 to the upper flank. The stress within this sector is a simple uniaxial compression parallel to the crack flanks:

$$\sigma_{rr} = -\sqrt{3}\,k\cos^2\theta$$

$$\sigma_{\theta\theta} = -\sqrt{3}\,k\sin^2\theta$$

$$\sigma_{r\theta} = \frac{\sqrt{3}}{2}k\sin 2\theta \qquad (8.6)$$

where, $54.7^0 \leq \theta \leq 180^0$. On the lower flank a constant stress sector emerges in $-125.3^0 \geq \theta \geq -180^0$ from the fan to the crack flank. The stress within this sector is a simple uniaxial tension parallel to the crack flanks:

$$\sigma_{rr} = \sqrt{3}\,k\cos^2\theta$$

$$\sigma_{\theta\theta} = \sqrt{3}\,k\sin^2\theta$$

$$\sigma_{r\theta} = -\frac{\sqrt{3}}{2}k\sin 2\theta \qquad (8.7)$$

The remote loading condition, $K_I/K_{II} = 0.5$, gives a plastic mixity quite close to this critical configuration ($M_p = 0.41$, $\phi = -69.6^0$), but in the numerical calculations plasticity has just broken through on the upper flank, and is about to break through on the lower flank, where the elastic sector ranges from -122.87^0 to -180^0. The numerically constructed slip line field for this loading is shown in Figure 7.35 and the stress field in Figures 7.29a-c.

Calculations were also performed at $K_I/K_{II} = 0.45$, which is very close to the critical condition ($M_p = 0.38$, $\phi = -70.53^0$) at which plasticity completes to both upper and the lower crack flanks. A constant stress sector develops in the angular range $-125.3^0 \geq \theta \geq -180^0$. This sector is subject to uniaxial tension parallel to the crack flanks. On the upper flank a constant stress sector develops between $54.7^0 \leq \theta \leq 180^0$ and is subject to uniaxial compression parallel to the crack flanks. The slip line field for this loading is shown in Figure 7.36 and the corresponding stress field in Figures 7.30a-c. Although the transitional field can be determined from the local plastic mixity, an analytic method to relate the remote elastic and plastic mixitics has not yet been established.

With increase levels of applied shear a fan emerges at $\theta = 125.3^0$ and a constant stress sector at $\theta = -70.53^0$ which is the asymptotic angle of the fan ahead of the crack. This gives rise to the near mode II fields. Near mode II fields consist of constant stress sectors on the upper and lower crack flanks leading to curved fan sectors and two further constant stress sectors which adjoin a curved fan directly ahead of the crack. Consider the near mode II slip line field shown in Figure 7.37. The method of solution starts by determining the angle ϕ_1 for the fan directly ahead of the crack using Equations 8.4 and 8.5. The constant stress sector angle, $\theta_7 = 125.3^\circ$ and continuity of stresses across this sector boundary gives the asymptotic fan angle for the fan at 125.3^0, $\phi_2 = 70.53^0$. The field above the crack plane is fixed by the span of the constant stress sector between θ_5 and θ_6. The angle between the slip lines in a constant stress sector gives the relation:

$$\tan(\theta_6 - \theta_5) = 2\tan(\phi_1 - \phi_2) \tag{8.8}$$

Equating the mean stresses at θ_5 and θ_6 gives the relation:

$$(\theta_5 + \theta_6) = (\pi + \phi_1 + \phi_2) \tag{8.9}$$

These equations are solved simultaneously to give numerical values of θ_5 and θ_6. A similar procedure gives the sector boundaries θ_3 and θ_4 on the lower flank. Numerical calculations have been performed at $K_I/K_{II} = 0.25$ and $M_p = 0.23$ for the slip line field shown in Figure 7.37. The sector angles are given in Table 7.5, and the stress field in Figures 7.31a-c. Finally in pure shear, $K_I/K_{II} = 0$, the slip line field, shown in Figure 7.38 is constructed and is identical to that proposed by Shih (1973). The corresponding stress field is given in Figures 7.32a-c, and the sector angles in Table 7.5.

Chapter 9 Discussion

Perfectly plastic fields for plane strain and plane stress which are derived as the limit of the HRR fields (Hutchinson, 1968, Rice & Rosengren, 1968) as the strain hardening exponent approaches zero necessarily exhibit plasticity at all angles around the crack tip. For mode I plane strain conditions this leads to the Prandtl field whose relevance as the limit of the HRR fields as the strain hardening exponent approaches zero has been recognised by Rice (1982). In this field plasticity fully surrounds the crack tip at all angles giving rise to a unique high constraint crack tip field which is fully characterised by J or the crack tip opening displacement. However this field only occurs when the T-stress is positive (tensile) which occurs in deeply edge-cracked bend bars in tension and bending (Betegón & Hancock, 1991). At very small applied loads in any configuration the T-stress is close to zero, and an elastic wedge appears on the crack flanks and the stress ahead of the crack decreases by a hydrostatic term which O'Dowd and Shih (1991a, 1991b) have denoted by Q. In configurations such as centre cracked panels negative (compressive) T-stresses develop. Here the angular span of the elastic wedge on the crack flanks increases further and the mean stress ahead of the crack further decreases. This family of plane strain mode I fields arises in perfect plasticity because plasticity does not fully surround the crack tip, and the loss of crack tip constraint is accompanied by an increase in the angular span of the elastic wedge on the crack flanks. The loss of crack tip constraint gives rise to an increase in fracture toughness in cleavage (Betegón & Hancock,1991) and an enhanced resistance to ductile tearing (Hancock et al., 1993). The mode I fields ($T = 0, \pm 0.5\sigma_0$), discussed in present work are consistent with the three sector solution presented by Li and Hancock (1999).

Plane strain mixed mode I/II fields have been discussed by Shih (1974), on the assumption that plasticity surrounds the crack tip at all angles. This requires the introduction of a discontinuity in radial stress between trailing sectors. This is permitted by the equilibrium equations, and has been interpreted as the limit of an angular zone with steep radial stress gradients in the mixed mode HRR fields. However, the problem of stress discontinuity can be avoided by allowing the possibility of elastic sector on the crack flank, which allows a fully continuous distribution for all stress components. Li and Hancock (1999) have presented five sector solutions for mixed mode I/II fields, where sectors from the lower crack flanks can be given as: constant stress sector 1, fan 1, constant stress sector 2, fan 2 and an elastic sector on the upper crack flank. Zhu and Chao (2001) have presented six sector solutions for mixed mode fields as the modification of the five sector solutions, where a constant stress sector has been included between fan 2 and elastic sector on the upper crack flank. According to Zhu and Chao (2001), five sector solution presented by Li and Hancock (1999) for mixed mode loading is the special case of six sector solution and is valid for the field containing an elastic wedge with a span, $\varphi \geq \pi/4$. Unlike mixed mode fields by Li and Hancock (1999), the fields discussed in present work show an incomplete constant stress sector adjacent to the elastic sector on the upper crack flank, which is consistent with the six sector solution of Zhu and Chao (2001). A comparison of the present numerical solution and the six sector analytical solution for mixed mode, $K_I/K_{II}=2$ is shown in Figure 9.4. Li and Hancock (1999) mixed mode fields for $K_I/K_{II} = 2$ are shown in Figures 9.1 and 9.2. For this loading ($K_I/K_{II} = 2$), a comparison of stress fields from the analytical solution of Li and Hancock (1999) and current numerical solution is shown in Figure 9.3. Both solutions presented for the plastic mixity, $M_p = 0.82$, show identical stresses in the leading sectors and differ only slightly in the trailing sectors. The toughness predicted by applying local fracture criteria to either field would thus give identical results, and the minor difference in the trailing sectors does not appear to have any significant effect on toughness.

Under mode I loading in plane strain, the effect of T-stress is to change the constraint of the field leading to a family of fields parameterised by constraint. If plasticity breaks through to one crack flank in the corresponding mixed mode fields, the effect of the T-stress is to change the local mixity, but not to create a new family of fields. The mixed mode toughness is thus fully characterised by J at any given local crack tip mixity. It may however be noted that the T-stress changes the relationship between the local and remote mixities, so that the remote ratio of tension to shear (K_I/K_{II}) does not lead to a unique toughness measured by J. Using the six sector solutions at $K_I/K_{II}=2$ but differing T-stress, the effect of T-stress is illustrated in Figures 9.5 and 9.6 and Table 9.1. These Figures compare the numerical solutions with analytical solutions. The trend is that increasingly tensile T-stresses decrease the span of the constant stress sector between the fan and the elastic sector, and change the plastic mixity. The mixed mode fields can be unified with unconstraint mode I fields into a single constraint-mixity locus. This allows mode I toughness to be extended to mixed mode loading configurations. The effects become significant when assessing structural integrity on shallow cracked components subjected to mixed mode loading.

In plane stress, mode I and near mode I fields have been discussed by Hutchinson (1968), Shih (1973) and Dong and Pan (1990) on the assumption that plasticity surrounds the crack tip at all angles. Statically admissible fields developed on this basis requires a discontinuity in radial stress which is allowed by the equilibrium equations. However in the present work, the problem of a stress discontinuity has been avoided by allowing the possibility of elastic sectors on the crack flanks. Unlike mode I and near mode I fields discussed by Dong and Pan (1990), in the fields (mode I and mixed mode I/II) discussed in present work, the crack line ahead of crack always lies in the curved fan throughout the transition from mode I to mode II. In mode I loading, the maximum hoop stress occurs in the curved fans, when the stress is uniquely defined. As a result, although the T-stress has an effect on the shape of the plastic zone, it has no effect on the asymptotic field, which is uniquely characterised by J. In mode I, the present work recovers the field discussed by Sham and Hancock (1999), however in mode II and near mode II, the fields identified by Shih (1973) emerge in which plasticity surrounds the tip at all angles.

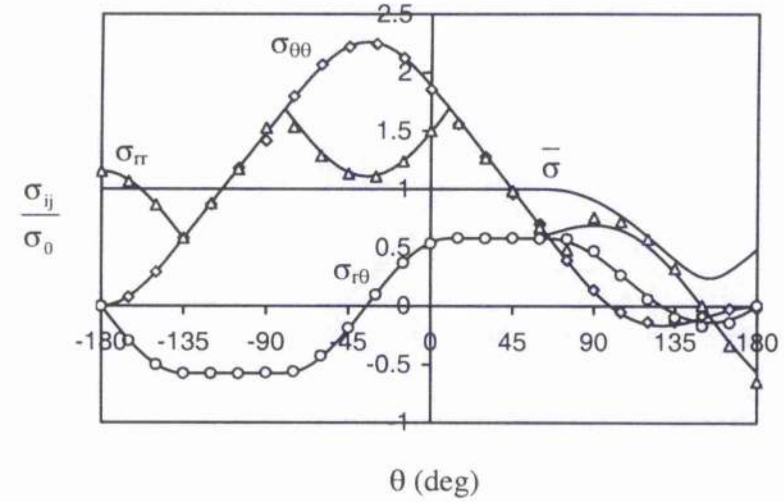

Figure 9.1: Asymptotic crack tip field under mixed mode (K_I/K_{II}=2) loading in plane strain (Li & Hancock, 1999).

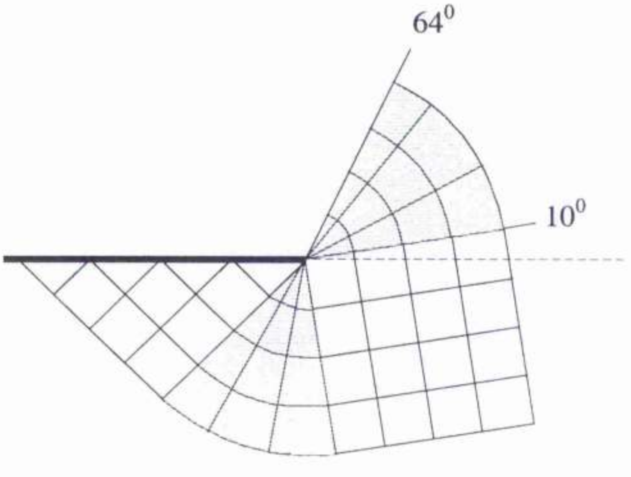

Figure 9.2: Li & Hancock (1999) plane strain mixed mode (K_I/K_{II}=2) slip line field.

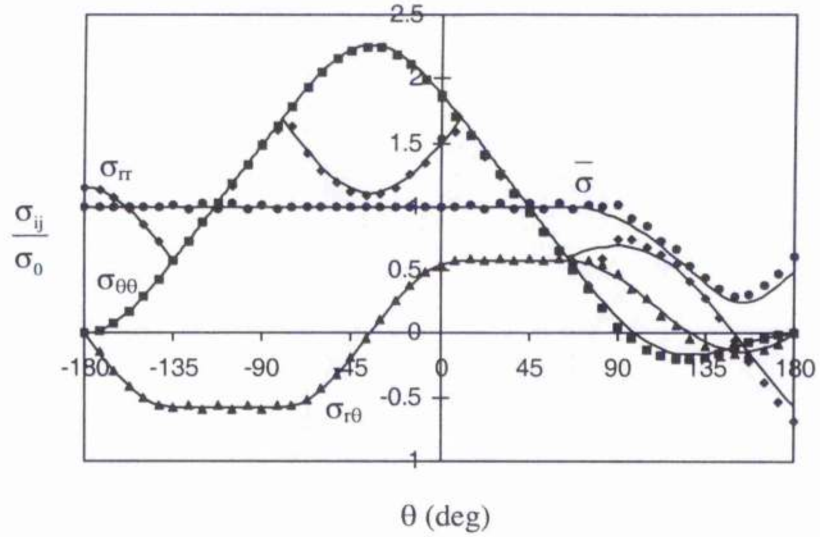

Figure 9.3: Comparison of plane strain mixed mode ($K_I/K_{II}=2$) numerical result (data points) with analytical solution (solid lines) of Li & Hancock (1999).

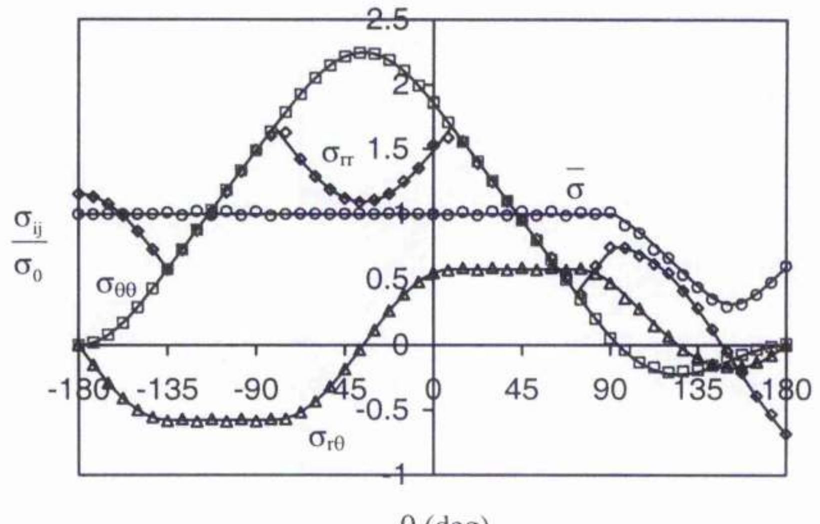

Figure 9.4: Comparison of plane strain mixed mode ($K_I/K_{II}=2$) numerical result (data points) with six-sector analytical solution (solid lines), T=0.

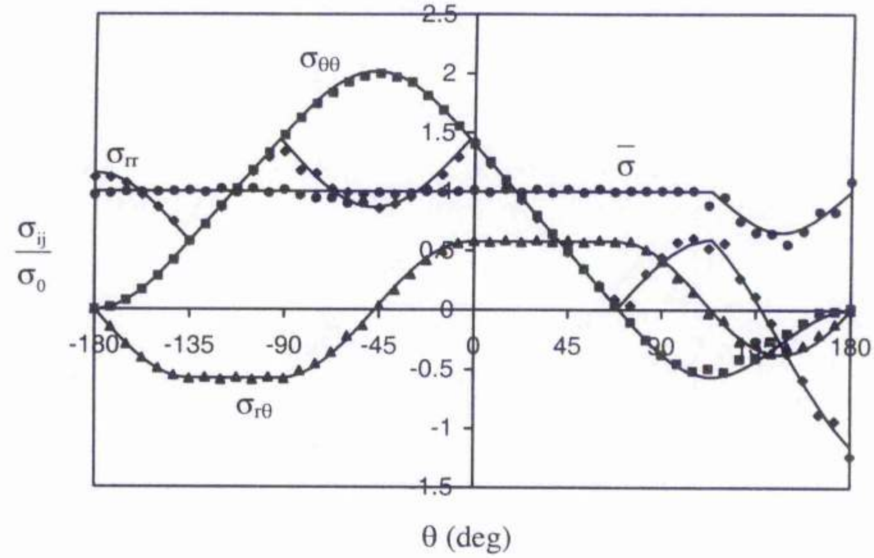

Figure 9.5: Comparison of plane strain mixed mode ($K_I/K_{II}=2$) numerical result (data points) with six-sector analytical solution (solid lines), $T=-0.5\sigma_0$.

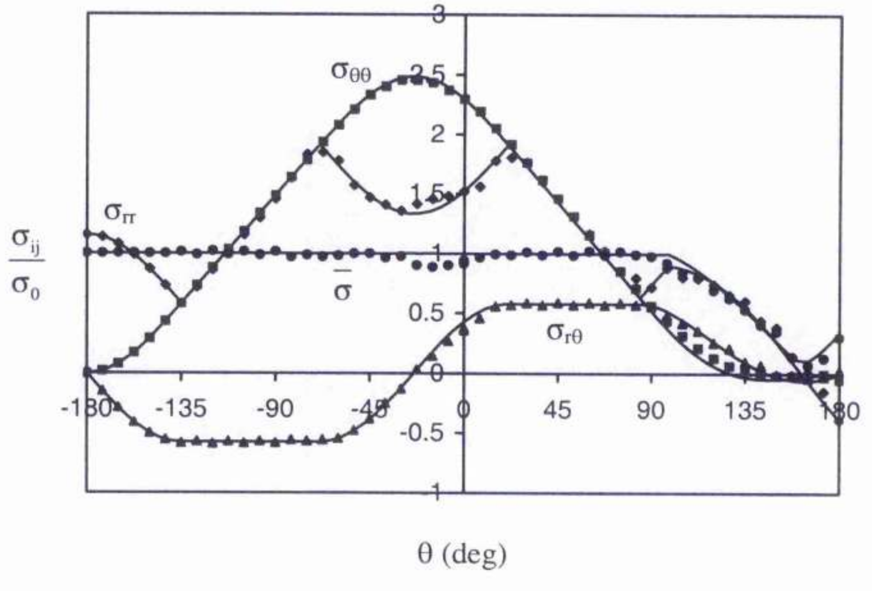

Figure 9.6: Comparison of plane strain mixed mode ($K_I/K_{II}=2$) numerical result (data points) with six-sector analytical solution (solid lines), $T=+0.5\sigma_0$.

Angle (degree)	$T=-0.5\sigma_0$		$T=0$		$T=+0.5\sigma_0$	
	Analytic	Numerical	Analytic	Numerical	Analytic	Numerical
θ_1	-135	-135	-135	-135	-135	-135
θ_2	-92.07	-90	-80.71	-81	-68.96	-67
θ_3	-2.07	0	9.29	9	21.04	23
θ_4	68.88	75	72.84	74	84.48	90
θ_5	113.88	107	92.02	92	98.43	90

Table 9.1: Sector angles of the slip line fields under mixed mode, $K_I/K_{II}=2$ in plane strain.

Chapter 10 Conclusion

Mode I, mode II and mixed mode I/II crack tip fields have been investigated under contained yielding conditions. The asymptotic crack tip fields for an elastic perfectly-plastic material response have been determined analytically, and verified numerically using boundary layer formulations in plane strain and plane stress conditions. The crack tip fields have been represented in terms of slip line fields.

The effects of the non-singular T-stress on the plastic zone at the crack tip as well as on the asymptotic crack tip field have been determined in plane strain. T-stress changes the size and shape of the plastic zone at the crack tip under mode I and mixed modes I/II. Under mode I loading, T-stress changes the constraint of the crack tip field leading to a family of fields, but does not change local mixity. Under mixed mode loading, T-stress changes local mixity without creating a new family of fields. In plane strain mode I, the numerical results are consistent with the analytical solutions of Li and Hancock (1999), while in mixed mode I/II loading, the data are consistent with the extension to the Li and Hancock fields proposed by Zhu and Chao (2001). However, this is a minor difference which only slightly affects the trailing sectors and does not change the form of the leading sectors.

Under mode I loading in plane stress, the effect of T-stress on plastic zone at the crack tip has been determined. Both positive and negative T-stresses change the size and shape of the plastic zone, although they do not have noticeable effects on the crack tip field.

Analytical solutions for plane stress mode I and mixed mode I/II problems have been developed by assembling constant stress, fan and elastic sectors. Analytical solutions show good agreement with the numerical results, and unlike fields presented by Hutchinson (1968), Shih (1973) and Dong and Pan (1990), the fields exhibit full continuity of stresses, and feature incomplete plasticity around the crack tip. In mode I, field discussed by Sham and Hancock (1999) emerges, and in mode II and near mode II, fields discussed by Shih (1973) develop.

Chapter 11 References

Aoki, S., Kishimoto, K., Yoshida, T. and Sakata, M., (1987), A finite element study of the near crack tip deformation of a ductile material under mixed mode loading, J. Mech. Phys. Solids 35, pp. 431-455.

Brown, W.F. Jr. and Srawley, J.E., (1966), Plane Strain Crack Toughness Testing of High Strength Metallic Materials, ASTM STP 410, American Society for Testing and Materials, Philadelphia, PA.

Betegón, C. and Hancock. J.W., (1991), Two-Parameter Characterisation of Elastic-Plastic Crack-Tip Fields, Journal of Applied Mechanics, Vol. 58, pp.104-110.

Bhattacharjee, D. and Knott, J.F., (1994), Ductile fracture in HY100 steel under mixed mode I/ mode II loading, Acta metal. mater., Vol. 42, No. 5, pp. 1747-1754.

Bhattacharjee, D. and Knott, J.F., (1993), Micro-mechanisms of fracture in steel tested under mixed-mode loading above the transition temperature, Mixed-Mode Fatigue and Fracture, ESIS 14, Mechanical Engineering Publications, London, pp. 99-109.

Budden, P.J., (1988), The effect of blunting on the strain field at a crack tip under mixed modes 1 and 2, J. Mech. Phys. Solids 36, pp. 503-518.

BS 5447: (1974), Methods of Testing for Plane Strain Fracture Toughness (K_{IC}) of Metallic Materials, British Standards Institution, London.

Du, Z.-Z. and Hancock, J.W., (1991), The Effect of Non-singular Stresses on Crack-tip Constraint, Journal of the Mechanics and Physics of Solids, Vol. 39, No. 4, pp. 555-567.

Dong, P. and Pan, J., (1990), Asymptotic Crack-Tip Fields for Perfectly Plastic Solids Under Plane-Stress and Mixed-Mode Loading Conditions, Journal of Applied Mechanics, Vol. 57, pp. 635-638.

E 399-83: (1983), Standard Test Method for Plane-Strain Fracture Toughness of Metallic Materials, American Society for Testing and Materials, Philadelphia.

Erdogan, F. and Sih, G.C., (1963), On the crack extension in plates under plane loading and transverse shear, Journal of Basic Engineering, Vol. 85, pp. 519-527.

Griffith, A.A., (1920), The Phenomena of Rupture and Flow in Solids, Philosophical Transactions, Series A, Vol. 221, pp. 163-198.

Ghosal, A.K. and Narasimhan, R., (1994), A finite element analysis of mixed-mode fracture initiation by ductile fracture mechanisms, Journal of Mechanics and Physics of Solids, Vol. 42, pp. 953-978.

Ghosal, A.K. and Narasimhan, R., (1996), Numerical simulations of hole growth and ductile fracture initiation under mixed mode loading, International Journal of Fracture, Vol. 77, pp. 281-304.

Gao, H., Wang, Z., Yang, C. and Zhou, A., (1979), An investigation on the brittle fracture of K_I-K_{II} composite mode cracks, Acta Met. Sin. 15, pp. 380-391 (in Chinese).

Graves, C., (1992), Effects of Cobalt Content on the Mixed Mode I/III Fracture Toughness of WC-Co Alloys, M.S. thesis, Washington State University.

Hibbitt, Karlsson & Sorensen, Inc., (1998), ABAQUS version 5.8, ABAQUS manual.

Hill, R., (1950), The Mathematical Theory of Plasticity, Oxford University Press, London.

Hill, R., (1952), On discontinuous plastic states with special reference to localised necking in thin sheets, J. Mech. Phys. Solids, 1, 19.

Hodge, P.G. Jnr., (1951), Yield conditions in plane plastic stress, J. Math. Phys., 29, 38.

Hutchinson, J.W., (1968), Singular behaviour at the end of a tensile crack in a hardening material, Journal of the Mechanics and Physics of Solids, Vol. 16, pp. 13-31.

Hutchinson, J.W., (1968), Plastic stress and strain fields at a crack tip, J. Mech. Phys. Solids, Vol. 16, pp. 337-347.

Hencky, H., (1923), Ueber einige statisch bestimmte Faelle des Gleichgewichts in plastischen Koerpern Z. angew. Math Mech., 3, pp. 245-251.

Hussain, M.A., Pu, S.L. and Underwood, J., (1974), ASTM STP 560, p.2, Am. Soc. Test. Mater., Philadelphia, Pa, Cited by Bhattacharjee & Knott (1994).

Hancock, J.W., Reuter, W.A. and Parks, D.M., (1993), Toughness and Constraint Parameterised by T, Constraint Effects in Fracture ASTM STP 1171, pp. 121-140, Philadelphia, PA: American Society for Testing and Materials.

Inglis, C.E., (1913), Stresses in a Plate Due to the Presence of Cracks and Sharp Corners, Transactions of the Institute of the Naval Architects, Vol. 55, pp. 219-241.

Irwin, G.R., (1948), "Fracture Dynamics", Fracturing of Metals, American Society for Metals, Cleveland, pp. 147-166.

Irwin, G.R. and Kies, J.A., (1954), Critical energy rate analysis of fracture strength, Weld. J. Res. Suppl. 33, pp. 193-198.

Kamat, S.V. and Hirth, J.P., (1995), Mixed Mode I/II Fracture Toughness of 2034 Aluminium Alloys, Accepted for publication in Acta Metallurgica et Materialia.

Kamat, S.V. and Hirth, J.P., (1995), Mixed mode fracture toughness of engineering materials, Journal of Engineering Materials and Technology, Vol. 117, pp. 391-394.

Li, J. and Hancock, J.W., (1999), Mode I and mixed mode fields with incomplete crack tip plasticity, International Journal of Solids and Structures, Vol. 36, pp. 711-725.

Li, F.Z., Shih, C.F. and Needleman, A., (1985), A comparison of methods for calculating energy-release rates, Engineering Fracture Mechanics, Vol. 21, pp. 405-421.

Mises, R., (1913), Göttinger Nachrichten Math. Phys. Klasse p. 582, Cited by Karstensen (1996).

Maccagno, T.M. and Knott, J.F., (1989), The fracture behaviour of PMMA in mixed modes I and II, Engng Fracture Mech., Vol. 34, pp. 65-86.

Maccagno, T.M. and Knott, J.F., (1991), The low temperature brittle fracture behaviour of steel in mixed modes I and II, Engng Fracture Mech., Vol. 38, No. 2/3, pp. 111-128.

Manoharan, M., Hirth, J.P. and Rosenfield, A.R., (1989), Combined Mode I-Mode III Fracture of a High Carbon Steel, Scripta Metallurgica, Vol. 29, pp. 763-766.

Manoharan, M., Raghavachary, S., Hirth, J.P. and Rosenfield, A.R., (1989), Fracture Surface Orientation under Mixed Mode Loading, ASME Journal of Engineering Materials and Technology, Vol. 111, pp. 440-442.

Orowan, E., (1948), Fracture and Strength of Solids, Reports on Progress in Physics, Vol. XII, p.185.

O'Dowd, N.P. and Shih, C.F., (1991a), Family of Crack Tip Fields Characterised by a Triaxiality Parameter: Part I - Structure of Fields, Journal of the Mechanics and Physics of Solids, Vol. 39, pp. 939-963.

O'Dowd, N.P. and Shih, C.F., (1991b), Family of Crack Tip Fields Characterised by a Triaxiality Parameter: Part II - Fracture Applications, Journal of the Mechanics and Physics of Solids, Vol. 39, pp. 989-1015.

Parks, D.M., (1974), A Stiffness Derivative Finite Element Technique for Determination of Crack Tip Stress Intensity Factors, International Journal of Fracture, Vol. 10, pp. 487-502.

Rice, J.R. and Rosengren, G.F., (1968), Plane strain deformation near a crack tip in a power law hardening material, Journal of the Mechanics and Physics of Solids, Vol. 16, pp. 1-12.

Rice, J.R., (1968), A Path Independent Integral and the Approximate Analysis of Strain Concentration by Notches and Cracks, Journal of Applied Mechanics, Vol. 35, pp. 379-386.

Rice, J.R. and Tracey, D.M., (1973). In Numerical and Computational Methods in Structural Mechanics, edited by S. J. Fenves et al., Academic Press, New York.

Rice, J. R., (1974), Limitations to the Small Scale Yielding Approximation for Crack Tip Plasticity, Journal of the Mechanics and Physics of Solids, Vol. 22, pp.17-26.

Rice, J.R., (1982), Elastic-plastic Crack Growth In: Hopkins H.G. and Sewell M.J. eds., Mechanics of Solids, the Rodney Hill Anniversary Volume, 539-562.

Saka, M., Tanaka, S. and Abe, H., (1986), Computl Mech. 1, V 175, Cited by Bhattacharjee & Knott (1994).

Sham, T.L., Li, J. and Hancock, J.W., (1999), A family of plane strain crack tip stress fields for interface cracks in strength-mismatched elastic-perfectly plastic solids, Journal of the Mechanics and Physics of Solids, Vol. 47, pp. 1963-2010.

Sham, T.L. and Hancock, J.W., (1999), Mode I crack tip fields with incomplete crack tip plasticity in plane stress, J. Mech. Phys. Solids, 47, pp. 2011-2027.

Shih, C.F., (1973), Elastic-Plastic Analysis of Combined Mode Crack Problems, Ph.D. thesis, Harvard University, Cambridge, Mass.

Shih, C.F., (1974), Small-Scale Yielding Analysis of Mixed Mode Plane-Strain Crack Problems, Fracture Analysis, ASTM STP 560, American Society for Testing and Materials, pp. 187-210.

Tresca, H., (1864), Comptes Rendus Acad. Sci, Paris 59, 754, Cited by Karstensen (1996).

Timoshenko, S. P. and Goodier, J. N., (1970), Theory of Elasticity, 3rd Edition, McGraw-Hill Book Company.

Tohgo, K., Otsuka, A. and Gao, H.W., (1988), Proceedings of Far East Fracture Group Workshop (Edited by M. Sakata), Tokyo Institute of Technology, Japan, pp. 101-108.

Westergaard, H.M., (1939), Bearing Pressures and Cracks, Journal of Applied Mechanics, Vol. 6, pp. 49-53.

Williams, M. L., (1957), On the Stress Distribution at the Base of a Stationary Crack, Journal of Applied Mechanics, Vol. 24, pp. 109-114.

Yokobori, T., Yokobori Jr, A.T., Sato, K. and Omotani, M., (1983), The effects of ferrite grain size on fracture of low carbon steel under mixed modes I and II, Engng Fracture Mech., Vol. 17, pp. 75-85.

Zywicz, Z. and Parks, D.M., (1989), Elastic yield zone around an interfacial crack tip, Journal of Applied Mechanics, Vol. 56, pp. 577-584.

Zywicz, Z. and Parks, D.M., (1992), Small-scale yielding interfacial crack-tip fields, Journal of the Mechanics and Physics of Solids, Vol. 40, No. 3, pp. 511-536.

Zhu, X.K. and Chao, Y.J., (2001), Constraint effects on crack-tip fields in elastic-perfectly plastic materials, Journal of the Mechanics and Physics of Solids, Vol. 49, pp. 363-399.

Appendix I

The computer programs fullfan3.go and fullfanodd3.go are used in conjunction with the ABAQUS post processor ABAQUS Post (Hibbitt, Karlsson and Sorensen, 1998) to write radial distances and Cartesian stresses at 7.5^0 intervals surrounding the crack tip. The data are written in a file named abaqus.rpt.

The program fullfan3.go

```
delete curves, name=all names

detail, elset = s1

path,absolute,distance,name=s11d180,nodelist,undeformed=on,var=s11,
D180

print c
s11d180

path,absolute,distance,name=s11d165,nodelist,undeformed=on,var=s11,
D165

print c
s11d165

path,absolute,distance,name=s11d150,nodelist,undeformed=on,var=s11,
D150

print c
s11d150

path,absolute,distance,name=s11d135,nodelist,undeformed=on,var=s11,
d135

print c
s11d135

path,absolute,distance,name=s11d120,nodelist,undeformed=on,var=s11,
D120

print c
s11d120

path,absolute,distance,name=s11d105,nodelist,undeformed=on,var=s11,
D105

print c
s11d105

path,absolute,distance,name=s11d90,nodelist,undeformed=on,var=s11,
D90

print c
s11d90

path,absolute,distance,name=s11d75,nodelist,undeformed=on,var=s11
D75
```

```
print c
s11d75

path,absolute,distance,name=s11d60,nodelist,undeformed=on,var=s11,
D60

print c
s11d60

path,absolute,distance,name=s11d45,nodelist,undeformed=on,var=s11
D45

print c
s11d45

path,absolute,distance,name=s11d30,nodelist,undeformed=on,var=s11
D30

print c
s11d30

path,absolute,distance,name=s11d15,nodelist,undeformed=on,var=s11
D15

print c
s11d15

detail, elset = upper

path,absolute,distance,name=s11d00u,nodelist,undeformed=on,var=s11,
D00

print c
s11d00u

detail, elset = bottom

path,absolute,distance,name=s11d00b,nodelist,undeformed=on,var=s11,
D00

print c
s11d00b

detail, elset = s1

path,absolute,distance,name=s11d345,nodelist,undeformed=on,var=s11,
D345

print c
s11d345

path,absolute,distance,name=s11d330,nodelist,undeformed=on,var=s11,
D330

print c
s11d330

path,absolute,distance,name=s11d315,nodelist,undeformed=on,var=s11,
d315

print c
```

```
s11d315

path,absolute,distance,name=s11d300,nodelist,undeformed=on,var=s11,
D300

print c
s11d300

path,absolute,distance,name=s11d285,nodelist,undeformed=on,var=s11,
D285

print c
s11d285

path,absolute,distance,name=s11d270,nodelist,undeformed=on,var=s11,
D270

print c
s11d270

path,absolute,distance,name=s11d255,nodelist,undeformed=on,var=s11
D255

print c
s11d255

path,absolute,distance,name=s11d240,nodelist,undeformed=on,var=s11,
D240

print c
s11d240

path,absolute,distance,name=s11d225,nodelist,undeformed=on,var=s11
D225

print c
s11d225

path,absolute,distance,name=s11d210,nodelist,undeformed=on,var=s11
D210

print c
s11d210

path,absolute,distance,name-s11d195,nodelist,undeformed=on,var=s11
D195

print c
s11d195

path,absolute,distance,name=s11d181,nodelist,undeformed=on,var=s11
D181

print c
s11d181

display,all curves

path,absolute,distance,name=s22d180,nodelist,undeformed=on,var=s22,
D180
```

```
print c
s22d180

path,absolute,distance,name=s22d165,nodelist,undeformed=on,var=s22,
D165

print c
s22d165

path,absolute,distance,name=s22d150,nodelist,undeformed=on,var=s22,
D150

print c
s22d150

path,absolute,distance,name=s22d135,nodelist,undeformed=on,var=s22,
d135

print c
s22d135

path,absolute,distance,name=s22d120,nodelist,undeformed=on,var=s22,
D120

print c
s22d120

path,absolute,distance,name=s22d105,nodelist,undeformed=on,var=s22,
D105

print c
s22d105

path,absolute,distance,name=s22d90,nodelist,undeformed=on,var=s22,
D90

print c
s22d90

path,absolute,distance,name=s22d75,nodelist,undeformed=on,var=s22
D75

print c
s22d75

path,absolute,distance,name=s22d60,nodelist,undeformed=on,var=s22,
D60

print c
s22d60

path,absolute,distance,name=s22d45,nodelist,undeformed=on,var=s22
D45

print c
s22d45

path,absolute,distance,name=s22d30,nodelist,undeformed=on,var=s22
D30

print c
```

```
s22d30

path,absolute,distance,name=s22d15,nodelist,undeformed=on,var=s22
D15

print c
s22d15

detail, elset = upper

path,absolute,distance,name=s22d00u,nodelist,undeformed=on,var=s22,
D00

print c
s22d00u

detail, elset = bottom

path,absolute,distance,name=s22d00b,nodelist,undeformed=on,var=s22,
D00

print c
s22d00b

detail, elset = s1

path,absolute,distance,name=s22d345,nodelist,undeformed-on,var=s22,
D345

print c
s22d345

path,absolute,distance,name=s22d330,nodelist,undeformed=on,var=s22,
D330

print c
s22d330

path,absolute,distance,name=s22d315,nodelist,undeformed=on,var=s22,
d315

print c
s22d315

path,absolute,distance,name=s22d300,nodelist,undeformed=on,var=s22,
D300

print c
s22d300

path,absolute,distance,name=s22d285,nodelist,undeformed=on,var=s22,
D285

print c
s22d285

path,absolute,distance,name=s22d270,nodelist,undeformed=on,var=s22,
D270

print c
s22d270
```

```
path,absolute,distance,name=s22d255,nodelist,undeformed=on,var=s22
D255

print c
s22d255

path,absolute,distance,name=s22d240,nodelist,undeformed=on,var=s22,
D240

print c
s22d240

path,absolute,distance,name=s22d225,nodelist,undeformed=on,var=s22
D225

print c
s22d225

path,absolute,distance,name=s22d210,nodelist,undeformed=on,var=s22
D210

print c
s22d210

path,absolute,distance,name=s22d195,nodelist,undeformed=on,var-s22
D195

print c
s22d195

path,absolute,distance,name=s22d181,nodelist,undeformed=on,var=s22
D181

print c
s22d181

display,all curve

path,absolute,distance,name=s12d180,nodelist,undeformed=on,var=s12,
D180

print c
s12d180

path,absolute,distance,name=s12d165,nodelist,undeformed=on,var=s12,
D165

print c
s12d165

path,absolute,distance,name=s12d150,nodelist,undeformed=on,var=s12,
D150

print c
s12d150

path,absolute,distance,name=s12d135,nodelist,undeformed=on,var=s12,
d135

print c
s12d135
```

```
path,absolute,distance,name=s12d120,nodelist,undeformed=on,var=s12,
D120

print c
s12d120

path,absolute,distance,name=s12d105,nodelist,undeformed=on,var=s12,
D105

print c
s12d105

path,absolute,distance,name=s12d90,nodelist,undeformed=on,var=s12,
D90

print c
s12d90

path,absolute,distance,name=s12d75,nodelist,undeformed=on,var=s12
D75

print c
s12d75

path,absolute,distance,name=s12d60,nodelist,undeformed=on,var=s12,
D60

print c
s12d60

path,absolute,distance,name=s12d45,nodelist,undeformed=on,var=s12
D45

print c
s12d45

path,absolute,distance,name=s12d30,nodelist,undeformed=on,var=s12
D30

print c
s12d30

path,absolute,distance,name=s12d15,nodelist,undeformed=on,var=s12
D15

print c
s12d15

detail, elset = upper

path,absolute,distance,name=s12d00u,nodelist,undeformed=on,var=s12,
D00

print c
s12d00u

detail, elset = bottom

path,absolute,distance,name=s12d00b,nodelist,undeformed=on,var=s12,
D00
```

```
print c
s12d00b

detail, elset = s1

path,absolute,distance,name=s12d345,nodelist,undeformed=on,var=s12,
D345

print c
s12d345

path,absolute,distance,name=s12d330,nodelist,undeformed=on,var=s12,
D330

print c
s12d330

path,absolute,distance,name=s12d315,nodelist,undeformed=on,var=s12,
d315

print c
s12d315

path,absolute,distance,name=s12d300,nodelist,undeformed=on,var=s12,
D300

print c
s12d300

path,absolute,distance,name=s12d285,nodelist,undeformed=on,var=s12,
D285

print c
s12d285

path,absolute,distance,name=s12d270,nodelist,undeformed=on,var=s12,
D270

print c
s12d270

path,absolute,distance,name=s12d255,nodelist,undeformed=on,var=s12
D255

print c
s12d255

path,absolute,distance,name=s12d240,nodelist,undeformed=on,var=s12,
D240

print c
s12d240

path,absolute,distance,name=s12d225,nodelist,undeformed=on,var=s12
D225

print c
s12d225

path,absolute,distance,name=s12d210,nodelist,undeformed=on,var=s12
D210
```

```
print c
s12d210

path,absolute,distance,name=s12d195,nodelist,undeformed=on,var=s12
D195

print c
s12d195

path,absolute,distance,name=s12d181,nodelist,undeformed=on,var=s12
D181

print c
s12d181

display,all curve

detail, elset = s1

path,absolute,distance,name=misd180,nodelist,undeformed=on,var=mises,
D180

print c
misd180

path,absolute,distance,name=misd165,nodelist,undeformed=on,var=mises,
D165

print c
misd165

path,absolute,distance,name=misd150,nodelist,undeformed=on,var=mises,
D150

print c
misd150

path,absolute,distance,name=misd135,nodelist,undeformed=on,var=mises,
d135

print c
misd135

path,absolute,distance,name=misd120,nodelist,undeformed=on,var=mises,
D120

print c
misd120

path,absolute,distance,name=misd105,nodelist,undeformed=on,var=mises,
D105

print c
misd105

path,absolute,distance,name=misd90,nodelist,undeformed=on,var=mises,
D90

print c
misd90
```

```
path,absolute,distance,name=misd75,nodelist,undeformed=on,var=mises
D75

print c
misd75

path,absolute,distance,name=misd60,nodelist,undeformed=on,var=mises,
D60

print c
misd60

path,absolute,distance,name=misd45,nodelist,undeformed=on,var=mises
D45

print c
misd45

path,absolute,distance,name=misd30,nodelist,undeformed=on,var=mises
D30

print c
misd30

path,absolute,distance,name=misd15,nodelist,undeformed=on,var=mises
D15

print c
misd15

detail, elset = upper

path,absolute,distance,name=misd00u,nodelist,undeformed=on,var=mises,
D00

print c
misd00u

detail, elset = bottom

path,absolute,distance,name=misd00b,nodelist,undeformed=on,var=mises,
D00

print c
misd00b

detail, elset = s1

path,absolute,distance,name=misd345,nodelist,undeformed=on,var=mises,
D345

print c
misd345

path,absolute,distance,name=misd330,nodelist,undeformed=on,var=mises,
D330

print c
misd330

path,absolute,distance,name=misd315,nodelist,undeformed=on,var=mises,
```

```
d315

print c
misd315

path,absolute,distance,name=misd300,nodelist,undeformed=on,var=mises,
D300

print c
misd300

path,absolute,distance,name=misd285,nodelist,undeformed=on,var=mises,
D285

print c
misd285

path,absolute,distance,name=misd270,nodelist,undeformed=on,var=mises,
D270

print c
misd270

path,absolute,distance,name=misd255,nodelist,undeformed=on,var=mises
D255

print c
misd255

path,absolute,distance,name=misd240,nodelist,undeformed=on,var=mises,
D240

print c
misd240

path,absolute,distance,name=misd225,nodelist,undeformed=on,var=mises
D225

print c
misd225

path,absolute,distance,name=misd210,nodelist,undeformed=on,var=mises
D210

print c
misd210

path,absolute,distance,name-misd195,nodelist,undeformed=on,var=mises
D195

print c
misd195

path,absolute,distance,name=misd181,nodelist,undeformed=on,var=mises
D181

print c
misd181

display,all curves
```

```
delete curves, name=all names

detail, elset = s1

path,absolute,distance,name=presd180,nodelist,undeformed=on,var=press,
D180

print c
presd180

path,absolute,distance,name=presd165,nodelist,undeformed=on,var=press,
D165

print c
presd165

path,absolute,distance,name=presd150,nodelist,undeformed=on,var=press,
D150

print c
presd150

path,absolute,distance,name=presd135,nodelist,undeformed=on,var=press,
d135

print c
presd135

path,absolute,distance,name=presd120,nodelist,undeformed=on,var=press,
D120

print c
presd120

path,absolute,distance,name=presd105,nodelist,undeformed=on,var=press,
D105

print c
presd105

path,absolute,distance,name=presd90,nodelist,undeformed=on,var=press,
D90

print c
presd90

path,absolute,distance,name=presd75,nodelist,undeformed=on,var=press
D75

print c
presd75

path,absolute,distance,name=presd60,nodelist,undeformed=on,var=press,
D60

print c
presd60

path,absolute,distance,name=presd45,nodelist,undeformed=on,var=press
D45
```

```
print c
presd45

path,absolute,distance,name=presd30,nodelist,undeformed=on,var=press
D30

print c
presd30

path,absolute,distance,name=presd15,nodelist,undeformed=on,var=press
D15

print c
presd15

detail, elset = upper

path,absolute,distance,name=presd00u,nodelist,undeformed=on,var=press,
D00

print c
presd00u

detail, elset = bottom

path,absolute,distance,name=presd00b,nodelist,undeformed=on,var=press,
D00

print c
presd00b

detail, elset = s1

path,absolute,distance,name=presd345,nodelist,undeformed=on,var=press,
D345

print c
presd345

path,absolute,distance,name=presd330,nodelist,undeformed=on,var=press,
D330

print c
presd330

path,absolute,distance,name=presd315,nodelist,undeformed=on,var=press,
d315

print c
presd315

path,absolute,distance,name=presd300,nodelist,undeformed=on,var=press,
D300

print c
presd300

path,absolute,distance,name=presd285,nodelist,undeformed-on,var=press,
D285

print c
```

```
presd285

path,absolute,distance,name=presd270,nodelist,undeformed=on,var=press,
D270

print c
presd270

path,absolute,distance,name=presd255,nodelist,undeformed=on,var=press
D255

print c
presd255

path,absolute,distance,name=presd240,nodelist,undeformed=on,var=press,
D240

print c
presd240

path,absolute,distance,name=presd225,nodelist,undeformed=on,var=press
D225

print c
presd225

path,absolute,distance,name=presd210,nodelist,undeformed=on,var=press
D210

print c
presd210

path,absolute,distance,name=presd195,nodelist,undeformed=on,var=press
D195

print c
presd195

path,absolute,distance,name=presd181,nodelist,undeformed=on,var=press
D181

print c
presd181

display,all curves
```

The program fullfanodd3.go

```
NSET,NSET=D00K,GENERATE
1,481,20

NSET, NSET = D8, GENERATE
2,482,20

NSET, NSET = D23, GENERATE
4,484,20

NSET, NSET = D38, GENERATE
6,486,20

NSET, NSET = D53, GENERATE
```

```
8,488,20

NSET, NSET = D68, GENERATE
10,490,20

NSET, NSET = D83, GENERATE
12,492,20

NSET, NSET = D98, GENERATE
494,926,18

NSET, NSET = D113, GENERATE
496,928,18

NSET, NSET = D128, GENERATE
498,930,18

NSET, NSET = D143, GENERATE
500,932,18

NSET, NSET = D158, GENERATE
502,934,18

NSET, NSET = D173, GENERATE
504,936,18

NSET, NSET = D188, GENERATE
938,1370,18

NSET, NSET = D203, GENERATE
940,1372,18

NSET, NSET = D218, GENERATE
942,1374,18

NSET, NSET = D233, GENERATE
944,1376,18

NSET, NSET = D248, GENERATE
946,1378,18

NSET, NSET = D263, GENERATE
948,1380,18

NSET, NSET = D278, GENERATE
1382,1766,16

NSET, NSET = D293, GENERATE
1384,1768,16

NSET, NSET = D308, GENERATE
1386,1770,16

NSET, NSET = D323, GENERATE
1388,1772,16

NSET, NSET = D338, GENERATE
1390,1774,16

NSET, NSET = D353, GENERATE
1392,1776,16
```

```
delete curves, name=all names
detail, elset = s1

path,absolute,distance,name=s11d173,nodelist,undeformed=on,var=s11,
D173

print c
s11d173

path,absolute,distance,name=s11d158,nodelist,undeformed=on,var=s11,
D158

print c
s11d158

path,absolute,distance,name=s11d143,nodelist,undeformed=on,var=s11,
D143

print c
s11d143

path,absolute,distance,name=s11d128,nodelist,undeformed=on,var=s11,
D128

print c
s11d128

path,absolute,distance,name=s11d113,nodelist,undeformed=on,var=s11,
D113

print c
s11d113

path,absolute,distance,name=s11d98,nodelist,undeformed=on,var=s11,
D98

print c
s11d98

path,absolute,distance,name=s11d83,nodelist,undeformed=on,var=s11,
D83

print c
s11d83

path,absolute,distance,name=s11d68,nodelist,undeformed=on,var=s11
D68

print c
s11d68

path,absolute,distance,name=s11d53,nodelist,undeformed=on,var=s11,
D53

print c
s11d53

path,absolute,distance,name=s11d38,nodelist,undeformed=on,var=s11
D38

print c
```

```
s11d38

path,absolute,distance,name=s11d23,nodelist,undeformed=on,var=s11
D23

print c
s11d23

path,absolute,distance,name=s11d8,nodelist,undeformed=on,var=s11
D8

print c
s11d8

detail, elset = upper

path,absolute,distance,name=s11d00u,nodelist,undeformed=on,var=s11,
D00K

print c
s11d00u

detail, elset = bottom

path,absolute,distance,name=s11d00b,nodelist,undeformed=on,var=s11,
D00K

print c
s11d00b

detail, elset = s1

path,absolute,distance,name=s11d353,nodelist,undeformed=on,var=s11,
D353

print c
s11d353

path,absolute,distance,name=s11d338,nodelist,undeformed=on,var=s11,
D338

print c
s11d338

path,absolute,distance,name=s11d323,nodelist,undeformed=on,var=s11,
D323

print c
s11d323

path,absolute,distance,name=s11d308,nodelist,undeformed=on,var=s11,
D308

print c
s11d308

path,absolute,distance,name=s11d293,nodelist,undeformed=on,var=s11,
D293

print c
s11d293
```

```
path,absolute,distance,name=s11d278,nodelist,undeformed=on,var=s11,
D278

print c
s11d278

path,absolute,distance,name=s11d263,nodelist,undeformed=on,var=s11
D263

print c
s11d263

path,absolute,distance,name=s11d248,nodelist,undeformed=on,var=s11,
D248

print c
s11d248

path,absolute,distance,name=s11d233,nodelist,undeformed=on,var=s11
D233

print c
s11d233

path,absolute,distance,name=s11d218,nodelist,undeformed=on,var=s11
D218

print c
s11d218

path,absolute,distance,name=s11d203,nodelist,undeformed=on,var=s11
D203

print c
s11d203

path,absolute,distance,name=s11d188,nodelist,undeformed=on,var=s11
D188

print c
s11d188

display,all curves

path,absolute,distance,name=s22d173,nodelist,undeformed=on,var=s22,
D173

print c
s22d173

path,absolute,distance,name=s22d158,nodelist,undeformed=on,var=s22,
D158

print c
s22d158

path,absolute,distance,name=s22d143,nodelist,undeformed=on,var=s22,
D143

print c
s22d143
```

```
path,absolute,distance,name=s22d128,nodelist,undeformed=on,var=s22,
d128

print c
s22d128

path,absolute,distance,name=s22d113,nodelist,undeformed=on,var=s22,
D113

print c
s22d113

path,absolute,distance,name=s22d98,nodelist,undeformed=on,var=s22,
D98

print c
s22d98

path,absolute,distance,name=s22d83,nodelist,undeformed=on,var=s22,
D83

print c
s22d83

path,absolute,distance,name=s22d68,nodelist,undeformed=on,var=s22
D68

print c
s22d68

path,absolute,distance,name=s22d53,nodelist,undeformed=on,var=s22,
D53

print c
s22d53

path,absolute,distance,name=s22d38,nodelist,undeformed=on,var=s22
D38

print c
s22d38

path,absolute,distance,name=s22d23,nodelist,undeformed=on,var=s22
D23

print c
s22d23

path,absolute,distance,name=s22d8,nodelist,undeformed=on,var=s22
D8

print c
s22d8

detail, elset = upper

path,absolute,distance,name=s22d00u,nodelist,undeformed=on,var=s22,
D00K

print c
s22d00u
```

```
detail, elset = bottom

path,absolute,distance,name=s22d00b,nodelist,undeformed=on,var=s22,
D00K

print c
s22d00b

detail, elset = s1

path,absolute,distance,name=s22d353,nodelist,undeformed=on,var=s22,
D353

print c
s22d353

path,absolute,distance,name=s22d338,nodelist,undeformed=on,var=s22,
D338

print c
s22d338

path,absolute,distance,name=s22d323,nodelist,undeformed=on,var=s22,
d323

print c
s22d323

path,absolute,distance,name=s22d230,nodelist,undeformed=on,var=s22,
D308

print c
s22d230

path,absolute,distance,name=s22d293,nodelist,undeformed=on,var=s22,
D293

print c
s22d293

path,absolute,distance,name=s22d278,nodelist,undeformed=on,var=s22,
D278

print c
s22d278

path,absolute,distance,name=s22d263,nodelist,undeformed=on,var=s22
D263

print c
s22d263

path,absolute,distance,name=s22d248,nodelist,undeformed=on,var=s22,
D248

print c
s22d248

path,absolute,distance,name=s22d233,nodelist,undeformed=on,var=s22
D233
```

```
print c
s22d233

path,absolute,distance,name=s22d218,nodelist,undeformed=on,var=s22
D218

print c
s22d218

path,absolute,distance,name=s22d203,nodelist,undeformed=on,var=s22
D203

print c
s22d203

path,absolute,distance,name=s22d188,nodelist,undeformed=on,var=s22
D188

print c
s22d188

display,all curve

path,absolute,distance,name-s12d173,nodelist,undeformed=on,var=s12,
D173

print c
s12d173

path,absolute,distance,name=s12d158,nodelist,undeformed=on,var=s12,
D158

print c
s12d158

path,absolute,distance,name=s12d143,nodelist,undeformed=on,var=s12,
D143

print c
s12d143

path,absolute,distance,name-s12d128,nodelist,undeformed=on,var=s12,
d128

print c
s12d128

path,absolute,distance,name=s12d113,nodelist,undeformed=on,var=s12,
D113

print c
s12d113

path,absolute,distance,name=s12d98,nodelist,undeformed=on,var=s12,
D98

print c
s12d98

path,absolute,distance,name=s12d83,nodelist,undeformed=on,var=s12,
D83
```

```
print c
s12d83

path,absolute,distance,name=s12d68,nodelist,undeformed=on,var=s12
D68

print c
s12d68

path,absolute,distance,name=s12d53,nodelist,undeformed=on,var=s12,
D53

print c
s12d53

path,absolute,distance,name=s12d38,nodelist,undeformed=on,var=s12
D38

print c
s12d38

path,absolute,distance,name=s12d23,nodelist,undeformed=on,var=s12
D23

print c
s12d23

path,absolute,distance,name=s12d8,nodelist,undeformed=on,var=s12
D8

print c
s12d8

detail, elset = upper

path,absolute,distance,name=s12d00u,nodelist,undeformed=on,var=s12,
D00K

print c
s12d00u

detail, elset = bottom

path,absolute,distance,name=s12d00b,nodelist,undeformed=on,var=s12,
D00K

print c
s12d00b

detail, elset = s1

path,absolute,distance,name=s12d353,nodelist,undeformed=on,var=s12,
D353

print c
s12d353

path,absolute,distance,name=s12d338,nodelist,undeformed=on,var=s12,
D338

print c
```

```
s12d338

path,absolute,distance,name=s12d323,nodelist,undeformed=on,var=s12,
d323

print c
s12d323

path,absolute,distance,name=s12d230,nodelist,undeformed=on,var=s12,
D308

print c
s12d230

path,absolute,distance,name=s12d293,nodelist,undeformed=on,var=s12,
D293

print c
s12d293

path,absolute,distance,name=s12d278,nodelist,undeformed=on,var=s12,
D278

print c
s12d278

path,absolute,distance,name=s12d263,nodelist,undeformed=on,var=s12
D263

print c
s12d263

path,absolute,distance,name=s12d248,nodelist,undeformed=on,var=s12,
D248

print c
s12d248

path,absolute,distance,name=s12d233,nodelist,undeformed=on,var=s12
D233

print c
s12d233

path,absolute,distance,name-s12d218,nodelist,undeformed=on,var=s12
D218

print c
s12d218

path,absolute,distance,name=s12d203,nodelist,undeformed=on,var=s12
D203

print c
s12d203

path,absolute,distance,name=s12d188,nodelist,undeformed=on,var=s12
D188

print c
s12d188
```

```
display,all curve
detail, elset = s1

path,absolute,distance,name=misd173,nodelist,undeformed=on,var=mises,
d173

print c
misd173

path,absolute,distance,name=misd158,nodelist,undeformed=on,var=mises,
d158

print c
misd158

path,absolute,distance,name=misd143,nodelist,undeformed=on,var=mises,
d143

print c
misd143

path,absolute,distance,name=misd128,nodelist,undeformed=on,var=mises,
d128

print c
misd128

path,absolute,distance,name=misd113,nodelist,undeformed=on,var=mises,
d113

print c
misd113

path,absolute,distance,name=misd98,nodelist,undeformed=on,var=mises,
d98

print c
misd98

path,absolute,distance,name=misd83,nodelist,undeformed=on,var=mises,
d83

print c
misd83

path,absolute,distance,name=misd68,nodelist,undeformed=on,var=mises
d68

print c
misd68

path,absolute,distance,name=misd53,nodelist,undeformed=on,var=mises,
d53

print c
misd53

path,absolute,distance,name=misd38,nodelist,undeformed=on,var=mises
d38

print c
```

```
misd38

path,absolute,distance,name=misd23,nodelist,undeformed=on,var=mises
d23

print c
misd23

path,absolute,distance,name=misd8,nodelist,undeformed=on,var=mises
d8

print c
misd8

detail, elset = upper

path,absolute,distance,name=misd00u,nodelist,undeformed=on,var=mises,
D00K

print c
misd00u

detail, elset = bottom

path,absolute,distance,name=misd00b,nodelist,undeformed=on,var=mises,
D00K

print c
misd00b

detail, elset = s1

path,absolute,distance,name=misd353,nodelist,undeformed=on,var=mises,
d353

print c
misd353

path,absolute,distance,name=misd338,nodelist,undeformed=on,var=mises,
d338

print c
misd338

path,absolute,distance,name=misd323,nodelist,undeformed=on,var=mises,
d323

print c
misd323

path,absolute,distance,name=misd308,nodelist,undeformed=on,var=mises,
d308

print c
misd308

path,absolute,distance,name=mis293,nodelist,undeformed=on,var=mises,
d293

print c
mis293
```

```
path,absolute,distance,name=misd278,nodelist,undeformed=on,var=mises,
d278

print c
misd278

path,absolute,distance,name=misd263,nodelist,undeformed=on,var=mises
d263

print c
misd263

path,absolute,distance,name=misd248,nodelist,undeformed=on,var=mises,
d248

print c
misd248

path,absolute,distance,name=misd233,nodelist,undeformed=on,var=mises
d233

print c
misd233

path,absolute,distance,name=misd218,nodelist,undeformed=on,var=mises
d218

print c
misd218

path,absolute,distance,name=misd203,nodelist,undeformed=on,var=mises
d203

print c
misd203

path,absolute,distance,name=misd188,nodelist,undeformed=on,var=mises
D188

print c
misd188

display,all curves

display,all curves

detail, elset = s1

path,absolute,distance,name=presd173,nodelist,undeformed=on,var=press,
D173

print c
presd173

path,absolute,distance,name=presd158,nodelist,undeformed=on,var=press,
D158

print c
presd158

path,absolute,distance,name=presd143,nodelist,undeformed=on,var=press,
```

```
D143

print c
presd143

path,absolute,distance,name=presd128,nodelist,undeformed=on,var=press,
d128

print c
presd128

path,absolute,distance,name=presd113,nodelist,undeformed=on,var=press,
D113

print c
presd113

path,absolute,distance,name=presd98,nodelist,undeformed=on,var=press,
D98

print c
presd98

path,absolute,distance,name=presd83,nodelist,undeformed=on,var=press,
D83

print c
presd83

path,absolute,distance,name=presd68,nodelist,undeformed=on,var=press
D68

print c
presd68

path,absolute,distance,name=presd53,nodelist,undeformed=on,var=press,
D53

print c
presd53

path,absolute,distance,name=presd38,nodelist,undeformed=on,var=press
D38

print c
presd38

path,absolute,distance,name=presd23,nodelist,undeformed=on,var=press
D23

print c
presd23

path,absolute,distance,name=presd8,nodelist,undeformed=on,var=press
D8

print c
presd8

detail, elset = upper
```

```
path,absolute,distance,name=presd00u,nodelist,undeformed=on,var=press,
D00K

print c
presd00u

detail, elset = bottom

path,absolute,distance,name=presd00b,nodelist,undeformed=on,var=press,
D00K

print c
presd00b

detail, elset = s1

path,absolute,distance,name=presd353,nodelist,undeformed=on,var=press,
D353

print c
presd353

path,absolute,distance,name=presd338,nodelist,undeformed=on,var=press,
D338

print c
presd338

path,absolute,distance,name=presd323,nodelist,undeformed-on,var=press,
d323

print c
presd323

path,absolute,distance,name=presd308,nodelist,undeformed=on,var=press,
D308

print c
presd308

path,absolute,distance,name=presd293,nodelist,undeformed=on,var=press,
D293

print c
presd293

path,absolute,distance,name=presd278,nodelist,undeformed-on,var-press,
D278

print c
presd278

path,absolute,distance,name=presd263,nodelist,undeformed=on,var=press
D263

print c
presd263

path,absolute,distance,name=presd248,nodelist,undeformed=on,var=press,
D248
```

```
print c
presd248

path,absolute,distance,name=presd233,nodelist,undeformed=on,var=press
D233

print c
presd233

path,absolute,distance,name=presd218,nodelist,undeformed=on,var=press
D218

print c
presd218

path,absolute,distance,name=presd203,nodelist,undeformed-on,var=press
D203

print c
presd203

path,absolute,distance,name-presd188,nodelist,undeformed=on,var=press
D188

print c
presd188

display,all curves
```

Appendix II

The programs fullfan3.m and fullfanodd3.m are Matlab programs, which read data (radial distances and Cartesian stresses at 7.5^0 interval surrounding the crack tip) from an abaqus.rpt file and arrange the data in matrix form. The stress data are then extrapolated to the crack tip in Cartesian form and finally transformed to polar co-ordinate system. The angle versus cylindrical stresses at the crack tip are written in an output file named general.out.

The program fullfan3.m

```
%%%%%%%%%%%%%%%%%%%%%%%%%%%%%%%%%%%%%%%%%%%%%%%%%%%%%%%%%%%%%%%%%%%%%%%%%%%%%%%
%This programme reads abaqus data stored in a file called abaqus.rpt. The first
%part of the programme strips the text from the file and stores the stresses in
%a matrix b
%%%%%%%%%%%%%%%%%%%%%%%%%%%%%%%%%%%%%%%%%%%%%%%%%%%%%%%%%%%%%%%%%%%%%%%%%%%%%%%
b=[];
f=fopen('abaqus.rpt','r');
count=0;
foundtext=0;
count1=1;
while 1
line=fgetl(f);
if ~isstr(line),break,end;
a=sscanf(line,'%f');
if size(a,1) > 0
if foundtext == 1, count1 = count1 + 1;, end;
b([1,count1],count+1)=a;
count=count + 1;
foundtext=0;
else
count=0;
foundtext=1;
end
end
fclose(f);
%%%%%%%%%%%%%%%%%%%%%%%%%%%%%%%%%%%%%%%%%%%%%%%%%%%%%%%%%%%%%%%%%%%%%%%%%%%%%%%
% This programme reads abaqus data stored in a file called abaqus.rpt
%The data is assumed to come from a blf with 26 radial lines of variables
% The data is read and reformatted to a matrix b(ij)
% The first row  i  = 1 contains distances from the tip

% j loops around angles from 2 to 26 in 15 degree intervals
%directly ahead of the crack there may be a discontinuity , so this angle is
%treated twice, extrapolating to the nodes on the crack line from above and
%below the crack, in the abaqus post-processing

%s11 is in  row i   2 thro 27
% s22 is in row i  28 thro 53
% s12 is in row i  54 thro 79
%mises is in rows 80 thro 105
%press is in rows 106 thro131 !!! not for plane stress  !!!

%For plane strain this version extrapolates mises and pressure directly instead
%of calculating them from the extrapolted stresses.For plane stress cannot read
%pressure directly only mises.

%The stresses are extrapolated to the tip as cartesian stresses and then
%transformed to cylindrical co-ords.  The upper crack flank is located along
```

```
%theta %= +180 degrees and the lower crack flank along theta - 180    i.e theta
%is measured anti- clockwise!!

%The programme is set for both plane strain ( nu  = 0.5 ) and plane stress,
%with plane strain currently commented out

%%%%%%%%%%%%%%%%%%%%%%%%%%%%%%%%%%%%%%%%%%%%%%%%%%%%%%%%%%%%%%%%%%%%%%%%%%%%%%%
%The data is plotted against distance  and curve fitted
% the ploting is normally supressed but can be reactivated to check the curve
%fit.
%Data can be written to an externqal file compatible with excel, and this
%is also currently commented out
%%%%%%%%%%%%%%%%%%%%%%%%%%%%%%%%%%%%%%%%%%%%%%%%%%%%%%%%%%%%%%%%%%%%%%%%%%%%%%%
                        %Firstly sigma11

                                         %figure
 for i = 2:27
                                         %plot (b(1,2:20),b(i,2:20),'bd')
                                         %xlabel('sigmaxx versus distance')
                                         % hold on
                                         %axis([0 20 -2e8 3e8])

                                         %curve fit sigmaxx stress

sxx = polyfit(b(1,2:4),b(i,2:4),1);
                                          disti = 0:1:100;
                                          sxxi = polyval(sxx,disti);
                                          %plot(disti,sxxi)

%interpolate to crack tip, stress held as stressxx
%there are 26 stresses including zero which is held twice
count = i-1;
stressxx(count) = sxx(2)/2e8;
% if the count is greater than 13 kount is set back one to catch the direction
%ahead of the crack twice
if count > 13
kount = count - 1;
else
kount = count;
end
%angle is held in degrees, the minus makes it positive anti-clockwise
angle(count) = 180-((kount-1)*15);
end

%%%%%%%%%%%%%%%%%%%%%%%%%%%%%%%%%%%%%%%%%%%%%%%%%%%%%%%%%%%%%%%%%%%%%%%%%%%%%%%
                        %Now sigma22
for i = 28:53
                                          % plot (b(1,2:20),b(i,2:20),'rd')
                                          %xlabel('sigmayy versus distance')
                                          % hold on
                                          %axis([0 20 -2e8 3e8])
                                          %end

                                          % curve fit sigmayy

syy = polyfit(b(1,2:4),b(i,2:4),1);
                                          %disti = 0:1:100;
                                          %syyi = polyval(syy,disti);
                                          %plot(disti,syyi)
%interpolate to crack tip, stress held as stressyy
count = i-27;
```

```
stressyy(count) = syy(2)/2e8;
end

%%%%%%%%%%%%%%%%%%%%%%%%%%%%%%%%%%%%%%%%%%%%%%%%%%%%%%%%%%%%%%%%%%%%%%%%%%%%%%%%%%%
                         %Now sigma12

%figure
for i = 54:79
%plot (b(1,5:20),b(i,5:20),'gd')
%label('sigmaxy versus distance')
% hold on
%axis([0 50 -2e8 3e8])

%Interpolate stress to tip and plot

%curve fit sigmaxy stress

sxy = polyfit(b(1,2:4),b(i,2:4),1);
                         %disti = 0:1:100;
                         %sxyi = polyval(sxy,disti);
                         %plot(disti,sxxi)

%interpolate to crack tip
count = i-53;
stressxy(count) = sxy(2)/2e8;
end
%%%%%%%%%%%%%%%%%%%%%%%%%%%%%%%%%%%%%%%%%%%%%%%%%%%%%%%%%%%%%%%%%%%%%%%%%%%%%%%%%%%

% Plot cartesian stresses at tip

figure
axis([-180 180 -2 5.0])
hold on
grid on
title(' Cartesian stresses for plane stress non hardening solution Homogeneous')
%title(' Cartesian stresses for plane strain non hardening solution Material
mismatch =1.6 ')
plot(angle(1:26),stressxx(1:26),'bd')
plot(angle(1:26),stressyy(1:26),'rd')
plot(angle(1:26),stressxy(1:26),'gd')
legend ('stressxx','stressyy','stressxy')

%%%%%%%%%%%%%%%%%%%%%%%%%%%%%%%%%%%%%%%%%%%%%%%%%%%%%%%%%%%%%%%%%%%%%%%%%%%%%%%%%%%

%It is most accurate to read mises and mean from the abaqus file, but  the
%stress components and the mean and mises may not be exactly conistent

%If you want to use the calculated  values of mises and mean comment this
%section out

%%%%%%%%%%%%%%%%%%%%%%%%%%%%%%%%%%%%%%%%%%%%%%%%%%%%%%%%%%%%%%%%%%%%%%%%%%%%%%%%%%%
                         %Now mises
for i = 80:105
                                        % plot (b(1,2:20),b(i,2:20),'rd')
                                        %xlabel('mises versus distance')
                                        % hold on
                                        %axis([0 20 -2e8 3e8])
                                        %end

                                        % curve fit mises
mis = polyfit(b(1,3:6),b(i,3:6),1);
```

```
                                        %disti = 0:1:100;
                                        %misesi = polyval(mises,disti);
                                        %plot(disti,misesi)
%interpolate to crack tip, stress held as mises
count = i-79;
mises(count) = mis(2)/2e8;
end

%%%%%%%%%%%%%%%%%%%%%%%%%%%%%%%%%%%%%%%%%%%%%%%%%%%%%%%%%%%%%%%%%%%%%%%%%%%%%%%%%%%
%%%%%%%%%%%%%%%%%%%%%%%%%%%%%%%%%%%%%%%%%%%%%%%%%%%%%%%%%%%%%%%%%%%%%%%%%%%%%%%%%%%
                         %Now mean stress (commment out for plane stress)
%for i = 106:131
                                        % plot (b(1,2:20),b(i,2:20),'rd')
                                        %xlabel('press versus distance')
                                        % hold on
                                        %axis([0 20 -2e8 3e8])
                                        %end

                                        % curve fit press

%press = polyfit(b(1,3:6),b(i,3:6),1);
                                        %disti = 0:1:100;
                                        %pressi = polyval(press,disti);
                                        %plot(disti,press)

%interpolate to crack tip, stress held as press

%count = i-105;

%Change pressure into mean stress by change of sign

%stressm(count) = -press(2)/2e8;

%end

%%%%%%%%%%%%%%%%%%%%%%%%%%%%%%%%%%%%%%%%%%%%%%%%%%%%%%%%%%%%%%%%%%%%%%%%%%%%%%%%%%%

                              % Transform to polar co-ords

for count = 1:26

% The minus sign on the angle makes the sign convention positrive anti-clockwise
theta = angle(count)*pi/180;

stressrr(count) = (stressxx(count) +stressyy(count))/2 +((stressxx(count) -
stressyy(count))/2)*cos(2*theta) + stressxy(count)*sin(2*theta);

stressqq(count) = (stressxx(count) + stressyy(count))/2 -((stressxx(count) -
stressyy(count))/2)*cos(2*theta) - stressxy(count)*sin(2*theta);

stressrq(count) = -((stressxx(count) - stressyy(count))/2)*sin(2*theta) +
stressxy(count)*cos(2*theta);

%%%%%%%%%%%%%%%%%%%%%%%%%%%%%%%%%%%%%%%%%%%%%%%%%%%%%%%%%%%%%%%%%%%%%%%%%%%%%%%%%%

                         % mises and mean stress

%It is most accurate to read mises and mean from the abaqus file, but  the
stress components and the mean and mises maynot be exactly conistent
%If you want to use the directly read values comment this section out
%von mises yield criterion in plane stress
```

```
%mises(count) = sqrt(stressxx(count)^2 + stressyy(count)^2 - stressxx(count) *
%stressyy(count) +3*stressxy(count)^2);


%von mises yield criterion  in plane strain
%mises(count)=sqrt(0.75*(stressxx(count)-
stressyy(count))^2+3*stressxy(count)^2);

%mean stress in plane strain
%stressm(count)=(stressxx(count)+stressyy(count))/2;

%mean stress in plane stress
stressm(count)=(stressxx(count)+stressyy(count))/3;

                                %stress deviators

sqq(count) = stressqq(count)-stressm(count);
srr(count) = stressrr(count)-stressm(count);

end

%%%%%%%%%%%%%%%%%%%%%%%%%%%%%%%%%%%%%%%%%%%%%%%%%%%%%%%%%%%%%%%%%%%%%%%%%

                        % Plot polar stresses at tip

figure
axis([-180 180 -2 4.0])
hold on
grid on
%title(' Cylindrical stresses for plane strain non hardening solution Material
mismatch =1.6 ')
title(' Cylindrical stresses for plane stress non hardening solution
Homogeneous')

plot(angle(1:26),stressrr(1:26),'b*')
plot(angle(1:26),stressqq(1:26),'r+')
plot(angle(1:26),stressrq(1:26),'gd')
legend('stressrr','stressqq','stressrq')

%%%%%%%%%%%%%%%%%%%%%%%%%%%%%%%%%%%%%%%%%%%%%%%%%%%%%%%%%%%%%%%%%%%%%%%%%
%Plot Deviators at Tip

figure
axis([-180 180 -2 4.0])
hold on
grid on
%title(' Cylindrical stresses for plane strain non hardening solution, Material
mismatch =1.2 ')
title(' Cylindrical stress deviators for plane stress non hardening solution,
Homogeneous')

plot(angle(1:26),srr(1:26),'b*')
plot(angle(1:26),sqq(1:26),'r+')
legend('srr','sqq')

%%%%%%%%%%%%%%%%%%%%%%%%%%%%%%%%%%%%%%%%%%%%%%%%%%%%%%%%%%%%%%%%%%%%%%%%%
% Note there is an option of either calculating mises and mean or using the
%directly read values
figure
axis([-180 180 -2 4.0])
hold on
```

```
grid on
%title(' mean and mises stress for plane strain non hardening solution Material
mismatch =1.6')
title(' mean and mises stress for plane stress non hardening solution
Homogeneous')

plot(angle(1:26),mises(1:26),'g*')
plot(angle(1:26),stressm(1:26),'r+')
legend('mises','stressm')

%%%%%%%%%%%%%%%%%%%%%%%%%%%%%%%%%%%%%%%%%%%%%%%%%%%%%%%%%%%%%%%%%%%%%%%%%%%%

%figure
%axis([-180 180 -2 5.0])
%hold on
%grid on
%title(' mises stress for plane strain non hardening solution ')
%title(' mises stress for plane stress non hardening solution ')

%plot(angle(1:26),mises(1:26),'k*')

%%%%%%%%%%%%%%%%%%%%%%%%%%%%%%%%%%%%%%%%%%%%%%%%%%%%%%%%%%%%%%%%%%%%%%%%%%%%

%figure
%axis([-180 180 -2 5.0])
%hold on
%grid on
%title(' mean stress for plane strain non hardening solution ')
%title(' mean stress for plane stress non hardening solution ')
%plot(angle(1:26),stressm(1:26),'r+')

%%%%%%%%%%%%%%%%%%%%%%%%%%%%%%%%%%%%%%%%%%%%%%%%%%%%%%%%%%%%%%%%%%%%%%%%%%%%
                    % write output to external files

%fn = 'data.out'

%fprintf(fn, 'dimensional distance strress qq theta = 0 \n')

%for l=4:141
%fprintf(fn, '%20.5f%20.5f\n', b(1,1),b(39,1))
%end
%%%%%%%%%%%%%%%%%%%%%%%%%%%%%%%%%%%%%%%%%%%%%%%%%%%%%%%%%%%%%%%%%%%%%%%%%%
%            write general output to external file

fn = 'general.out'

fprintf(fn,'angle  stressxx  stressyy  stressxy  stressrr  stressqq  stressrq
srr  sqq  stressm   mises\n')

for i = 1:26
fprintf(fn,
'%10.5f%10.5f%10.5f%10.5f%10.5f%10.5f%10.5f%10.5f%10.5f%10.5f%10.5f\n',
angle(i),stressxx(i),stressyy(i),stressxy(i),stressrr(i),stressqq(i),stressrq(i)
,srr(i),sqq(i),stressm(i),mises(i))
end
```

The program fullfanodd3.m

```
%%%%%%%%%%%%%%%%%%%%%%%%%%%%%%%%%%%%%%%%%%%%%%%%%%%%%%%%%%%%%%%%%%%%%%%%%%%%
%This programme reads abaqus data stored in a file called abaqus.rpt. The first
```

```
%part of the programme strips the text from the file and stores the stresses in
%a matrix b
%%%%%%%%%%%%%%%%%%%%%%%%%%%%%%%%%%%%%%%%%%%%%%%%%%%%%%%%%%%%%%%%%%%%%%%%%%%%%%%%
b=[];
f=fopen('abaqus.rpt','r');
count=0;
foundtext=0;
count1=1;
while 1
line=fgetl(f);
if ~isstr(line),break,end;
a=sscanf(line,'%f');
if size(a,1) > 0
if foundtext == 1, count1 = count1 + 1;, end;
b([1,count1],count+1)=a;
count=count + 1;
foundtext=0;
else
count=0;
foundtext=1;
end
end
fclose(f);
%%%%%%%%%%%%%%%%%%%%%%%%%%%%%%%%%%%%%%%%%%%%%%%%%%%%%%%%%%%%%%%%%%%%%%%%%%%%%%%%
%This programme reads abaqus data stored in a file called abaqus.rpt
%The data is assumed to come from a blf with 26 radial lines of variables
%The data is read and reformatted to a matrix b(ij)
%The first row  i  = 1 contains distances from the tip

% j loops around angles from 2 to 26 in 15 degree intervals
%directly ahead of the crack there may be a discontinuity , so this angle is
%treated twice, extrapolating to the nodes on the crack line from above and
%below the crack, in the abaqus post-processing

%s11 is in  row i   2 thro 27
% s22 is in row i  28 thro 53
% s12 is in row i  54 thro 79
%mises is in rows 80 thro 105
%press is in rows 106 thro131!!!not for plane stress!!!

%For plane strain this version extrapolates mises and pressure directly instead
%of calculating them from the extrapolted stresses.For plane stress cannot read
%pressure directly only mises.

%The stresses are extrapolated to the tip as cartesian stresses and then
%transformed to cylindrical co-ords.  The upper crack flank is located along
%theta %= +180 degrees and the lower crack flank along theta = 180    i.e theta
%is measured anti- clockwise!!

%The programme is set for both plane strain ( nu  = 0.5 ) and plane stress,
%with plane strain currently commented out

%%%%%%%%%%%%%%%%%%%%%%%%%%%%%%%%%%%%%%%%%%%%%%%%%%%%%%%%%%%%%%%%%%%%%%%%%%%%%%%%
%The data is plotted against distance  and curve fitted
%the ploting is normally supressed but can be reactivated to check the curve
%fit.
%Data can be written to an externqal file compatible with excel, and this
%is also currently commented out
%%%%%%%%%%%%%%%%%%%%%%%%%%%%%%%%%%%%%%%%%%%%%%%%%%%%%%%%%%%%%%%%%%%%%%%%%%%%%%%%
                         %Firstly sigma11
                                        %figure
```

```
 for i = 2:27
                                                  %plot (b(1,2:20),b(i,2:20),'bd')
                                                  %xlabel('sigmaxx versus distance')
                                                  % hold on
                                                  %axis([0 20 -2e8 3e8])

                                                  %curve fit sigmaxx stress

sxx = polyfit(b(1,2:4),b(i,2:4),1);
                                                   disti = 0:1:100;
                                                   sxxi = polyval(sxx,disti);
                                                   %plot(disti,sxxi)

%interpolate to crack tip, stress held as stressxx
%there are 26 stresses including zero which is held twice
count = i-1;
stressxx(count) = sxx(2)/2e8;

%The count is  set back two to catch the direction ahead of the crack twice

if count <  13
kount = count;

elseif count > 14
kount = count - 2;

else
kount = 12.5
end

%angle is held in degrees, the minus makes it positive anti-clockwise
angle(count) = 172.5-((kount-1)*15);
end

%%%%%%%%%%%%%%%%%%%%%%%%%%%%%%%%%%%%%%%%%%%%%%%%%%%%%%%%%%%%%%%%%%%%%%%%%%%%%%%%
                        %Now sigma22
for i = 28:53
                                                   % plot (b(1,2:20),b(i,2:20),'rd')
                                                   %xlabel('sigmayy versus distance')
                                                   % hold on
                                                   %axis([0 20 -2e8 3e8])
                                                   %end

                                                   % curve fit sigmayy

syy = polyfit(b(1,2:4),b(i,2:4),1);
                                                   %disti = 0:1:100;
                                                   %syyi = polyval(syy,disti);
                                                   %plot(disti,syyi)
%interpolate to crack tip, stress held as stressyy
count = i-27;
stressyy(count) = syy(2)/2e8;
end

%%%%%%%%%%%%%%%%%%%%%%%%%%%%%%%%%%%%%%%%%%%%%%%%%%%%%%%%%%%%%%%%%%%%%%%%%%%%%%%%
                        %Now sigma12

%figure
for i = 54:79
%plot (b(1,5:20),b(i,5:20),'gd')
%label('sigmaxy versus distance')
```

```
%hold on
%axis([0 50 -2e8 3e8])

%Interpolate stress to tip and plot

%curve fit sigmaxy stress

sxy = polyfit(b(1,2:4),b(i,2:4),1);
                            %disti = 0:1:100;
                            %sxyi = polyval(sxy,disti);
                            %plot(disti,sxxi)

%interpolate to crack tip
count = i-53;
stressxy(count) = sxy(2)/2e8;
end
%%%%%%%%%%%%%%%%%%%%%%%%%%%%%%%%%%%%%%%%%%%%%%%%%%%%%%%%%%%%%%%%%%%%%%%%%%%%
% Plot cartesian stresses at tip
figure
axis([-180 180 -2 5.0])
hold on
grid on
title(' Cartesian stresses for plane stress non hardening solution Homogeneous')
%title(' Cartesian stresses for plane strain non hardening solution Material
mismatch =1.6 ')
plot(angle(1:26),stressxx(1:26),'bd')
plot(angle(1:26),stressyy(1:26),'rd')
plot(angle(1:26),stressxy(1:26),'gd')
legend ('stressxx','stressyy','stressxy')
%%%%%%%%%%%%%%%%%%%%%%%%%%%%%%%%%%%%%%%%%%%%%%%%%%%%%%%%%%%%%%%%%%%%%%%%%%%%
                           % Transform to polar co-ords

for count = 1:26
% The minus sign on the angle makes the sign convention positrive anti-clockwise
theta = angle(count)*pi/180;

stressrr(count) = (stressxx(count) +stressyy(count))/2 +((stressxx(count) -
stressyy(count))/2)*cos(2*theta) + stressxy(count)*sin(2*theta);

stressqq(count) = (stressxx(count) +stressyy(count))/2 -((stressxx(count) -
stressyy(count))/2)*cos(2*theta) - stressxy(count)*sin(2*theta);

stressrq(count) = -((stressxx(count) - stressyy(count))/2)*sin(2*theta) +
stressxy(count)*cos(2*theta);

%%%%%%%%%%%%%%%%%%%%%%%%%%%%%%%%%%%%%%%%%%%%%%%%%%%%%%%%%%%%%%%%%%%%%%%%%%%%
                           % mises and mean stress

% It is most accurate to read mises and mean from the abaqus file, but the
stress components and the mean and mises maynot be exactly conistent

%If you want to use the directly read values comment this section out
%von mises yield criterion in plane stress

%mises(count) = sqrt(stressxx(count)^2 - stressyy(count)^2 - stressxx(count) *
%stressyy(count) +3*stressxy(count)^2);

% von mises yield criterion  in plane strain
%mises(count)=sqrt(0.75*(stressxx(count)-
stressyy(count))^2+3*stressxy(count)^2)%;
%mean stress in plane strain
```

```
%stressm(count)=(stressxx(count)+stressyy(count))/2;

%mean stress in plane stress
stressm(count)=(stressxx(count)+stressyy(count))/3;

                              %stress deviators

sqq(count) = stressqq(count)-stressm(count);
srr(count) = stressrr(count)-stressm(count);

end

%%%%%%%%%%%%%%%%%%%%%%%%%%%%%%%%%%%%%%%%%%%%%%%%%%%%%%%%%%%%%%%%%%%%%%%%%%%%%%%
%%%%%%%%%%%%%%%%%%%%%%%%%%%%%%%%%%%%%%%%%%%%%%%%%%%%%%%%%%%%%%%%%%%%%%%%%%%%%%%%
%                  Now mean stress (comment out for plane stress)

%It is most accurate to read mises and the  mean from the abaqus file, but  the
%stress components and the mean and mises may not be exactly conistent

%If you want to use the calculated  values of mises and mean comment this
%section out

                         %for i = 106:131
                                        % plot (b(1,2:20),b(i,2:20),'rd')
                                        %xlabel('press versus distance')
                                        % hold on
                                        %axis([0 20 -2e8 3e8])
                                        %end

                                        % curve fit press

%press = polyfit(b(1,3:6),b(i,3:6),1);
                                        %disti = 0:1:100;
                                        %pressi = polyval(press,disti);
                                        %plot(disti,press)
% interpolate to crack tip, stress held as press

%count = i-105;

%Change pressure into mean stress by change of sign

%stressm(count) = -press(2)/2e8;
%end

%%%%%%%%%%%%%%%%%%%%%%%%%%%%%%%%%%%%%%%%%%%%%%%%%%%%%%%%%%%%%%%%%%%%%%%%%%%%%%%

%It is most accurate to read mises a from the abaqus file, but the stress
%components and the mean and mises may not be exactly conistent

%If you want to use the calculated  values of mises and mean comment this
%section out

                       %Now mises
for i = 80:105
                                        % plot (b(1,2:20),b(i,2:20),'rd')
                                        %xlabel('mises versus distance')
                                        % hold on
                                        %axis([0 20 -2e8 3e8])
                                        %end

                                        % curve fit mises
```

```
mis = polyfit(b(1,3:6),b(i,3:6),1);
                                                    %disti = 0:1:100;
                                                    %misesi = polyval(mises,disti);
                                                    %plot(disti,misesi)
%interpolate to crack tip, stress held as mises
count = i-79;
mises(count) = mis(2)/2e8;
end

%%%%%%%%%%%%%%%%%%%%%%%%%%%%%%%%%%%%%%%%%%%%%%%%%%%%%%%%%%%%%%%%%%%%%%%%%%%%%%%%%%%%%%%%%%%%%%%
%%%%%%%%%%%%%%%%%%%%%%%%%%%%%%%%%%%%%%%%%%%%%%%%%%%%%%%%%%%%%%%%%%%%%%%%%%%%%%%%%%%%%%%%%%%%%%
%Plot polar stresses at tip

figure
axis([-180 180 -2 4.0])
hold on
grid on
%title(' Cylindrical stresses for plane strain non hardening solution Material
mismatch =1.6 ')
title(' Cylindrical stresses for plane stress non hardening solution
Homogeneous')

plot(angle(1:26),stressrr(1:26),'b*')
plot(angle(1:26),stressqq(1:26),'r+')
plot(angle(1:26),stressrq(1:26),'gd')
legend('stressrr','stressqq','stressrq')
%%%%%%%%%%%%%%%%%%%%%%%%%%%%%%%%%%%%%%%%%%%%%%%%%%%%%%%%%%%%%%%%%%%%%%%%%%%%%%%%%%%%%%%%%%%%%%%

%%%%%%%%%%%%%%%%%%%%%%%%%%%%%%%%%%%%%%%%%%%%%%%%%%%%%%%%%%%%%%%%%%%%%%%%%%%%%%%%%%%%%%%%%%%%%%%
%Plot Deviators at Tip

figure
axis([-180 180 -2 4.0])
hold on
grid on
%title('Cylindrical stresses for plane strain non hardening solution,
Homogeneous ')
title('Cylindrical stress deviators for plane stress non hardening solution,
Homogeneous')

plot(angle(1:26),srr(1:26),'b*')
plot(angle(1:26),sqq(1:26),'r+')
legend('srr','sqq')
%%%%%%%%%%%%%%%%%%%%%%%%%%%%%%%%%%%%%%%%%%%%%%%%%%%%%%%%%%%%%%%%%%%%%%%%%%%%%%%%%%%%%%%%%%%%%%
figure
axis([-180 180 -2 4.0])
hold on
grid on
%title('mean and mises stress for plane strain non hardening solution Materia
%mismatch =1.6')
title(' mean and mises stress for plane stress non hardening solution
Homogeneous')
plot(angle(1:26),mises(1:26),'g*')
plot(angle(1:26),stressm(1:26),'r+')
legend('mises','stressm')

%%%%%%%%%%%%%%%%%%%%%%%%%%%%%%%%%%%%%%%%%%%%%%%%%%%%%%%%%%%%%%%%%%%%%%%%%%%%%%%%%%%%%%%%%%%%%

%figure
%axis([-180 180 -2 5.0])
%hold on
```

```
%grid on
%title(' mises stress for plane strain non hardening solution ')
%title(' mises stress for plane stress non hardening solution ')

%plot(angle(1:26),mises(1:26),'k*')

%%%%%%%%%%%%%%%%%%%%%%%%%%%%%%%%%%%%%%%%%%%%%%%%%%%%%%%%%%%%%%%%%%%%%%%%%%%%%%%%

%figure
%axis([-180 180 -2 5.0])
%hold on
%grid on
%title(' mean stress for plane strain non hardening solution ')
%title(' mean stress for plane stress non hardening solution ')
%plot(angle(1:26),stressm(1:26),'r+')

%%%%%%%%%%%%%%%%%%%%%%%%%%%%%%%%%%%%%%%%%%%%%%%%%%%%%%%%%%%%%%%%%%%%%%%%%%%%%%%%
                    % write output to external files

%fn = 'data.out'

%fprintf(fn, 'dimensional distance  strress qq theta = 0 \n')

%for l=4:141
%fprintf(fn, '%20.5f%20.5f\n', b(1,l),b(39,l))
%end
%%%%%%%%%%%%%%%%%%%%%%%%%%%%%%%%%%%%%%%%%%%%%%%%%%%%%%%%%%%%%%%%%%%%%%%%%%%%%
%           write general output to external file

fn = 'general.out'

fprintf(fn,'angle  stressxx  stressyy  stressxy  stressrr  stressqq  stressrq
srr  sqq  stressm  mises\n')

for i = 1:26
fprintf(fn,
'%10.5f%10.5f%10.5f%10.5f%10.5f%10.5f%10.5f%10.5f%10.5f%10.5f%10.5f\n',
angle(i),stressxx(i),stressyy(i),stressxy(i),stressrr(i),stressqq(i),stressrq(i
,srr(i),sqq(i),stressm(i),mises(i))
end
```